

## ABSTRACT

Title of Document: STRUCTURAL AND FUNCTIONAL STUDIES OF THE DNA DAMAGE-INDUCIBLE UBL-UBA PROTEIN DDI1

Urszula Krystyna Nowicka, Doctor of Philosophy, 2014

Directed By: Professor David Fushman  
Department of Chemistry and Biochemistry

The ubiquitin-proteasome system plays an essential role in the biology of eukaryotes. Through turnover of short-lived proteins, it regulates vital processes such as cell cycle progression, transcription, misfolded-protein degradation, and immune response. One scenario of how ubiquitinated proteins are driven to the 26S proteasome for degradation involves shuttle proteins (Rad23, Dsk2, or Ddi1), which recognize their substrate through a ubiquitin associated (UBA) domain and identify the proteasome through their ubiquitin like (UBL) domain.

Ddi1 (DNA Damage-Inducible 1) protein has an unusual composition for a UBL-UBA protein as it also contains a conserved retroviral protease fold domain (RVP). The detailed substrate specificity of Ddi1 as a shuttle is not known; however, it was found that Ddi1 is required for degradation of Ho endonuclease and F-box protein Ufo1, two proteins involved in cell cycle progression and regulation. In *Saccharomyces*

*cerevisiae*, both UBA and UBL domains of Ddi1 are required for its shuttling function. Interestingly, through evolution, Ddi1 lost its UBA domain in mammals, which raises the question of how this shuttle protein performs its function without the domain that binds Ub. Furthermore, the presence of a UBL domain is also questionable since the N-terminal gene sequence of Ddi1 in yeast shares low identity with Ub and other known UBL domains. In order to fully confirm that yeast Ddi1 is an UBL-UBA shuttle, the solution structure of the nominal UBL domain was obtained. In addition, the functional properties of UBL domains were examined. This work shows that Ddi1UBL does not recognize its expected binding partners, one example being the ubiquitin interactive motif (UIM) domains of the Ufo1 protein. However, it is capable of recognizing ubiquitin (Ub) and its conjugates as well as the UBL domain of Dsk2, which is a novel interaction and is uncharacteristic for all known UBL domains.

To date, UBL-UBA shuttle proteins are well-studied proteins in the ubiquitin proteasomal pathway. Nevertheless, the details of target protein delivery to the proteasome for degradation are not well known. This work characterizes Ddi1 as an UBL-UBA protein, confirming its potential as a shuttle protein like other UBL-UBA proteins, such as Dsk2 and Rad23.

STRUCTURAL AND FUNCTIONAL STUDIES OF THE DNA DAMAGE-  
INDUCIBLE UBL-UBA PROTEIN DDI1

By

Urszula Krystyna Nowicka

Thesis submitted to the Faculty of the Graduate School of the  
University of Maryland, College Park, in partial fulfillment  
of the requirements for the degree of  
Doctor of Philosophy  
2014

Advisory Committee:

Professor David Fushman, Chair  
Professor Dorothy Beckett  
Professor Kwaku Dayie  
Professor Jonathan Dinman  
Professor Nicole LaRonde

© Copyright by  
Urszula Krystyna Nowicka  
2014

## Dedication

To the memory of my father, Wojciech Nowicki who passed away before he could see my graduation. With love to my mother Ewa Nowicka and my sister Monika for all the love, support and understanding. I also dedicate this work to my family and friends who were always there when I needed them.

## Acknowledgements

I cannot express enough thanks to my advisor Dr. David Fushman for his mentoring and support throughout the graduate program. I also would like to thank my committee Dr. Kwaku Dayie, Dr. Nicole LaRonde and especially Dr. Dorothy Beckett for their continued support and encouragement.

I would like to acknowledge my collaborators: Prof. Michael H. Glickman, Dr. Olivier Walker, Dr. Dasha Krutauz and Dr. Noa Reis for their contribution to my project.

I also wish to thank Dr. Dorothy Beckett for allowing me to use analytical centrifuge in her laboratory and her former student Dr. Poorni Adikaram for help in data collection and showing me how to use WinNonLin software. Their advice was very useful during data analysis.

I would like also to express my thanks to past and present members of the Fushman Lab: Adithya, Alex, Andrew, Andrew, Anja, Apurva, Carlos, Daoning, Donald, Dulith, Emma, Karina, Konstantin, Ming-Yih, Rajesh, Raquel, Shirley, Tanuja, and Tony, who helped me make first steps in the field of biochemistry and were always there to give me support and advice. In addition, I would like to thank Daoning for his involvement in the Ddi1 project, Shirley for helping me with cloning of Ubp6UBL. Carlos for providing me with Ub<sub>2</sub> samples for DUB assays and UbG75C, Emma for providing me with Ub<sub>2</sub> samples for DUB assays, Anja for providing Ub<sub>2</sub> for binding studies and Rajesh for UBQLN1 UBA sample.

I thank my fellow Biochemistry friends: Poorni and Katie and all the other friends I have made throughout the years in the department.

This work was funded by the National Institutes of Health Grants GM095755, US-Israel Binational Foundation grant and by Graduate Summer Research Fellowship from University of Maryland.

# Table of Contents

Dedication.....	ii
Acknowledgements .....	iii
Table of Contents .....	v
List of Tables .....	viii
List of Figures.....	ix
List of Abbreviations.....	xiii
Chapter 1. Introduction and specific aims .....	1
1.1 The ubiquitin proteasome system .....	1
1.2 Ubiquitin and ubiquitination .....	4
1.3 E1, E2, E3 enzymes .....	11
1.3.1 Hierarchical system of ubiquitination enzymes specificity.....	11
1.3.2 SCF <sup>Uf<sub>0</sub>1</sup> - E3 ligase enzymes .....	12
1.4 DNA Damage Inducible protein, Ddi1 .....	14
1.4.1 UBL-UBA protein Ddi1 and its evolution .....	14
1.4.2 Putative function of Ddi1 UBL and UBA domains.....	19
1.5 Research motivation and specific aims.....	21
Chapter 2. Structural studies of Ddi1UBL .....	24
2.1 Ddi1 domains can be studied independently .....	24
2.2 Sequential assignment.....	27
2.3 Structural constraints .....	29
2.3.1 NOE constraints.....	29
2.3.2 Dihedral angle constraints .....	31
2.3.3 Secondary structure prediction .....	32
2.3.4 Hydrogen bonds.....	35
2.3.5 Residual dipolar couplings .....	39
2.4 Structure calculations .....	40
2.5 Ddi1UBL structure.....	40
2.6 Ddi1UBL vs. Ubiquitin structure comparison .....	43
2.7 Dynamic properties of Ddi1UBL.....	48

2.8 Oligomeric state of Ddi1UBL .....	50
Chapter 3. Ddi1- novel ubiquitin receptor.....	53
3.1 Ddi1 as a multidomain protein.....	53
3.2 Ddi1 interacts with ubiquitin not only through the UBA domain.....	57
3.3 Ddi1UBL interacts with ubiquitin .....	58
3.4 Ubiquitin interacts with Ddi1UBL through the hydrophobic-patch residues ...	62
3.5 Ddi1 UBL pulls out ubiquitin conjugates from cell extract.....	66
3.6 Ub interacts with UBL domain of Ddi1 but not of Dsk2 or Rad23 .....	67
3.7 Structure of the Ub:Ddi1UBL complex .....	68
3.8 Ufo1UIMs interact with ubiquitin but not with Ddi1 .....	75
3.9 Ddi1UBL and Ub:Ddi1UBL complex crystallization .....	81
Chapter 4. Ddi1UBL, first known ubiquitin like domain with a UIM motif .....	83
4.1 Ddi1 heterodimerization with other shuttle proteins.....	83
4.2 Dsk2UBL binding to Ddi1UBL.....	90
4.3 Ddi1UBL has an additional binding site for Dsk2UBL.....	92
4.4 Ddi1UBL differentiates between different linkages of Ub <sub>2</sub> .....	97
4.5 Ddi1UBL has UIM-like motif sequence in its $\alpha$ -helix.....	102
4.6 Ddi1UBL mutants with altered UIM-like motif sequence.....	103
4.7 Effects of mutations on binding to Ub, Dsk2UBL, K48-Ub <sub>2</sub> and K63-Ub <sub>2</sub> ... ..	109
Chapter 5. UBL domain of Ubp6, purification and NMR data collection .....	121
5.1 Ubp6 construct design.....	121
5.2 Protein purification .....	122
5.3 Ubp6UBL NMR data collection for resonance assignment .....	124
5.4 Ubp6UBL has more than one conformation? .....	124
Chapter 6. Discussion and future project direction .....	129
6.1 Discussion .....	129
6.2 Future project direction .....	134
Chapter 7. Materials and methods .....	137
7.1 Proteins constructs and purifications .....	137
7.2 Sequence analysis .....	138
7.3 NMR experiments .....	138

7.4	NMR binding assays .....	139
7.5	HD exchange experiments .....	139
7.6	PRE experiments for complex structure calculations .....	140
7.7	Ddi1FL DUB activity assay.....	141
7.8	Sedimentation equilibrium.....	141
7.9	Mass spectrometry .....	142
7.10	Circular dichroism .....	142
	References .....	143

## List of Tables

Table 2-A. Summary of resonance assignments obtained from triple resonance experiments.....	28
Table 2-B. NMR unique NOE distance statistics for Ddi1UBL structure. ....	30
Table 2-C. Ddi1UBL sequence in TALOS+ .....	32
Table 2-D. NMR refinement statistics for Ddi1UBL structures .....	42
Table 3-A. Active and passive residues used for docking of Ub-Ddi1UBL complexes	69
Table 3-B. Distance constraints for Ub:Ddi1UBL complex based on MTS defense studies ...	70

# List of Figures

Figure 1-1. Ubiquitin proteasome system regulates majority of cellular events .....	1
Figure 1-2. Mono-/multi-/poly-ubiquitination schemes .....	2
Figure 1-3. Delivery of polyubiquitinated proteins for proteasomal degradation.....	3
Figure 1-4. Schematic representation of the gene structure of <i>S.cerevisiae</i> shuttle proteins: Ddi1, Rad23, and Dsk2 .....	4
Figure 1-5. Ribbon representation of Ub structure.....	5
Figure 1-6. Isopeptide bond between Ub and substrate/Ub .....	6
Figure 1-7. Ubiquitination pathway .....	7
Figure 1-8. Structure comparison of K48-Ub <sub>2</sub> and K63-Ub <sub>2</sub> .....	9
Figure 1-9. Different binding modes of UBA2 and Ub <sub>2</sub> chains .....	10
Figure 1-10. Hierarchical scheme of the enzymes involved in ubiquitination.....	12
Figure 1-11. Scheme architecture of the SCF E3 ligase with Ufo1 as F-box protein ....	13
Figure 1-12. Schematic representation of the Ddi1 gene structure from <i>S.cerevisiae</i> ...	14
Figure 1-13. Sequence alignments of the Ddi1UBL domain with Ub (yeast and human homolog), Rad23UBL and Dsk2UBL .....	15
Figure 1-14. Individual sequence comparison of Ddi1UBA domain with UBA domains of Rad23 and Dsk2 .....	16
Figure 1-15. Sequence alignment of the Ddi1UBA and Ddi1UBL with the UBA and UBL domains of other shuttle proteins (Dsk2 and Rad23) .....	17
Figure 1-16. Ddi1 gene structure among different eukaryotes .....	18
Figure 2-1. <sup>1</sup> H- <sup>15</sup> N TROSY spectra of the full length Ddi1 .....	25
Figure 2-2. Comparison of <sup>15</sup> N T1 relaxation rates for the Ddi1UBL and UBL domain of Ddi1FL .....	26
Figure 2-3. Prediction of secondary structures and order parameters for Ddi1UBL ....	34
Figure 2-4. Changes in the spectrum of Ddi1UBL upon HD exchange.....	36
Figure 2-5. Ddi1UBL peaks attenuations in the HD exchange experiment .....	37
Figure 2-6. Structure of Ddi1UBL .....	41
Figure 2-7. Ddi1UBL structure evaluation based on RDC .....	42

Figure 2-8. Comparison of Ddi1UBL and Ub.....	44
Figure 2-9. Ddi1UBL and Ub structure packing.....	44
Figure 2-10. Ddi1UBL and Ub structure comparison.....	46
Figure 2-11. Electrostatic potential of the surface of Ub and the UBL domains from shuttle proteins: Ddi1, Rad23, and Dsk2.....	47
Figure 2-12. Comparison of the <sup>15</sup> N relaxation data in Ddi1UBL and Ub.....	49
Figure 2-13. Sedimentation equilibrium analysis of Ddi1UBL .....	51
Figure 2-14. ESI-MS spectrum of DdiUBL .....	52
Figure 3-1. Heteronuclear NOE spectrum of full length Ddi1 .....	54
Figure 3-2. Time resolved deubiquitinating enzyme (DUB) activity assay, testing for Ddi1 protease activity against K6-, K11-, K27-, K29-, K33-, K48- and K63-Ub <sub>2</sub> s .....	55
Figure 3-3. Model structure of Ddi1FL .....	56
Figure 3-4. Ddi1FL binding to Ub .....	58
Figure 3-5. Ub binding to Ddi1UBL .....	59
Figure 3-6. Amide chemical shift differences in Ddi1UBL upon Ub binding .....	60
Figure 3-7. Putative Ub-binding site on Ddi1UBL .....	61
Figure 3-8. Titration curves for Ub binding to Ddi1UBL .....	62
Figure 3-9. Titration spectra of <sup>15</sup> N-Ub with Ddi1UBL .....	63
Figure 3-10. CSP between free Ub and Ub upon saturation with Ddi1UBL .....	64
Figure 3-11. Putative binding side for Ub on Ddi1UBL structure .....	65
Figure 3-12. Representative titration curves for <sup>15</sup> N-Ub binding to Ddi1UBL .....	65
Figure 3-13. <sup>6xHis</sup> Ub Co-immunoprecipitates Ddi1UBL.....	66
Figure 3-14. Ddi1UBL pull out ubiquitin conjugates from cell extract .....	67
Figure 3-15. NMR titration of Ub with the UBL domains from Dsk2 and Rad23 .....	68
Figure 3-16. Haddock derived structure of the Ub:Ddi1UBL complex .....	71
Figure 3-17. Validation of the NMR-derived (HADDOCK) structure of Ub:Ddi1UBL complex using site-specific paramagnetic spin-labeling .....	73
Figure 3-18. Interface between Ddi1UBL and Ub .....	74
Figure 3-19. Side chains contacts at the interface of the Ub:Ddi1UBL complex .....	75
Figure 3-20. Ufo1UIMs binding to Ddi1UBL .....	76

Figure 3-21. Lack of interaction of Ufo1UIM with Ddi1UBL and Ddi1FL .....	77
Figure 3-22. CD spectrum of Ufo1UIM .....	78
Figure 3-23. Ufo1UIMs recognize Ub .....	79
Figure 3-24. Ub recognizes Ufo1UIMs through the hydrophobic patch.....	80
Figure 3-25. Representative titration curves for Ufo1UIMs binding to Ub .....	80
Figure 3-26. Potential crystal hits of Ub:Ddi1UBL complex from the INDEX screening suite.....	82
Figure 4-1. Binding of UBL domains of Dsk2 and Rad23 to full length Ddi1 .....	84
Figure 4-2. Binding of UBL domain of Ddi1UBL to full length Dsk2 and Rad23 .....	86
Figure 4-3. Ddi1UBL binding to Rad23UBL.....	87
Figure 4-4. Ddi1UBL interaction with hDsk2UBA and hRad23UBA2.....	89
Figure 4-5. Interaction of UBL domains from Dsk2 and Ddi1 .....	90
Figure 4-6. Chemical shift perturbations of Ddi1UBL binding to Dsk2UBL.....	91
Figure 4-7. Putative Ddi1UBL binding site on the surface of Dsk2UBL .....	92
Figure 4-8. Dsk2UBL binding to Ddi1UBL.....	93
Figure 4-9. Chemical shift perturbations upon Dsk2UBL binding to <sup>15</sup> N-Ddi1UBL ....	94
Figure 4-10. Putative Dsk2UBL binding site on the surface of Ddi1UBL .....	95
Figure 4-11. Competition assay between Ub, Ddi1UBL and Dsk2UBL .....	96
Figure 4-12. Comparison of K48-Ub <sub>2</sub> and K63-Ub <sub>2</sub> binding to Ddi1UBL .....	98
Figure 4-13. Ddi1UBL differentiates between K48-Ub <sub>2</sub> and K63-Ub <sub>2</sub> . ....	100
Figure 4-14. CSP between free Ddi1UBL and Ddi1UBL bound to K48-Ub <sub>2</sub> and K63-Ub <sub>2</sub> at equal molar ratio.....	101
Figure 4-15. Sequence alignment of the $\alpha$ -helix amino acids of Ddi1UBL and $\alpha$ -helix sequence in Ub, Dks2UBL and Rad23UBL.....	102
Figure 4-16. Sequence alignment of the $\alpha$ -helix amino acids of Ddi1UBL and other known UIM motif sequences.....	103
Figure 4-17. Ddi1UBL mutants design .....	104
Figure 4-18. <sup>1</sup> H- <sup>15</sup> N SOFAST-HMQC spectra of Ddi1UBL_WT and its mutants.....	105
Figure 4-19. Overlay of the spectra of Ddi1UBL_WT, Ddi1UBL_S and Ddi1UBL_SK .....	106
Figure 4-20. Spectra of Ddi1UBL_KSK mutant.....	108

Figure 4-21. Ddi1UBL_SK and Ddi1UBL_KSK binding to mono Ub .....	110
Figure 4-22. Chemical shift perturbations of Ddi1UBL WT and Ddi1UBL_SK binding to Ub.....	111
Figure 4-23. HetNOE spectrum of <sup>15</sup> N-Ddi1UBL_KSK mutant in the presence of Ub .....	112
Figure 4-24. Ddi1UBL mutants binding to Dsk2UBL.....	113
Figure 4-25. Comparison of chemical shift perturbations of Ddi1UBL_WT and Ddi1UBL mutants in the presence of Dsk2UBL.....	115
Figure 4-26. Ddi1UBL_SK binding to K48-Ub <sub>2</sub> and K63-Ub <sub>2</sub> .....	116
Figure 4-27. Comparison of Ddi1UBL_SK binding to Ub, K48-Ub <sub>2</sub> and K63-Ub <sub>2</sub> ...	118
Figure 4-28. CSP between free Ddi1UBL_SK and Ddi1UBL_SK bound to Ub, K48- and K63-Ub <sub>2</sub> .....	119
Figure 4-29. Comparison of Ddi1UBL_SK spectra at bound states with K48-Ub <sub>2</sub> and K63-Ub <sub>2</sub> .....	120
Figure 5-1. Purification of unlabeled sample of Ubp6UBL .....	123
Figure 5-2. <sup>1</sup> H- <sup>15</sup> N-HSQC spectrum of Ubp6UBL in 20mM phosphate buffer, pH=6.8, at 25°C .....	125
Figure 5-3. HetNOE spectrum of Ubp6UBL .....	126
Figure 5-4. <sup>1</sup> H- <sup>15</sup> N SOFAST-HMQC spectra of Ubp6UBL sample collected at low temperature, 17°C and higher temperature 35°C .....	128
Figure 6-1. Ddi1 recognition of ubiquitinated substrates in <i>S.cerevisiae</i> .....	132
Figure 6-2. Schematic representation of a possible function of Ddi1 as a proteasomal shuttle in yeast and humans .....	133
Figure 6-3. Sequence alignment of UBL domain of Ddi1 from <i>S.cerevisiae</i> and from <i>H.sapiens</i> .....	135

## List of Abbreviations

$\mu\text{M}$	micro molar
Ala	alanine
AMP	adenosine monophosphate
APC	anaphase-promoting complex
ARIA	ambiguous constraints for iterative assignment
ATP	adenosine triphosphate
AUC	analytical ultracentrifugation
CARA	computer aided resonance assignment
CD	circular dichroism
CNS	crystallography and NMR system
CSI	chemical shift index
CSP	chemical shifts perturbations
CYM	cysteine residue with MTSL spin label bound
Cys	cysteine
Ddi1	DNA Damage-Inducible 1
DNA	deoxyribonucleic acid
Dsk2	dominant suppressor of Kar2
DUB	deubiquitinase / deubiquitinating enzyme
<i>E. coli</i>	Escherichia coli
ESI-MS	electrospray ionization mass spectrometry
Gly	glycine
h.s.	<i>Homo sapiens</i>
<i>H.sapiens</i>	<i>Homo sapiens</i>
HADDOCK	high ambiguity driven biomolecular docking
HD	hydrogen–deuterium exchange
hetNOE	heteronuclear nuclear Overhauser effect
HMQC	heteronuclear multiple-quantum correlation
Ho	homothallic switching endonuclease
HSQC	heteronuclear single quantum coherence

IB	immunoblot
IPAP-HSQC	in-phase/antiphase heteronuclear single quantum coherence
Kd	dissociation constant
Leu	leucine
	( <i>S</i> -(2,2,5,5-tetramethyl-2,5-dihydro-1H-pyrrol-3-yl)methyl methanesulfonothioate)
MTSL	
NaP	sodium phosphate
NEB	New England biolabs
NMR	nuclear magnetic resonance
NOE	nuclear Overhauser effect
NOESY	nuclear Overhauser effect spectroscopy
PEG	Polyethylene glycol
PRE	paramagnetic relaxation enhancement
Rad23	radiation gene 23
RCI	random coil index
RDC	residual dipolar coupling
RMS	root mean square
RMSD	root-mean-square deviation
rpm	revolutions per minute
Rpn10	regulatory particle non-ATPase 10
Rpn13	regulatory particle non-ATPase 13
RVP	retroviral protease fold domain
s.c.	<i>Saccharomyces cerevisiae</i>
<i>S.cerevisiae</i>	<i>Saccharomyces cerevisiae</i>
SCF	SKP1-CUL1-F-box protein) E3 ubiquitin-protein ligase complex
SOFAST-HMQC	band-selective optimized flip angle short transient HMQC
TALOS	torsion angle likelihood obtained from shift sequence similarity
Thr	threonine
TROSY	transverse relaxation optimized spectroscopy
Ub	ubiquitin
UBA	ubiquitin associated domain

UBC	ubiquitin conjugating enzyme
UBL	ubiquitin like domain
Ubp6	ubiquitin-specific protease-6
UBQLN1	ubiquitin-like protein 1
Ufo1	UV-F-box-HO 1
UIM	ubiquitin-interacting motif
UPS	ubiquitin proteasome system
UV	ultraviolet

# Chapter 1. Introduction and specific aims

## 1.1 The ubiquitin proteasome system

The ubiquitin proteasome system (UPS) is responsible for turnover of short-lived proteins by the 26S proteasome. The UPS mechanism for protein degradation plays a very important role in cellular regulation in eukaryotes, as it influences a variety of essential cellular pathways such as: cell cycle progression, transcription, misfolded proteins degradation, DNA repair, and the immune and stress response (Figure 1-1)<sup>1-11</sup>. Dysfunction of the UPS leads to the failures in cellular pathways, and as a consequence, to number of severe inflammatory diseases, cancer and neurological disorders<sup>6,12-16</sup>.

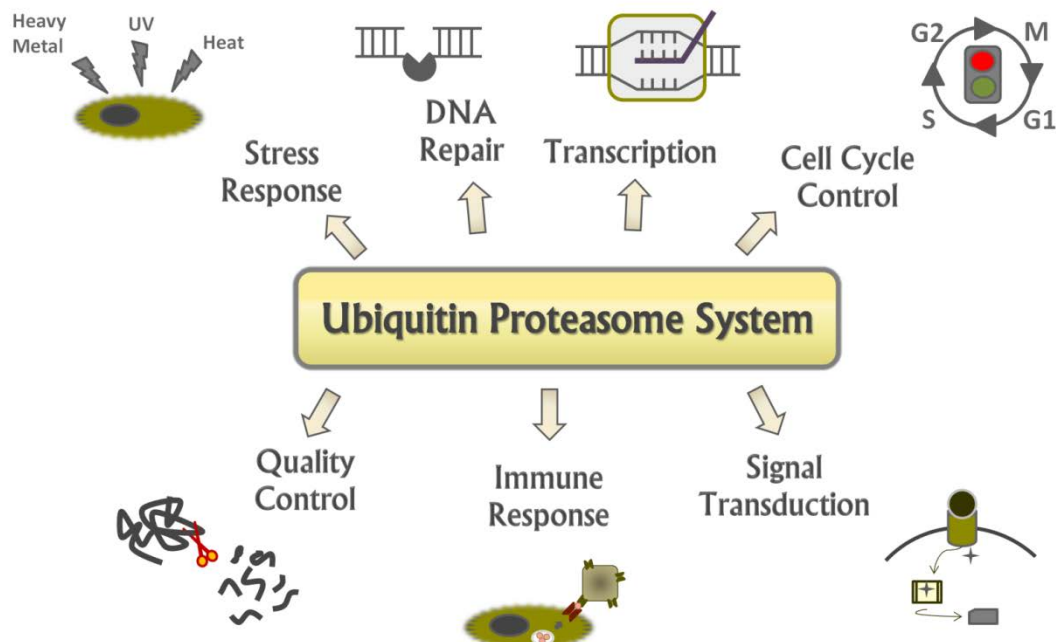


**Figure 1-1.** Ubiquitin proteasome system regulates majority of cellular events.

In the ubiquitin proteasome system, the protein of interest is modified with a signaling protein called ubiquitin (Ub). With the use of three enzymes, E1 (ubiquitin activating enzyme), E2 (ubiquitin conjugating enzyme) and E3 (ubiquitin protein ligase), Ub is attached to the target protein of interest. Depending on the final signaling pathway, the ubiquitinated protein can be mono-, multi- or polyubiquitinated (Figure 1-2).

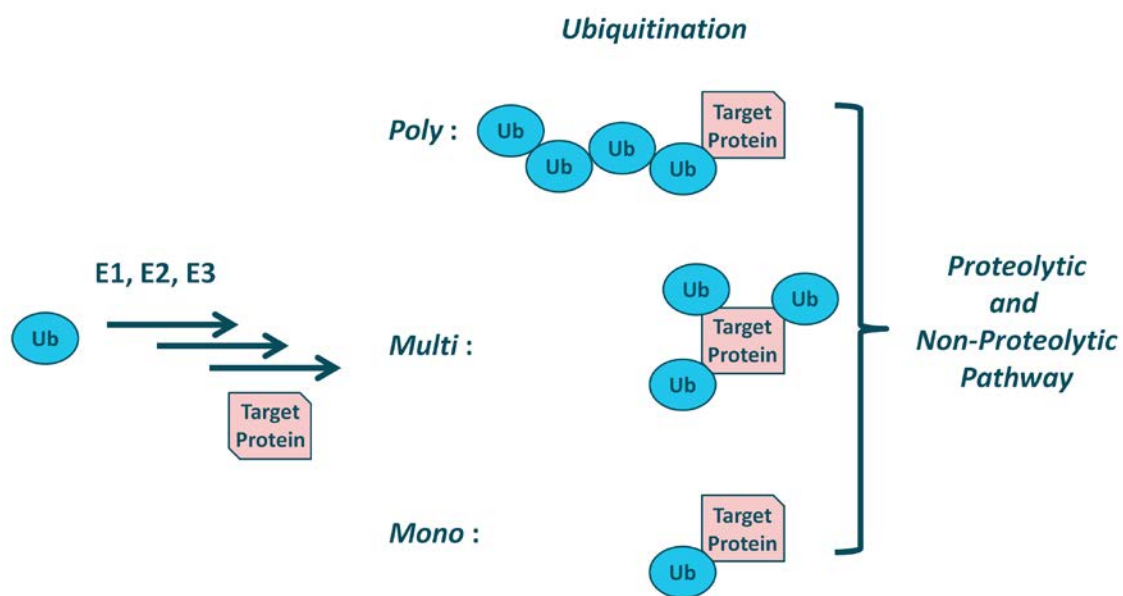


**Figure 1-2. Mono-/multi-/poly-ubiquitination schemes. In Eukaryotes, the mode of ubiquitination influences which signaling pathway target protein are delivered to.**

In *S.cerevisiae*, target proteins that are polyubiquitinated for 26S proteasomal degradation are either directly recognized by the intrinsic receptors: Rpn10 and Rpn13, that are part of 19S proteasomal subunit, or by the shuttle proteins: Rad23, Dsk2 and Ddi1, and subsequently driven to the proteasome (Figure 1-3)<sup>17-27</sup>. Ubiquitinated

substrates can be recognized by just one or both of the pathways simultaneously, which is supported by the discovery that the function of Ub receptors is redundant, and only concurrent deletion of two or more cause accumulation of ubiquitinated proteins<sup>26,28-31</sup>.

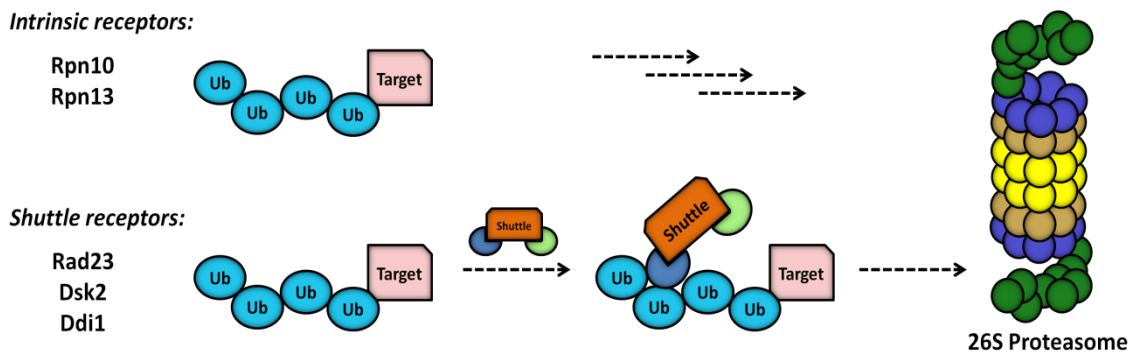


**Figure 1-3. Delivery of polyubiquitinated proteins for proteasomal degradation.** Target proteins can be directly recognized by the proteasome (Rpn10, Rpn13) or by shuttle proteins (Rad23, Dsk2, Ddi1) that will deliver target proteins to the 26S proteasome by binding to it.

Shuttle proteins such as Rad23, Dsk2, and Ddi1 are a group of proteins that have a Ubiquitin Like Domain (UBL) on their N-terminus and Ubiquitin Association Domain (UBA) on the C-terminus. Ddi1 and Dsk2 have just one UBA domain while Rad23 has two, a UBA1 that follows the UBL domain and a UBA2 domain at the C-terminal end (Figure 1-4). It has been hypothesized that UBL-UBA proteins perform their shuttle function by utilizing their UBL domains to interact with the proteasome, and their UBA domain to interact with Ub moieties of ubiquitinated proteins<sup>30,32-35</sup>.

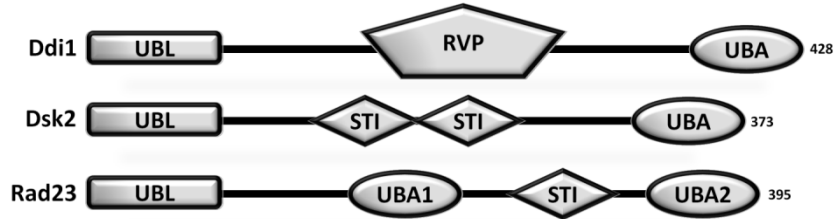


**Figure 1-4. Schematic representation of the gene structure of *S.cerevisiae* shuttle proteins: Ddi1, Rad23, and Dsk2. Abbreviation annotation: UBL, Ubiquitin Like Domain; RVP, retroviral protease fold domain; UBA, Ubiquitin Association Domain; STI, stress-inducible-1.**

## 1.2 Ubiquitin and ubiquitination

Ubiquitin is highly conserved among eukaryotic species. It consists of 76 amino acids with molecular mass of 8.5kDa. On the Ub surface there is a hydrophobic patch composed of the side chains from the amino acids L8, I44 and V70 that interact with Ub receptors (Figure 1-5)<sup>36-38</sup>. In the sequence there are also seven conserved lysines: K6, K11, K27, K29, K33, K48, and K63. Also present is a –GG motif (G75,G76) on the C-terminal end that is very important for Ub to perform its function (Figure 1-5).

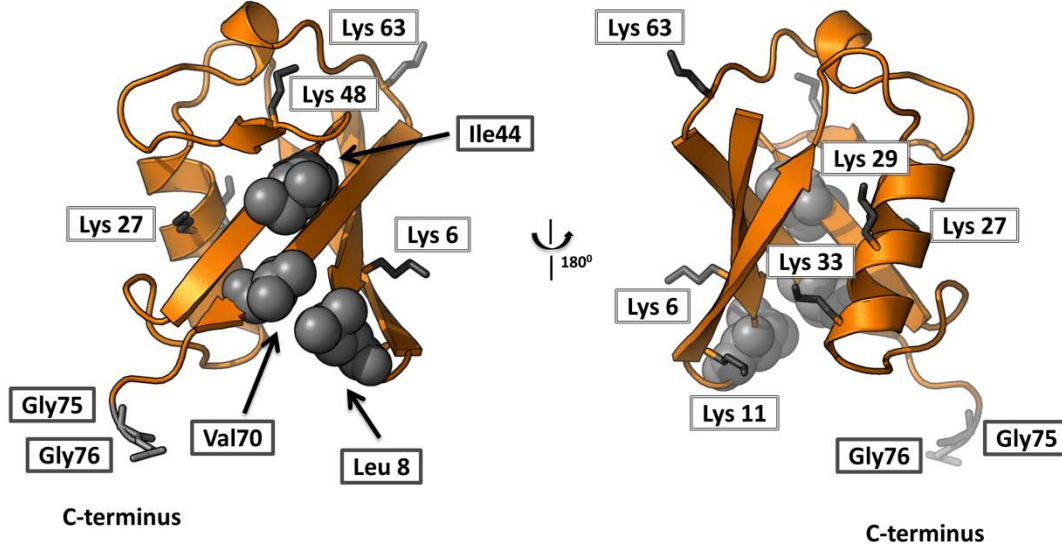


**Figure 1-5. Ribbon representation of Ub structure. Amino acids comprising the hydrophobic patch are shown as grey spheres. All conserved lysines are shown as dark grey sticks. –GG motif is shown as grey sticks. Ub structure was obtained from 1ubq.pdb.**

Upon posttranslational modification, a Ub molecule is covalently attached to the lysine side chain of the substrate protein. The amino group of this side chain forms an isopeptide bond with the carboxylic group of the carboxyl-terminal amino acid (G76) in the Ub molecule (Figure 1-6).

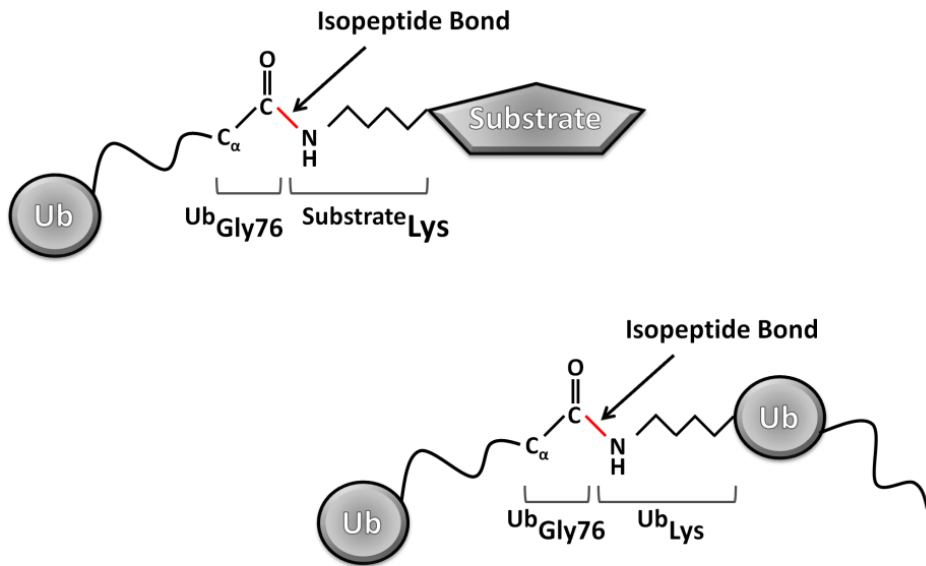


**Figure 1-6. Isopeptide bond between Ub and substrate/Ub.** Isopeptide bond is shown in red. Top figure shows the bond formed between Ub Gly 76 and the amino group of the Lys side chain from the substrate protein. The lower figure shows the isopeptide bond between two Ub molecules.

As mentioned above, ubiquitination is achieved by a cascade of multienzymatic reactions (Figure 1-7), which can be described by the following steps:

- Activation of Ub by the E1 enzyme. E1, with the use of ATP, synthesizes a Ub C-terminal adenylate, which as an enzyme bound substrate is used to form an E1-ubiquitin thiol ester bond.
- Transfer of Ub from E1 to the active site cysteine of an E2 enzyme. E2 enzymes are also called ubiquitin-conjugating (UBCs) or ubiquitin-carrier proteins as they carry the activated ubiquitin from E1 to the substrate.

- Transfer of activated Ub from E2 to a substrate-specific E3 enzyme. E3 is a ubiquitin-protein ligase that binds substrate protein and E2 enzyme. The isopeptide bond between the C-terminal glycine residue of Ub and the lysine residue of the target protein is created.

After this cascade of events the monoubiquitinated protein is created. To form the polyubiquitinated protein, the above steps are repeated, with the only difference being that the lysine of the previously bound Ub is used to create an isopeptide bond with the successive Ub protein.

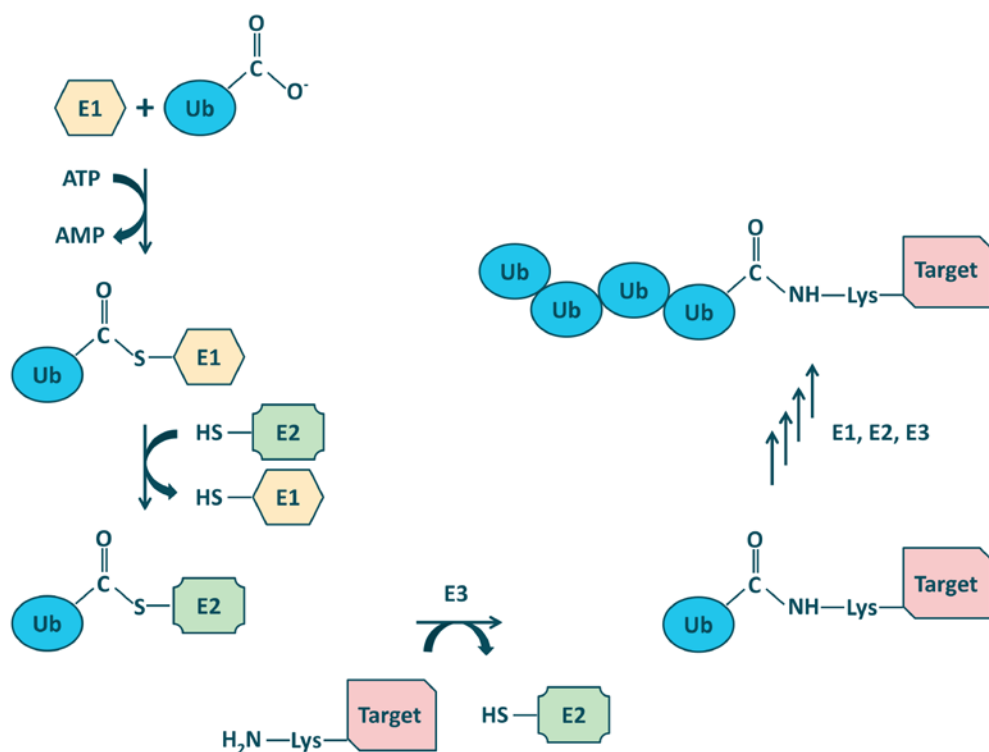


**Figure 1-7. Ubiquitination pathway.** Initially Ub is activated by E1 enzyme and then transferred to E2 enzyme. The specific substrate is recognized by the E3 ligase. In the last step, Ub is covalently linked to a lysine residue of the target protein, where an isopeptide bond is created. The process is repeated if the target protein needs to be polyubiquitinated.

In the case of poly-ubiquitination, Ub molecules are attached through either each of the seven lysines, or the free amino group at the N-terminus, which leads to various linkage chain formations. The Ub unit which has a free C-terminal end is referred to as “proximal”, while the Ub molecule which provides the C-terminus for isopeptide bond formation is called “distal”. It was previously shown that different linkages dictate diverse conformations of polyUb chains and as a result different orientations of the hydrophobic patches<sup>39</sup>.

It was shown that in the structure of K48-linked dimer (K48-Ub<sub>2</sub>) hydrophobic patches of both Ub units are in a closed conformation, indicating that the patches interact with each other to form a hydrophobic interface (Figure1-8)<sup>40</sup>. Meanwhile, the K63-linked dimer (K63-Ub<sub>2</sub>) has an open conformation with both hydrophobic patches fully accessible for ligands (Figure1-8)<sup>41</sup>.

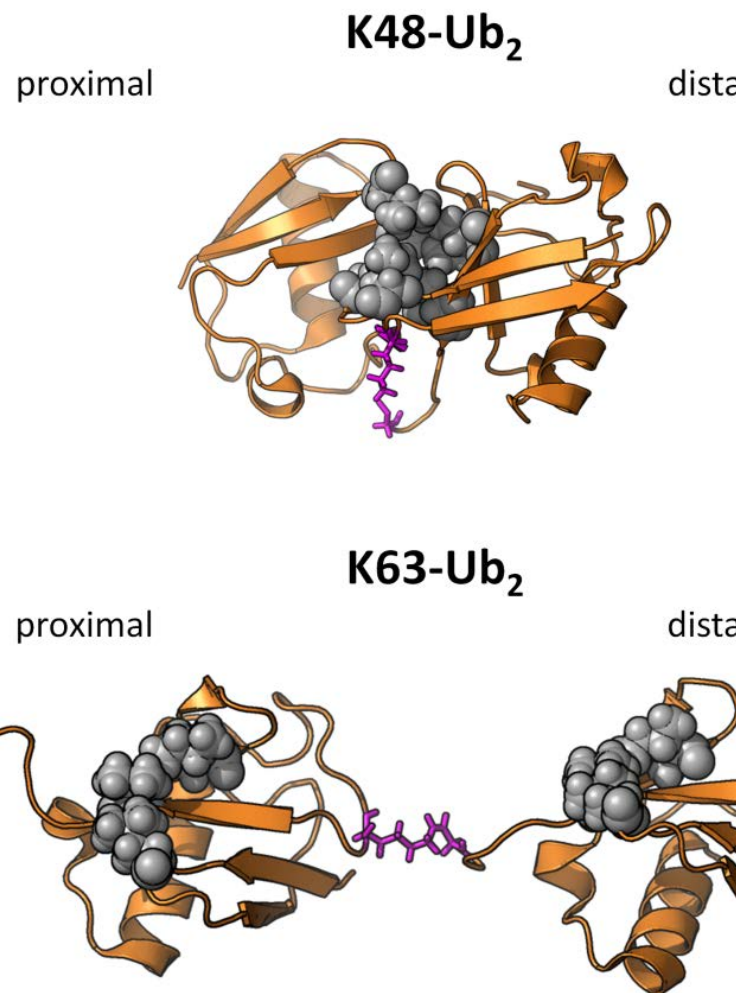


**Figure 1-8. Structure comparison of K48-Ub<sub>2</sub> and K63-Ub<sub>2</sub>.** Each of the chains has a different conformation. Hydrophobic patch for each Ub unit is shown as grey spheres. Isopeptide bond is shown in magenta. K48-Ub<sub>2</sub> structure was obtained from pdb with access number 2BGF, while K63-Ub<sub>2</sub> access number is 2RR9.

Different orientations of hydrophobic patches dictate differences in recognition of Ub receptors. For example, the UBA2 domain of the Rad23 human isoform (hHR23a) binds K48-Ub<sub>2</sub> in a sandwich mode, where UBA2 interacts with both hydrophobic patches simultaneously. In the case of K63-Ub<sub>2</sub> each hydrophobic patch binds one UBA2 domain (Figure 1-9)<sup>41,42</sup>.

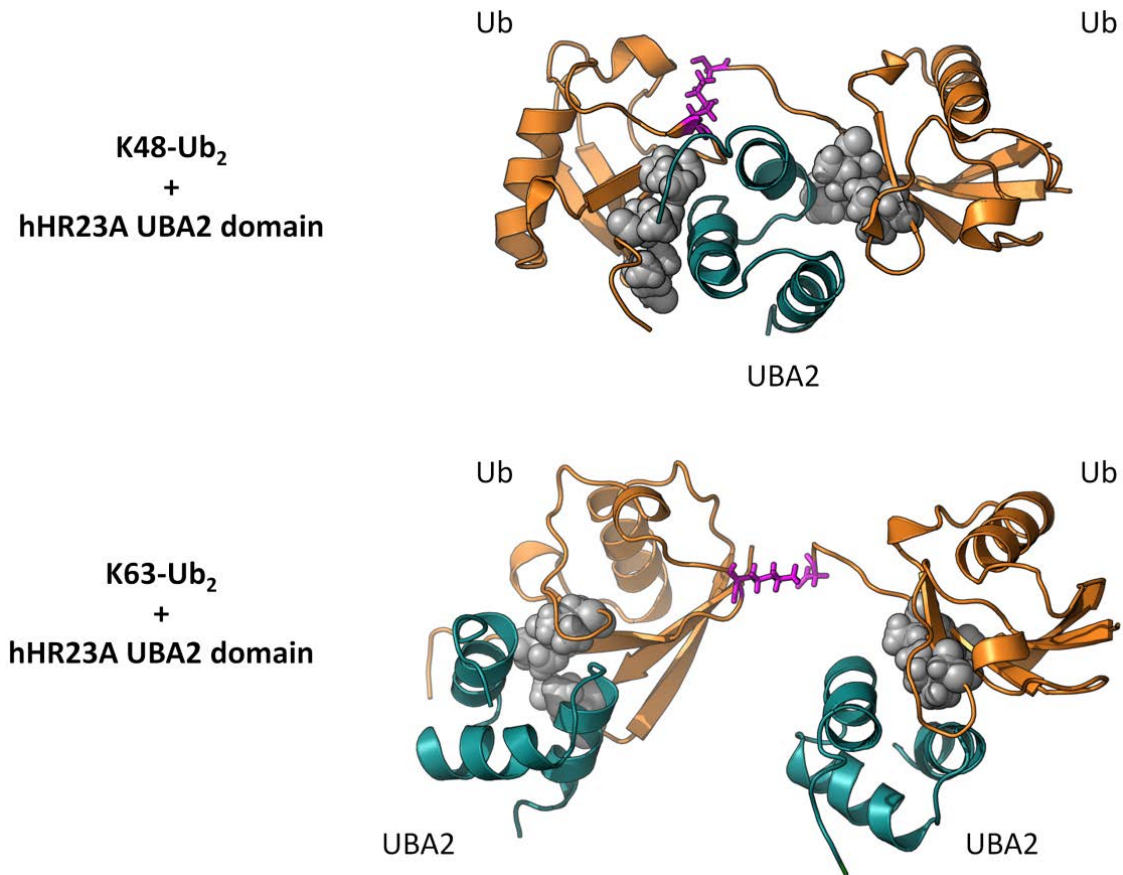


**Figure 1-9. Different binding modes of UBA2 and Ub<sub>2</sub> chains. UBA2 (dark cyan) domain from hHR23A receptor. K48-Ub<sub>2</sub> (orange, top panel) binds one UBA2 domain in sandwich like mode (1ZO6) and K63-Ub<sub>2</sub> (orange, bottom panel) binds two UBA2 domains (source R.Varadan/D.Fushman). The hydrophobic patches are shown as gray spheres; isopeptide bond is shown in magenta.**

Dissimilarity in the type of linkage also dictates to which signaling pathway the ubiquitinated protein will be targeted. It was shown that polyubiquitin chains linked through K48 and K11 are responsible for targeting proteins for proteasomal degradation, while polyUb which are linked through K63 are involved in DNA repair<sup>10,43-51</sup>.

## **1.3 E1, E2, E3 enzymes**

### **1.3.1 Hierarchical system of ubiquitination enzymes specificity**

The possibility of creating polyUb chains through different lysine residues is strongly related to the type and role of the target protein. A hierarchical system can be proposed to explain the substrate specificity of particular enzymes involved in the ubiquitination process (Figure 1-10).

A single E1 enzyme activates Ub, which is transferred to several E2 enzymes. E2 can then transfer Ub to a particular E3 or to a subclass of numerous E3 enzymes. E3 is responsible for the target protein selection and specificity. It can be dedicated just to one substrate or to a subset of substrates which present similar structural motifs<sup>52</sup>.

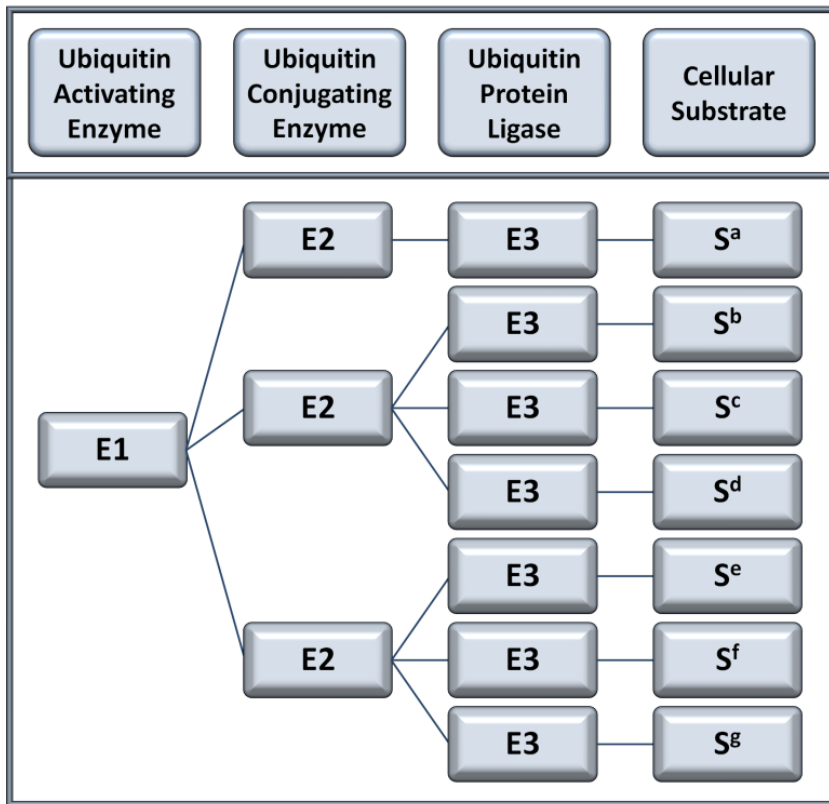


**Figure 1-10. Hierarchical scheme of the enzymes involved in ubiquitination. E1 enzyme activates ubiquitin for all E2 enzymes and E3s. E2 enzymes are E3 specific, whereas E3s are substrate specific.**

### 1.3.2 SCF<sup>Ufo1</sup> - E3 ligase enzymes

A few families of E3 ubiquitin-ligase enzymes have been characterized. One is the SCFs (Skp1-Cdc53/Cull-F-box protein), a class of E3 ligase proteins involved in cell cycle regulation. SCFs are comprised of common subunits as well as individual proteins that define substrate specificity<sup>52</sup>. In the SCF complex, the C-terminal domain of Cdc53/Cul1 binds the Rbx1 protein that interacts with the E2 enzyme. The N-terminus of Cdc53/Cul1 harbors the F-box protein and Skp1 adaptor (Figure 1-11). The

Skp1 adaptor is responsible for F-box protein recognition and binding, while F-box proteins define substrate specificity, and by binding to Skp1, they bring the substrate and E2 enzyme into close proximity<sup>53</sup>.

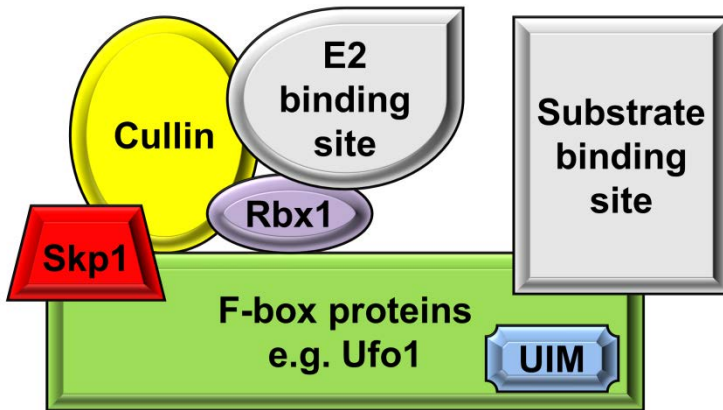


**Figure 1-11. Scheme architecture of the SCF E3 ligase with Ufo1 as F-box protein.**

F-box proteins are a group of proteins that mediate protein-protein interactions. Ufo1 is an unusual F-box protein among the SCF complex because it not only has a protein-protein interaction domain but also contains three copies of the ubiquitin-interacting motif (UIM). UIM is a motif that has a series of hydrophobic residues LALAL or LAMAL, which are terminated by the conserved Ser amino acid. Transcription of Ufo1 begins in response to DNA damage<sup>54,55</sup>. Ufo1 as well as other F-box proteins are short-lived proteins that undergo ubiquitination. Molecular biology studies propose that there is a specific interaction between the Ddi1 UBL domain, and Ufo1 UIM<sup>56</sup>. Moreover, this interaction seems to be essential for the turnover of the SCF<sup>Ufo1</sup> complex (SCF complex with Ufo1 as a F-box protein) and plays a role in cell cycle progression.

## 1.4 DNA Damage Inducible protein, Ddi1

### 1.4.1 UBL-UBA protein Ddi1 and its evolution

The Ddi1 (DNA Damage-Inducible 1) protein was first discovered in 1997 and was characterized as a gene whose transcription was induced in response to a variety of stress factors in yeast<sup>57</sup>. The composition of the shuttle protein Ddi1 from *S.cerevisiae* is unusual. In addition to a UBL and a UBA domain, between these domains it contains a conserved retroviral protease fold domain (RVP), followed by a putative PEST region and Sso1-binding domains (Sso1-BD) (Figure 1-12)<sup>58,59</sup>.



**Figure 1-12. Schematic representation of the Ddi1 gene structure from *S.cerevisiae*.**

The N-terminal UBL domain of Ddi1 (Ddi1UBL) has 19.8% and 11.0% sequence identity with Rad23 and Dsk2, respectively. The sequence identity with yeast Ub homolog is only 18.4% (19.5% for human Ub), compared to 23% sequence identity for the UBL domain of Rad23 (Figure 1-13).

Ddi1UBL	1 MDLTISNELTGEIYGPPIEVSEDMALTDLIALLOADCGFDKTKHDLYYNMD	50
Ub_Yeast	1 M <del>Q</del> I <del>F</del> VKT-LTGKTI-TLEVESSDTIDNVKS <del>K</del> I <del>Q</del> DKEGIPPD <del>Q</del> R <del>L</del> I <del>F</del> AGK	48
Ddi1UBL	51 ILDSNRTQSLKELGLKTDD---LLLIRGKISNS	80
Ub_Yeast	49 QLEDGRT--LSDYNIQKESTLHLVRLRGG	76
Ddi1UBL	1 MDLTISNELTGEIYGPPIEVSEDMALTDLIALI <del>Q</del> ADC <del>G</del> FDKTKHDLYYNMD	50
Ub_Human	1 M <del>Q</del> I <del>F</del> VKT-LTGKTI-TLEVEPSDTIENVKAKI <del>Q</del> DKEGIPPD <del>Q</del> R <del>L</del> I <del>F</del> AGK	48
Ddi1UBL	51 ILDSNRTQSLKELGLKTDD---LLLIRGKISNS	80
Ub_Human	49 QLEDGRT--LSDYNIQKESTLHLVRLRGG	76
Ddi1UBL	1 MDLTISNELTGEIYGPPIEVSEDMALTDLIALI <del>Q</del> ADC <del>G</del> FDKTKHDLYNM	49
Rad23UBL	1 M <del>V</del> S <del>L</del> T <del>F</del> KNF <del>K</del> KEKV--PLDLEPSNTILETKTKLAQSISCEESQIKL <del>I</del> YSG	48
Ddi1UBL	50 DILDSNRTQSLKELGLKTDD--LLLIRGKISNS	80
Rad23UBL	49 KVLQDSKTVS--ECGLKDGDQVVFMVSQKKS	77
Ddi1UBL	1 MDLTISNELTGEIYGPPIEVSEDMALTDLIALI <del>Q</del> ADC <del>G</del> FDKTKHDLYYNMD	50
Dsk2UBL	1 M <del>S</del> L <del>N</del> -----I <del>H</del> I <del>K</del> S <del>G</del> DK-----W <del>E</del> V <del>N</del>	17
Ddi1UBL	51 ILDSNRTQSLKELGLKTDD-----LLIRGKISNS	80
Dsk2UBL	18 V <del>A</del> P <del>E</del> S <del>T</del> V <del>L</del> Q <del>F</del> K <del>E</del> A <del>I</del> N <del>K</del> A <del>G</del> I <del>P</del> V <del>A</del> N <del>Q</del> R <del>L</del> I <del>Y</del> S <del>G</del> K <del>I</del> L <del>K</del> DDQ <del>T</del> V <del>E</del> S <del>Y</del> H <del>I</del> Q <del>D</del> G <del>H</del> S	67
Ddi1UBL	84	80
Dsk2UBL	68 VHLVKSQPK	76

**Figure 1-13. Sequence alignments of the Ddi1UBL domain with Ub (yeast and human homolog), Rad23UBL and Dsk2UBL. Lines (dark grey shading) indicate identity; colons (grey shading) indicate similarity in the sequence and dots indicate small similarity. The EMBOSS program was used to align the sequences<sup>60</sup>.**

The C-terminal UBA domain of Ddi1 (Ddi1UBA) has 29.3% sequence identity with the Rad23 UBA1 domain, 39.5% sequence identity with the Rad23 UBA2 domain and 29.8% sequence identity with the Dsk2 UBA domain (Figure 1-14).

Ddi1_UBA	1 TFP <span style="background-color: black; color: black;">E</span> QTI <span style="background-color: black; color: black;">K</span> QI <span style="background-color: black; color: black;">L</span> M <span style="background-color: black; color: black;">D</span> L <span style="background-color: black; color: black;">G</span> F <span style="background-color: black; color: black;">P</span> RDAV <span style="background-color: black; color: black;">V</span> K <span style="background-color: black; color: black;">A</span> L <span style="background-color: black; color: black;">K</span> Q <span style="background-color: black; color: black;">T</span> N <span style="background-color: black; color: black;">G</span> N <span style="background-color: black; color: black;">A</span> E <span style="background-color: black; color: black;">F</span> A <span style="background-color: black; color: black;">A</span> S <span style="background-color: black; color: black;">S</span> L <span style="background-color: black; color: black;">I</span> F <span style="background-color: black; color: black;">Q</span>	40
Rad23_UBA1	1 T <span style="background-color: black; color: black;">E</span> RNET <span style="background-color: black; color: black;">E</span> T <span style="background-color: black; color: black;">I</span> R <span style="background-color: black; color: black;">I</span> M <span style="background-color: black; color: black;">E</span> M <span style="background-color: black; color: black;">G</span> Y <span style="background-color: black; color: black;">Q</span> R <span style="background-color: black; color: black;">E</span> E <span style="background-color: black; color: black;">V</span> E <span style="background-color: black; color: black;">R</span> A <span style="background-color: black; color: black;">A</span> F <span style="background-color: black; color: black;">N</span> N <span style="background-color: black; color: black;">P</span> D <span style="background-color: black; color: black;">R</span> A <span style="background-color: black; color: black;">A</span> V <span style="background-color: black; color: black;">E</span> Y <span style="background-color: black; color: black;">Y</span> LL <span style="background-color: black; color: black;">M</span> G	41
<hr/>		
Ddi1_UBA	1 T <span style="background-color: black; color: black;">F</span> P <span style="background-color: black; color: black;">P</span> -- <span style="background-color: black; color: black;">Q</span> T <span style="background-color: black; color: black;">I</span> K <span style="background-color: black; color: black;">Q</span> I <span style="background-color: black; color: black;">L</span> M <span style="background-color: black; color: black;">D</span> L <span style="background-color: black; color: black;">G</span> F <span style="background-color: black; color: black;">P</span> RDAV <span style="background-color: black; color: black;">V</span> K <span style="background-color: black; color: black;">A</span> L <span style="background-color: black; color: black;">K</span> Q <span style="background-color: black; color: black;">T</span> N <span style="background-color: black; color: black;">G</span> N <span style="background-color: black; color: black;">A</span> E <span style="background-color: black; color: black;">F</span> A <span style="background-color: black; color: black;">A</span> S <span style="background-color: black; color: black;">S</span> L <span style="background-color: black; color: black;">I</span> F <span style="background-color: black; color: black;">Q</span>	40
Rad23_UBA2	1 P <span style="background-color: black; color: black;">E</span> D <span style="background-color: black; color: black;">D</span> O <span style="background-color: black; color: black;">A</span> I <span style="background-color: black; color: black;">S</span> R <span style="background-color: black; color: black;">I</span> C <span style="background-color: black; color: black;">E</span> L <span style="background-color: black; color: black;">G</span> F <span style="background-color: black; color: black;">E</span> R <span style="background-color: black; color: black;">D</span> L <span style="background-color: black; color: black;">V</span> I <span style="background-color: black; color: black;">Q</span> V <span style="background-color: black; color: black;">Y</span> F <span style="background-color: black; color: black;">A</span> C <span style="background-color: black; color: black;">D</span> K <span style="background-color: black; color: black;">N</span> E <span style="background-color: black; color: black;">E</span> A <span style="background-color: black; color: black;">A</span> N <span style="background-color: black; color: black;">I</span> L <span style="background-color: black; color: black;">F</span> S <span style="background-color: black; color: black;">D</span>	41
<hr/>		
Ddi1_UBA	1 T <span style="background-color: black; color: black;">F</span> P <span style="background-color: black; color: black;">P</span> -- <span style="background-color: black; color: black;">Q</span> T <span style="background-color: black; color: black;">I</span> K <span style="background-color: black; color: black;">Q</span> I <span style="background-color: black; color: black;">L</span> M <span style="background-color: black; color: black;">D</span> L <span style="background-color: black; color: black;">G</span> F <span style="background-color: black; color: black;">P</span> RDAV <span style="background-color: black; color: black;">V</span> K <span style="background-color: black; color: black;">A</span> L <span style="background-color: black; color: black;">K</span> Q <span style="background-color: black; color: black;">T</span> N <span style="background-color: black; color: black;">G</span> N <span style="background-color: black; color: black;">A</span> E <span style="background-color: black; color: black;">F</span> A <span style="background-color: black; color: black;">A</span> S <span style="background-color: black; color: black;">S</span> L <span style="background-color: black; color: black;">I</span> F <span style="background-color: black; color: black;">Q</span>	40
Dsk2_UBA	1 P <span style="background-color: black; color: black;">P</span> E <span style="background-color: black; color: black;">E</span> R <span style="background-color: black; color: black;">Y</span> E <span style="background-color: black; color: black;">H</span> Q <span style="background-color: black; color: black;">L</span> R <span style="background-color: black; color: black;">Q</span> I <span style="background-color: black; color: black;">N</span> D <span style="background-color: black; color: black;">M</span> G <span style="background-color: black; color: black;">F</span> F <span style="background-color: black; color: black;">D</span> F <span style="background-color: black; color: black;">D</span> R <span style="background-color: black; color: black;">N</span> V <span style="background-color: black; color: black;">A</span> A <span style="background-color: black; color: black;">L</span> R <span style="background-color: black; color: black;">R</span> S <span style="background-color: black; color: black;">G</span> G <span style="background-color: black; color: black;">S</span> V <span style="background-color: black; color: black;">Q</span> G <span style="background-color: black; color: black;">A</span> L <span style="background-color: black; color: black;">D</span> S <span style="background-color: black; color: black;">I</span> L <span style="background-color: black; color: black;">N</span> G	45

**Figure 1-14. Individual sequence comparison of Ddi1UBA domain with UBA domains of Rad23 and Dsk2. Lines (dark grey shading) indicate identity; colons (grey shading) indicate similarity in the sequence and dots indicate small similarity. The EMBOSS program was used to align the sequences<sup>60</sup>.**

Sequence alignment of the UBL domains and Ub with each other, as well as alignment of the UBA domains, indicates conserved residues (Figure 1-15). In the case of the UBL domain of Ddi1, these residues are: Leu45, Leu52 and Thr57. For UBA domain, these are: Gly402, Ala422, and Leu426 (residue numbering is with respect to the full length Ddi1 sequence).

Interestingly the analysis of Ddi1 gene conservation among different species shows that, with just one exception, the UBL domain is always present in the Ddi1 sequence, while the UBA domain is not present in mammals (Figure 1-16).

```

Ddi1UBA      ---TFPEQTIKQLMDLGFPF-DAVVKALKQTNQNAEFAASLLFQ-
Dsk2UBA      PPEERYEHQLRQLNDMGMFFDFDRNVAALRRSGGSVQGALDSLLNG
Rad23UBA1    ---TERNETIERIMEMGYQR-EEVERALRAAFNNPDRAVEYLLMG
Rad23UBA2    ---PEDDQAISRLCELGFER-DLVIQVYFACDKNEEAANILFSD

```

```

Ddi1UBL      -MDLTISNELTGEIYGPIEVSEDMALTDLIALLQADCGFDKTHDLYNNMDIIDSNRTQSLKELGLKTDDLLLIRGKISNS
Dsk2UBL      -MSLNIIHI-KSGQDKWEVNVAPESTVLQFKEAINKANGIPVANQRLIYSGKILKDDQTV--SYH1QDGHSVHLVKSQPK-
Rad23UBL     MVSLLTFK--NFKKEKVPLDLEPSNTILETKLAQSISCEESQIKLIYSGKVLQDSKTVS--ECGLKDGDQVVFMSQKKS
Ub Yeast     -MQIFVKT-LTG-KTITLEVESSDTIDNVKSQKIQDKEGIPPDQQRILFAGKQLEDGRTLS--DYNIQKESTLHLVLRRLRGG
Ub Human     -MQIFVKT-LTG-KTITLEVEPSDTIENVKAKIQDKEGIPPDQQRILFAGKQLEDGRTLS--DYNIQKESTLHLVLRRLRGG

```

	yeast Ub	human Ub	Rad23UBL	Dsk2UBL	Sequence Identity	Rad23UBA1	Rad23UBA2	Dks2UBA	Ddi1UBA
Ddi1UBL	18.4%	19.5%	19.8%	11.0%	Sequence Identity	29.3%	39.5%	29.8%	
	39.1%	39.1%	41.9%	20.2%	Sequence Similarity	56.1%	55.8%	46.8%	

**Figure 1-15.** Sequence alignment of the Ddi1UBA and Ddi1UBL with the UBA and UBL domains of other shuttle proteins (Dsk2 and Rad23). Top panel, sequence alignment of the Ddi1UBA domain with Dsk2 and Rad23 UBA domains. Bottom panel, Ddi1UBL alignment with Ub (yeast and human homolog) and Rad23UBL and Dsk2UBL. Dark grey shading indicates identity; grey shading indicates similarity in the sequence.

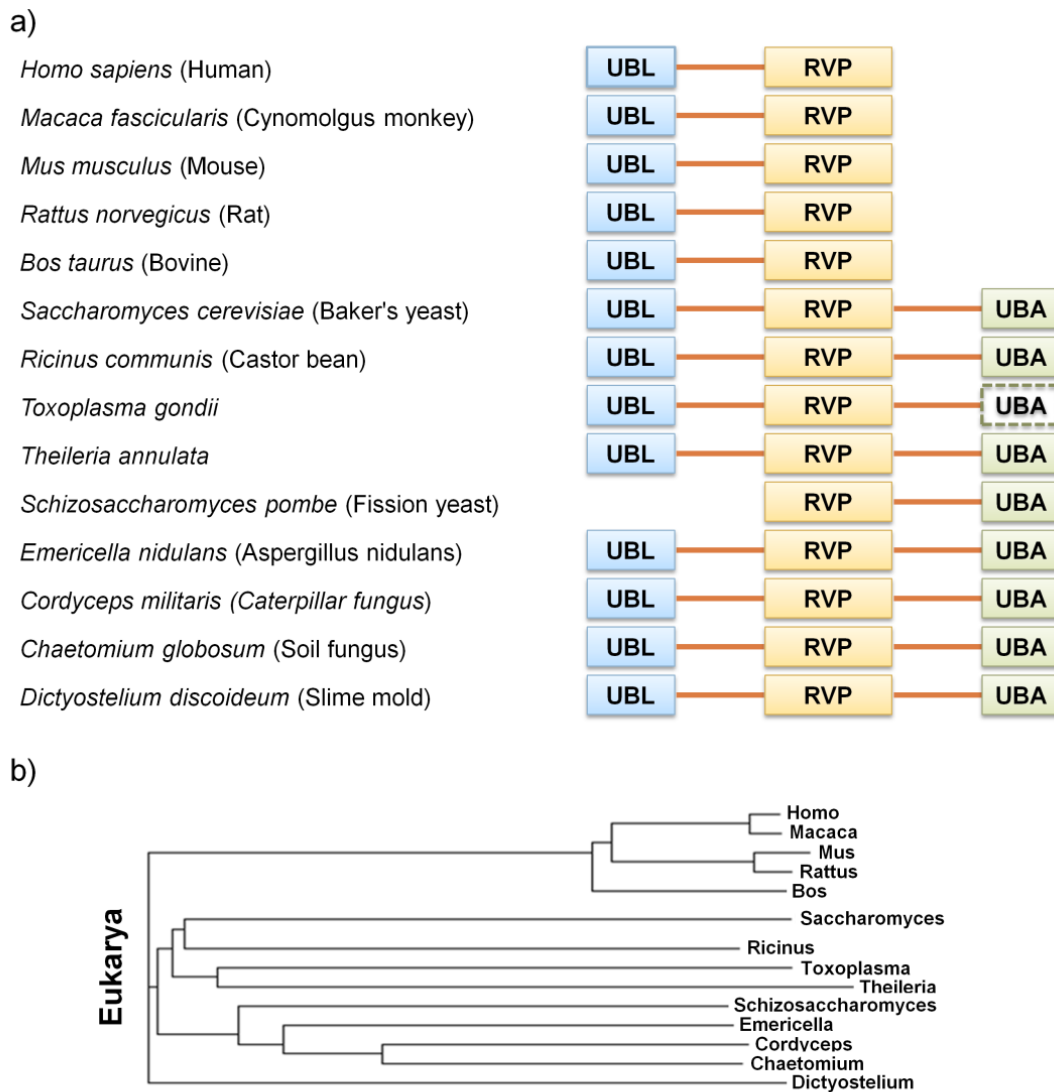


**Figure 1-16. Ddi1 gene structure among different eukaryotes.** (a) Domain representation for several eukaryotic organisms; UBL – ubiquitin like domain, RVP – retroviral protease-like domain, UBA – ubiquitin association domain, shown as solid blocks. The dashed block indicates the potential presence of an C-terminal sequence that was identified by the domain prediction software but did not pass the threshold criteria. (b) The phylogenetic tree of shown organisms (bottom panel).

### **1.4.2 Putative function of Ddi1 UBL and UBA domains.**

The detailed roles of the both UBL and UBA domains of Ddi1 are not known. However, a few processes in which these domains are involved have been discovered.

***Dimerization of shuttle proteins.*** The UBL-UBA proteins Ddi1, Rad23 and Dsk2 are known to have the ability to homodimerize. The Rad23 and Dsk2 proteins require UBA domains for their dimerization, while Ddi1 mediates it through the RVP domain<sup>61,62</sup>. Additionally, it was observed that Rad23 can heterodimerize with both Ddi1 and Dsk2<sup>29,62</sup>. The UBA domain of Rad23 is essential for Rad23-Dsk2 interaction, but it is not known which domain of Dsk2 is involved in this heterodimerization<sup>29</sup>. Two models have been proposed for Rad23 and Ddi1 dimerization. The first one suggests that both proteins utilize their UBA domains (UBA1 of Rad23 and UBA of Ddi1)<sup>61</sup>. On the contrary, according to the second model the UBA domain of Ddi1 and the UBL domain of Rad23 are responsible for this heterodimerization<sup>30</sup>.

**Ddi1 UBL-UBA potential binding partners.** UBA and UBL Ddi1 domains are not only involved in dimerization, but also in interactions with other binding partners. As mentioned previously, it was shown that the UBL domain of Ddi1 interacts with the F-box protein Ufo1 most probably through its UIM domain, yet unfortunately no biochemical parameters are known for this interaction<sup>56</sup>. Furthermore, it was shown that the Ddi1 UBL domain also binds the 19S regulatory subunit of the proteasome<sup>23</sup>. Interestingly, in other studies it was discovered that the hHR23A UBL domain binds to the human homolog Rpn10<sup>63</sup>. Therefore, Rpn10 might be a potential binding partner for Ddi1UBL domain binding.

Additionally, the regulation of the Pds1 protein depends on the presence of the Ddi1 protein. Pds1 inhibits cell cycle progression to the anaphase in *S.cerevisiae*. Deletion of Ddi1 and Rad23 genes rescues the temperature stability of Pds1. It is proposed that the binding between Ub moieties of ubiquitinated Pds1 and the UBA domain of Ddi1 prevents the polyUb chain from elongation<sup>17</sup>. Another role of the Ddi1 UBA domain was revealed in degradation of Ho endonuclease, the substrate for the SCF<sup>Ufo1</sup> ligase<sup>23</sup>. Ho endonuclease function is highly regulated: after performing its role in initiation of mating type interconversion it is recruited by Ufo1 to the SCF ubiquitin ligase complex for ubiquitination and subsequently degraded by the 26S proteasome<sup>23,64,65</sup>. The absence of the Ddi1 stabilizes the Ho endonuclease. As the ubiquitination of Ho endonuclease is required for degradation, it was proposed that the Ddi1UBA domain interacts with the Ub moieties.

The change in the role of Ddi1 from supporting degradation, as in the case of Ho endonuclease to preventing polyUb chain from elongation is not fully understood. It might be due to the fact that in both processes different E3 complexes are involved. Pds1 is ubiquitinated by the APC E3 ligase, while Ho endonuclease by SCF<sup>Ufo1</sup> complex<sup>17,23</sup>. The Pds1 stability regulation depends on the presence of both Ddi1 and Rad23 which may also indicate that the process of heterodimerization is involved in this phenomenon<sup>17</sup>. Despite the differences in both cases, it was the Ddi1UBA that was necessary for interaction with Ub moieties. Indeed, other studies show that the UBA domain of Ddi1 binds monoUb as well as polyUb chains<sup>32</sup>. Full length Ddi1 has a K<sub>d</sub> for monoUb around 10 μM unfortunately no K<sub>d</sub> value is known for polyUb chains<sup>32</sup>. Moreover, it is not known whether Ub binding by the UBA domain is affected by

heterodimerization with shuttle proteins or by interactions involving the UBL domain. Kang *et.al* 2006 made an attempt to study the effect of Ub binding upon dimerization, however the results do not give a clear answer<sup>30</sup>.

## 1.5 Research motivation and specific aims.

As emphasized above, the ubiquitin proteasome system plays a very crucial role in eukaryotes. In particular, it is very important to understand how shuttle proteins deliver polyubiquitinated proteins for proteasomal degradation. While Rad23 and Dsk2 have been pretty extensively characterized, information about Ddi1 is lacking. Some partial knowledge about its role in the cell is available from molecular biology studies; however the detailed functions of Ddi1 are not known. So far, it was shown that Ddi1 is a multi-domain protein and particularly that the UBL and UBA domains play an important part in the proteasomal degradation pathway. Furthermore, due to very low sequence identity between Ddi1 and Ub, as well as other UBL domains of shuttle proteins, it is unclear whether Ddi1 indeed contains a UBL domain and what its binding preferences are. Additionally, analysis of domain conservation among different species indicates that, with just one exception, the UBL domain is always present in Ddi1 sequence, while the UBA domain is not present in mammals. This loss of the UBA domain during evolution might be a result of its lack of functional importance in higher organisms, which then raises the question, of whether and how Ddi1 can act as a shuttle protein without a Ub-binding component. Finally, no RVP-domain activity as a protease was tested before in the context of the ubiquitin-proteasome system. In order to understand the complex role of Ddi1 in protein degradation, we performed structural

and functional characterization of this multi-domain protein. Structural studies confirmed the expected fold of the Ddi1UBL domain. Surprisingly, the first experiments for functional characterization of Ddi1 disclosed many unexpected properties of this protein.

Aims:

1. Structural studies of Ddi1UBL

The N-terminal domain of Ddi1UBL shares low sequence identity with ubiquitin and other UBL domains of shuttle proteins. Since the presence of the UBL domain in Ddi1 was only predicted through bioinformatics the first goal of the presented work was to test whether Ddi1 indeed has a domain that has a Ub fold. Having confirmed the relevance of studying individual Ddi1UBL, a series of spectra were collected in order to obtain full <sup>1</sup>H, <sup>13</sup>C and <sup>15</sup>N resonance assignment. This assignment was used further to obtain structural and distance constraints that allowed for three dimensional structure calculations.

2. Ddi1 – novel ubiquitin receptor

Ddi1 is a multi-domain protein; in this study we addressed the properties and functions of the previously uncharacterized RVP and UBL domains in the context of UPS system. It is already known that through its UBA domain Ddi1 interacts with Ub. Surprisingly, while monitoring UBA-Ub interaction in the Ddi1FL construct, we discovered that the UBL domain of Ddi1 also interacts with Ub. Interaction of any UBL domain and Ub has not been previously observed. Results presented here characterize the unique discovery and deliver information on affinity between Ddi1UBL and Ub, binding sites on both proteins and the structure of the complex. Additionally, we tested

the Ddi1UBL interaction with its known binding partner, UIM domains from Ufo1 protein, for which activity was also tested against Ub.

### 3. Ddi1UBL, first known ubiquitin like domain with UIM motif

Also of interest was determining whether Ub was the only unusual binding partner of Ddi1UBL. Since shuttle proteins can heterodimerize, we wanted to determine if Ddi1 utilizes its UBL domain to form such interaction. These studies led to the discovery that Ddi1UBL binds to the UBL domain of Dsk2 and the mode of its binding differs from the one with Ub. Detailed analysis revealed that Ddi1UBL appears to have two binding sites for Dsk2UBL and the second one involves an  $\alpha$ -helix. Interestingly, this second binding site is also used for distinguishing between binding monoUb and Ub dimers. Finally the focus of the studies was to understand what is special about the  $\alpha$ -helix of Ddi1UBL, as it has the potential to interact with Ub moieties and UBL domains.

## **Chapter 2. Structural studies of Ddi1UBL**

### **2.1 Ddi1 domains can be studied independently**

As mentioned above, it is believed that Ddi1 belongs to the UBL-UBA shuttle protein family. Such classification comes from the fact that the N- and C-terminal fragments of the Ddi1 gene were identified bioinformatically as the UBL and UBA domains, respectively<sup>17,61</sup>. First, it was essential to confirm that the spectral/structural properties of the isolated N- and C-terminal Ddi1 fragments (containing the putative UBL and UBA domains) are the same as in the context of the full-length (FL) Ddi1 construct.

For this purpose, 2D  $^1\text{H}$ - $^{15}\text{N}$  TROSY spectrum of FL Ddi1 was recorded and compared with the corresponding spectra of the isolated fragments. The majority of NMR signals overlaid almost perfectly, indicating that the chemical environment for each amide group is essentially the same in the FL protein and in the isolated fragments (Figure 2-1). Small discrepancies can be observed only for a few C-terminal residues in Ddi1UBL and are not unexpected, as they reflect a change in the chemical environment as a result of the truncation. Similarly, for the first few residues of the UBA domain, the lack of preceding amino acids that are present in the full-length construct explains the differences in peak positions in the NMR spectra of Ddi1UBA and FL Ddi1.

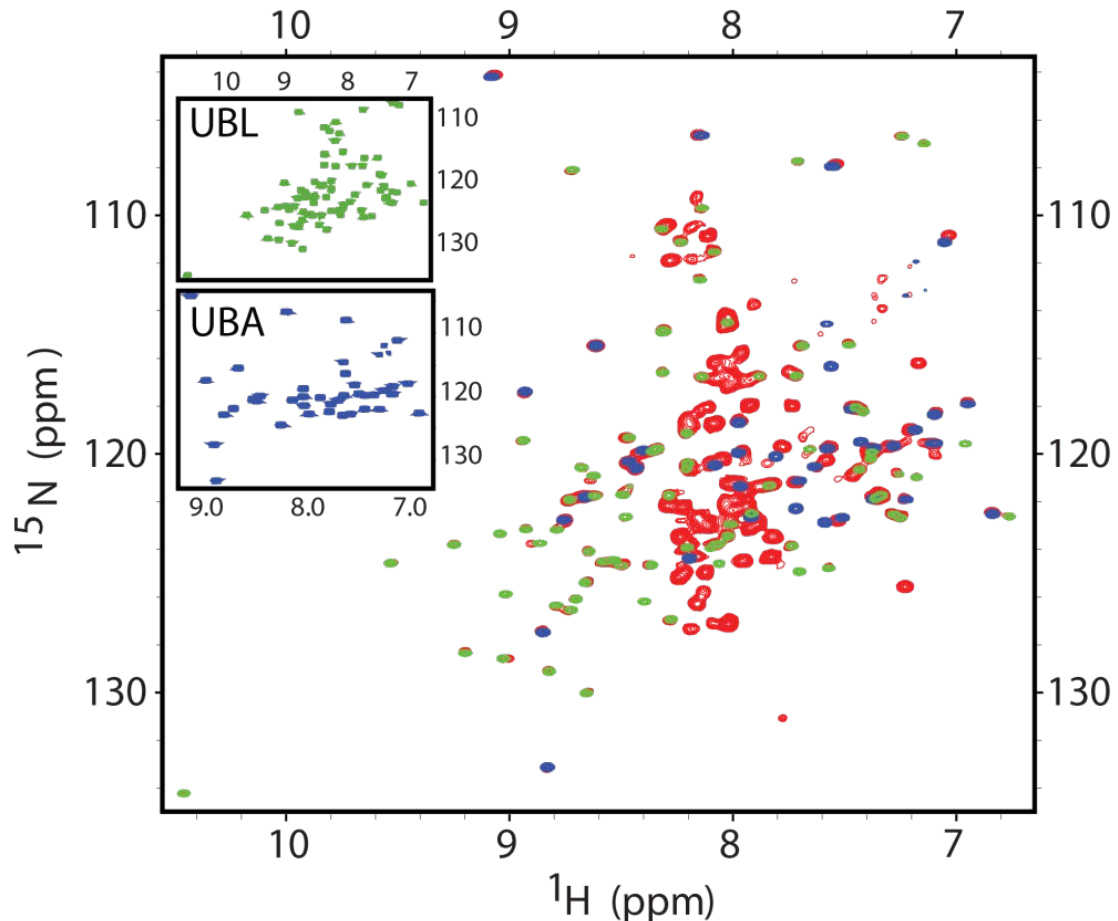


**Figure 2-1.**  $^1\text{H}$ - $^{15}\text{N}$  TROSY spectra of the full length Ddi1.  $^1\text{H}$ - $^{15}\text{N}$  TROSY spectra of the full length Ddi1 (red) overlaid with the spectra of the isolated fragments containing only UBA (blue) and UBL (green) domains; spectra of individual domains are shown in boxes with the same color coding.

Furthermore, because the Ddi1UBA construct is quite short (44 a.a.), even small changes at its N-terminus may affect other residues that are close in space. This explains some small changes in peak positions observed for the rest of the Ddi1UBA signals. It is noteworthy that the UBA and UBL signals in the spectrum of the FL Ddi1 (a 47 kDa protein) are relatively sharp, which indicates that both domains tumble somewhat independently from the rest of the protein and from each other. This is

further confirmed by analysis of the  $^{15}\text{N}$  longitudinal relaxation time ( $T_1$ ) which depends on the overall tumbling rate, and hence contains information about the size of the molecule<sup>42</sup>. Especially in the case of Ddi1UBL, the general pattern of  $^{15}\text{N}$   $T_1$  values is retained and the overall levels of  $T_1$  are quite similar for the isolated domain and in the FL protein (Figure 2-2). This indicates that in both cases the UBL domain tumbles in the same manner and is not affected by the rest of the FL Ddi1 protein.

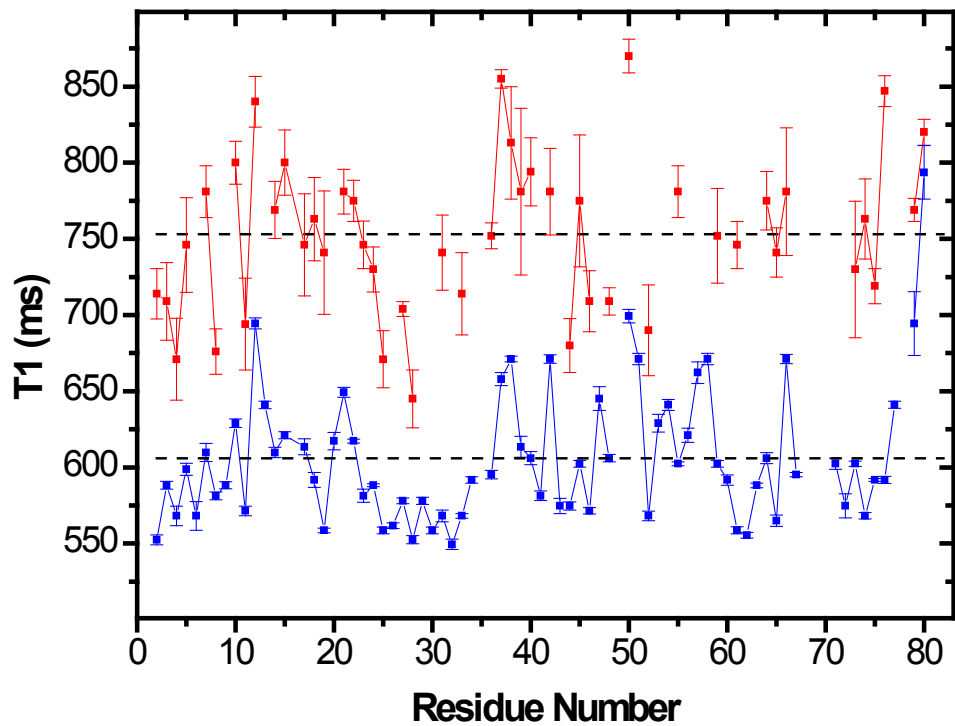


**Figure 2-2. Comparison of  $^{15}\text{N}$   $T_1$  relaxation rates for the Ddi1UBL and UBL domain of Ddi1FL.**  $^{15}\text{N}$   $T_1$  relaxation rates for the UBL domain of Ddi1UBL are shown in blue, for the Ddi1 full length construct are shown in red. For the full-length construct, only data for residues assigned with confidence are shown. The dash line indicates average  $T_1$  value, 753ms for Ddi1FL and 606ms for UBL domain.

## 2.2 Sequential assignment

In order to obtain the three dimensional structure of a protein by means of NMR it is necessary to assign resonance frequencies of proton, nitrogen and carbon atoms in the protein. Unfortunately, only protons ( $^1\text{H}$ ) have nonzero spin whose interactions with magnetic field can be monitored by NMR. The most abundant isotopes of carbon ( $^{12}\text{C}$ ) and nitrogen ( $^{14}\text{N}$ ) present in biological samples have zero spin and therefore are invisible for NMR spectroscopy. In order to record resonance frequencies of nitrogen and carbon atoms, the protein sample is enriched during preparation with NMR active isotopes such as  $^{13}\text{C}$  and  $^{15}\text{N}$ . A double labeled Ddi1sample ( $^{13\text{C},15\text{N}}\text{Ddi1UBL}$ ) was used to measure 3D triple resonance experiments such as: HNCO, HN(CA)CO, HN(CO)CA, HNCA, CBCA(CO)NH, HNCACB. These experiments allowed for basic assignments of  $\text{H}_\text{N}$ , N, C',  $\text{C}_\alpha$ ,  $\text{C}_\beta$  carbon atoms that are present in amino acids. The design of experiments also allows for linking resonances of particular residues ( $i$ ) to carbons in preceding amino acids ( $i-1$ ). This particular feature allows for linking amino acids resonances together, indicating which resonance belongs to which amino acid within the sequence. This so called sequential assignment is essential for protein structure calculation. The detailed resonance patterns that can be observed in the above experiments are summarized in Table 2-A.

Experiment name	Resonances observed
HNCO	${}^{i-1}C'$ $\leftarrow {}^iHN$
HN(CA)CO	${}^{i-1}C'$ $\leftarrow {}^iHN \rightarrow {}^iC'$
HN(CO)CA	${}^{i-1}C_\alpha \leftarrow {}^iHN$
HNCA	${}^{i-1}C_\alpha \leftarrow {}^iHN \rightarrow {}^iC_\alpha$
CBCA(CO)NH	${}^{i-1}C_\beta, {}^{i-1}C_\alpha \rightarrow {}^iHN$
HNCACB	${}^{i-1}C_\beta, {}^{i-1}C_\alpha \leftarrow {}^iHN \rightarrow {}^iC_\alpha, {}^iC_\beta$
CC(CO)NH	${}^{i-1}C_\varepsilon, {}^{i-1}C_\delta, {}^{i-1}C_\gamma, {}^{i-1}C_\beta, {}^{i-1}C_\alpha \rightarrow {}^iHN$
H(CCO)HN	${}^{i-1}H_\varepsilon, {}^{i-1}H_\delta, {}^{i-1}H_\gamma, {}^{i-1}H_\beta, {}^{i-1}H_\alpha \rightarrow {}^iHN$

**Table 2-A. Summary of resonance assignments obtained from triple resonance experiments.**

Having initial assignments for  $C'$ ,  $C_\alpha$ ,  $C_\beta$  of individual amino acids, CC(CO)NH, H(CCO)HN triple resonance experiments were analyzed in order to obtain the remaining carbon and proton side chain assignments. These two spectra show the “towers” of carbons/protons (respectively) of a particular residue being linked to an amide group of a preceding amino acid. Overall, this analysis allowed almost full assignment for carbons and protons present in the amino acid side chains. The complete proton assignment was confirmed by analysis of 2D and 3D TOCSY spectra that also show proton towers that are linked to its own amide resonances. Finally, the sequential assignment was verified by 2D and 3D NOESY experiments. The entire sequential assignment was performed using the CARA program<sup>66</sup>.

## 2.3 Structural constraints

The sequential assignment is essential, but not sufficient for structure calculation. In order to obtain high resolution NMR protein structure, a number of constraints that deliver information on the distance between atoms and bonds geometry is required.

### 2.3.1 NOE constraints

The main parameters used for structure calculations are dipolar cross-relaxation (NOE) rate constants that arise from the fact that dipolar-coupled spins do not relax independently. With some approximation, the intensity of the NOE peak is proportional to the inverse sixth power of the distance between two interacting <sup>1</sup>H spins:

$$\text{NOE} \propto 1/r^6 \quad (1)$$

The NOE cross-peaks that are observed in 2D and 3D NOESY experiments allow detecting cross-peaks of atoms that are separated by up to 5.5 Å distance in space. Depending whether the atoms belong to the same amino acid (*i-i*) or two different residues (*i-j*), the NOE constraints can be divided into two groups: intra- and inter residue. Furthermore, the inter-residue NOEs can be divided into three categories based on the proximity of amino acids with atoms that cause the cross-peak:

- sequential, *i* and *j* are neighboring residues;
- medium, *i* and *j* are less than four amino acids apart;
- long-range, cross-peak is between atoms of residues that are more than 4 amino acids apart in sequence;

The amount and type of NOEs distances used for Ddi1UBL structure calculations can be found in Table 2-B.

DISTANCE CONSTRAINTS STATISTICS	
Total NOEs	1101
Intra-residue	431
Inter-residue	670
Sequential ( $ i - j  = 1$ )	296
Medium-range ( $ i - j  < 4$ )	141
Long-range ( $ i - j  > 4$ )	233

**Table 2-B. NMR unique NOE distance statistics for Ddi1UBL structure.**

Despite the fact that both 2D and 3D NOESY experiments were used for NOE assignment, the 2D NOESY experiment was used to prepare the list of unique (above the diagonal) distance constraints in the format of \*.peaks file. The cross-peak intensities were obtained with use of the CARA Integration Tool that allows for tuning of the peak's base width and model<sup>66</sup>. Integration was performed with the Model-Based Linear Equation System. The list of NOEs was checked against unrealistic intensities that occasionally arise from peak overlaps and result in mistaken values during linear deconvolution of intensities.

### 2.3.2 Dihedral angle constraints

The polypeptide backbone is sterically constrained by torsion angles (dihedral angles): Phi ( $\Phi$ , around the  $C_\alpha$ -N bond) and PSI ( $\Psi$ , around the  $C_\alpha$ -C' bond). The torsion angles between peptide groups describe polypeptide chain conformations and define the geometric properties of peptide groups. The restrictions put on the allowed dihedral angles are summarized in a Ramachandran plot, which helps easily identify forbidden conformations of polypeptide chains. Interestingly,  $\Phi$  and  $\Psi$  angle values also help identify secondary structure elements since amino acids that are part of a particular secondary structure will show sequences of repeating torsion angle values.

As emphasized above, dihedral angles are a set of very important constraints for structure calculation. Fortunately, information about dihedral angles can be predicted based on secondary chemical shifts: differences between observed chemical shifts and chemical shifts for the same amino acid but in the random coil. The software TALOS+ is a useful tool that allows prediction of torsion angles based on secondary chemical shifts for the following nuclei:  $^1H_N$ ,  $^1H_\alpha$ ,  $^{13}C_\alpha$ ,  $^{13}C_\beta$ ,  $^{13}C'$ , and  $^{15}N$ , along with information about the protein sequence. Prediction is based on triplets of amino acids and the goal is to match all measured secondary shifts to secondary shifts of triplets that are available in the database. A good prediction is made when 10 different matches from the database give consensus secondary shift values for each amino acid within the triplet. The dihedral angles for triplets in database are known and therefore torsion angles will be known for the amino acids from the protein of interest.

TALOS+ predicted dihedral angels for the majority of amino acids in the Ddi1UBL sequence (Table 2-C). It can be easily noticed that based on prediction amino acids at the C-terminal end of Ddi1UBL show some dynamics, and it is therefore impossible to predict PSI and PHI angles. Even though a number of amino acids show ambiguous values (shown in yellow), it is worth mentioning that the majority had 9 out of 10 good matches. A total of 63 PSI and PHI angles that can be trusted were used as one of input files for structure calculation.

TALOS+		Ddi1UBL									
M1	D2	L3	T4	I5	S6	N7	E8	L9	T10		
G11	E12	I13	Y14	G15	P16	I17	E18	V19	S20		
E21	D22	M23	A24	L25	T26	D27	L28	I29	A30		
L31	L32	Q33	A34	D35	C36	G37	F38	D39	K40		
T41	K42	H43	D44	L45	Y46	Y47	N48	M49	D50		
I51	L52	D53	S54	N55	R56	T57	Q58	S59	L60		
K61	E62	L63	G64	L65	K66	T67	D68	D69	L70		
L71	T72	I73	R74	G75	K76	I77	S78	N79	S80		
K81	L82	N83									

**Table 2-C. Ddi1UBL sequence in TALOS+. Each residue has a specific color based on the software classification. Green - unambiguous/good prediction, Yellow - ambiguous/no prediction, Blue - dynamic/no prediction, Red - bad prediction relative to a known structure, Gray - no classification.**

### 2.3.3 Secondary structure prediction

Information from chemical shifts of backbone atoms can be also used for secondary structure prediction as it was observed that isotropic chemical shifts of  $^1\text{H}_\alpha$ ,

$^{13}\text{C}'$ ,  $^{13}\text{C}_\alpha$  and  $^{13}\text{C}_\beta$  backbone nuclei show dependence on secondary structures. It is well established that secondary chemical shifts have characteristic values that can be correlated to particular secondary structure elements<sup>67-69</sup>. This phenomenon is used for example in the chemical shift index method (CSI) that allows for identification of secondary structures<sup>70,71</sup>. Taking advantage of this well established approach, the  $^1\text{H}_\alpha$ ,  $^{13}\text{C}'$ ,  $^{13}\text{C}_\alpha$  and  $^{13}\text{C}_\beta$  chemical shifts from Ddi1 assignment were used to predict secondary structure elements (Figure 2-3).

The CSI method is not the only method that allows for secondary structure prediction. Talos+ is another program that allows for such analysis. In this approach  $^1\text{H}_\alpha$ ,  $^{13}\text{C}'$ ,  $^{13}\text{C}_\alpha$  and  $^{13}\text{C}_\beta$  and  $^{15}\text{N}$  chemical shifts of Ddi1UBL were used for identification of secondary structure elements. In addition to predicting secondary structures, Talos+ predicts order parameters ( $S^2$ ) based on the random coil index (RCI) method<sup>72</sup>. Order parameters help identify regions that are dynamically disordered and recognize complementary information required for predication of secondary structure elements.  $S^2$  values vary from 0 to 1, where 1 will correspond to most structured elements and  $S^2$  values smaller than 0.5 will belong to dynamic elements.

Both CSI and Talos+ identified similar regions in Ddi1UBL sequence as  $\alpha$ -helix (only difference between methods is the length of the helix) and  $\beta$ -strands. Similarly, the secondary structure composition of Ub also has one long  $\alpha$ -helix and 4  $\beta$ -strands.

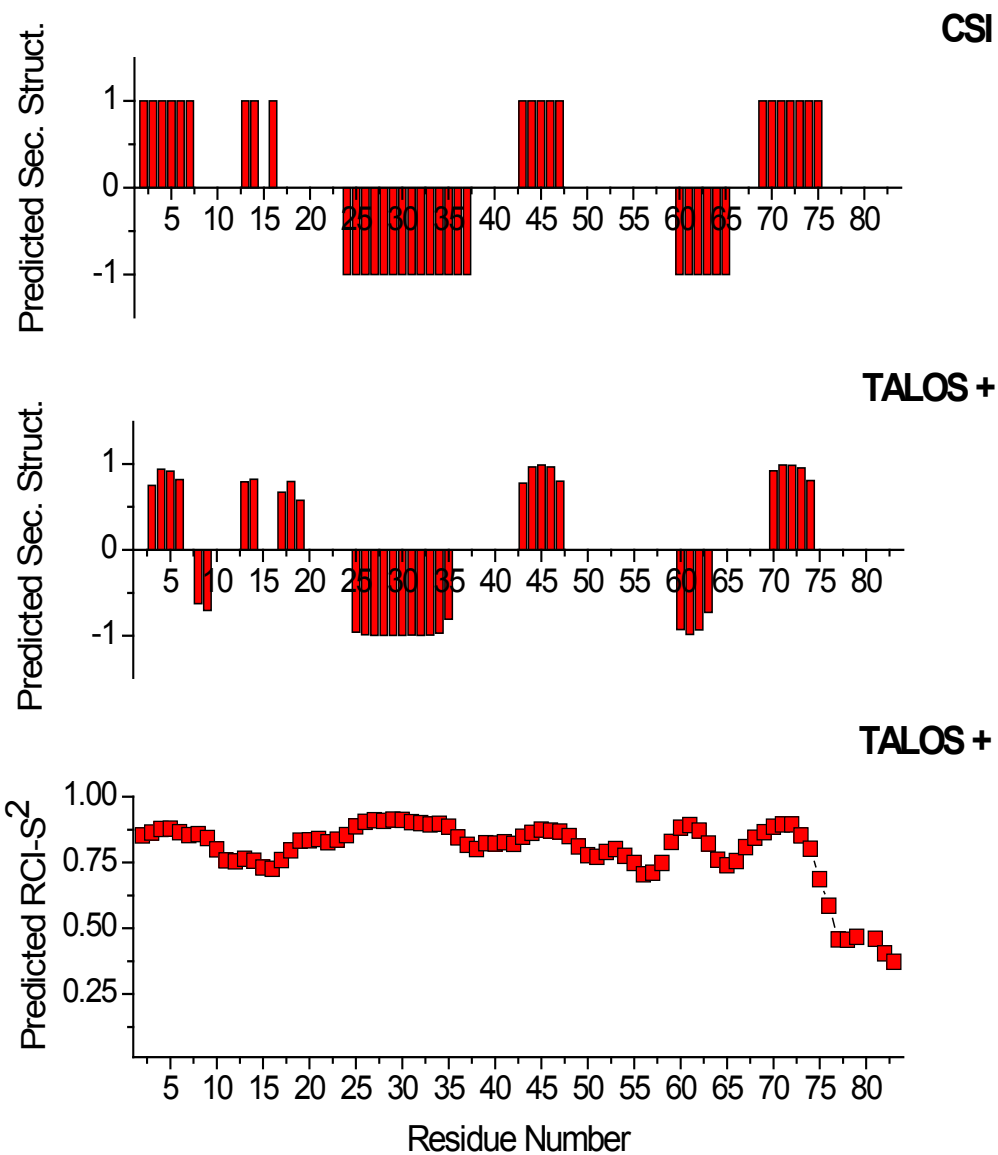


**Figure 2-3. Prediction of secondary structures and order parameters for Ddi1UBL.** Secondary structure prediction is presented in top (based on CSI method) and middle panel (based on TALOS+ approach). In both cases values presented on y axes corresponds to  $\beta$ -sheet secondary structure element for +1 values and  $\alpha$ -helix for values equal to -1. Additionally, probability of the prediction of TALOS+ method corresponds to the height of the bars. Bottom, predicted order parameters  $S^2$  based on RCI method.

### 2.3.4 Hydrogen bonds

Another set of essential information for structure calculation is hydrogen bonds (H-bonds). The preparation of H-bond constraints is a two-step process. Initially, it is important to identify which amide protons are involved in hydrogen bonding and secondly it is necessary to identify the donor and acceptor for a particular H-bond. Using the above shown prediction, which identified residues that might be part of the  $\alpha$ -helix and  $\beta$ -strands, is useful when identifying potential residues involved in H-bonds; however, this information is not sufficient for the final list of H-bond constraints in the calculation. With use of NMR, there are two approaches that help define hydrogen bond constraints: amide proton-solvent exchange experiments and information obtained from detailed analysis of NOESY type experiments. For the first approach, a  $^{15}\text{N}$ -Ddi1UBL sample was lyophilized from the  $\text{H}_2\text{O}$  based buffer and rapidly dissolved in the  $\text{D}_2\text{O}$ . Next, a series of  $^1\text{H}$ - $^{15}\text{N}$  SOFAST-HMQC spectra were collected to observe changes in peak intensities upon exchange of protons with deuterium (HD exchange). This HD exchange experiment takes advantage of the fact that amide protons involved in hydrogen bonding are shielded from the solvent and not easily accessible for deuterium exchange. Consequently, amides that are easily accessible exchange with  $\text{D}_2\text{O}$  solvent rapidly and therefore become invisible in the spectrum. For this particular study, 45  $^1\text{H}$ - $^{15}\text{N}$  SOFAST-HMQC spectra were collected over time with the same set of experimental parameters. The only difference between experiments was the number of scans that were collected; series 1-14 had 4 scans, for 15-34 each experiment had 8 scans, whereas for 35-45 series 16 scans were obtained. The information about the

number of scans is necessary to keep in mind when comparing peak intensities between different experiments.

As expected, in the first experiment a number of peaks already disappeared from the spectrum. This was an indication that these invisible signals belong to residues with amide bonds that are solvent exposed and not protected by hydrogen bonding or not buried in the three dimensional structure. For the purpose of comparing and illustrating the number of signals that disappeared from the spectrum, the first spectrum of the HD exchange series was overlaid onto the spectrum of Ddi1UBL at the same concentration in protonated buffer (Figure 2-4).

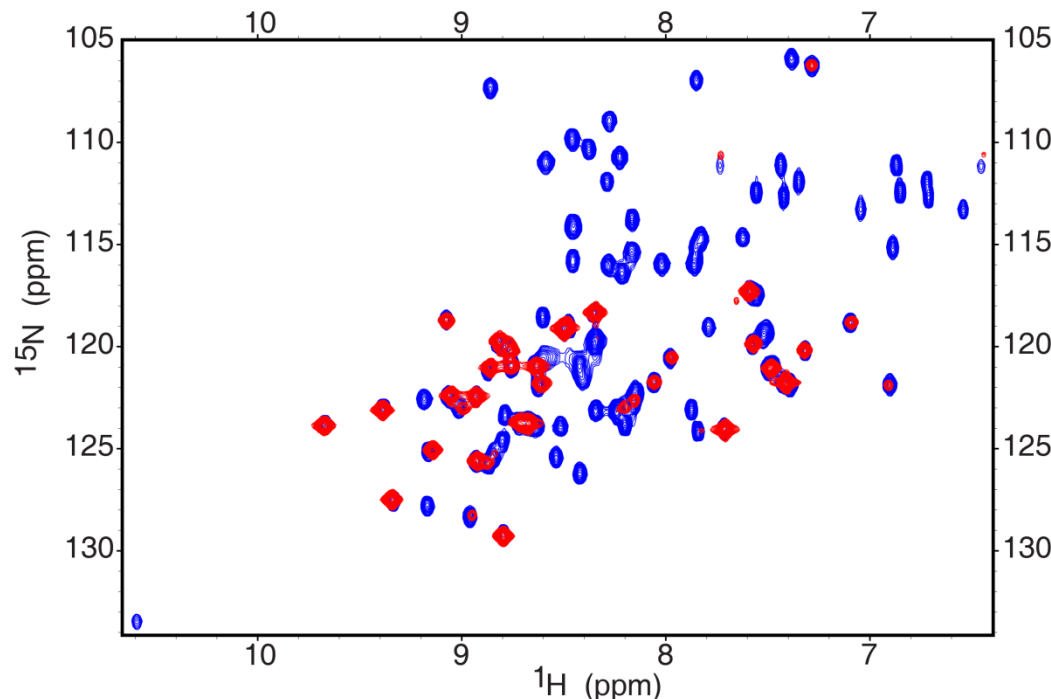


**Figure 2-4. Changes in the spectrum of Ddi1UBL upon HD exchange.**  $^1\text{H}$ - $^{15}\text{N}$  SOFAST-HMQC spectra overlay of 1mM  $^{15}\text{N}$ -Ddi1UBL in 20mM NaP buffer pH 6.8 in  $\text{H}_2\text{O}$  (blue) and first experiment from the HD exchange series of 1mM  $^{15}\text{N}$ -Ddi1UBL lyophilized from 20mM NaP pH 6.8  $\text{H}_2\text{O}$  buffer and resuspended in  $\text{D}_2\text{O}$  (red).

Interestingly, when peak intensities are plotted as a function of residue number, it can be easily observed that most residues predicted to be part of secondary structures, based on the dihedral angles analysis, are still visible in the first HD exchange experiment (Figure 2-5). As Ddi1UBL was being exposed to D<sub>2</sub>O, intensities of the peaks decreased with time. After approximately 30 minutes amino acids: 3-7, 12, 14, 17, 19, 42-47 and 69-74 lost on average half of their intensities. At the end of HD exchange experiment, after 245 minutes, these peaks almost disappeared from the spectrum. The region from residues 28 to 34 was more protected from the solvent, and half of these signals still had significant peak intensities at the end of the measurement.

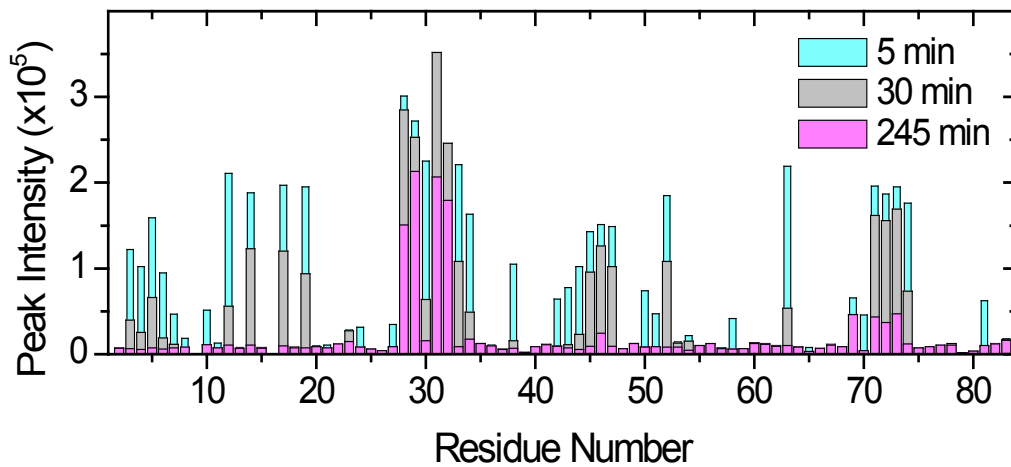


**Figure 2-5. Ddi1UBL peaks attenuations in the HD exchange experiment.** Peak intensities at three time points: 5min (cyan), 30min (gray), 245min (magenta) are showed as bars. Intensities at the last time point were divided by 4 due to the difference in the number of scans. For each amino acid data are overlaid on top of each other in order to emphasize change of peak intensity.

Results of HD experiment significantly supported the CSI and TALOS+ prediction of residues involved in secondary structures and consequently suggested which amino acids are involved in hydrogen bonding.

Secondly, it was necessary to define the pairs of amino acids that make the H-bond. Hydrogen bonds are made between amino acids that are close in space but are not neighbors in the primary sequence. NOESY experiments, which provide information about protons close in space, are very useful tools to identify both which residues are involved in bond formation and the type of secondary structure this bond participates in. There are a few characteristic cross peaks, and their assignment helps identify H-bonds. For residues that are part of the  $\alpha$ -helix, cross peaks between the amide protons of residue  $i$  and  $i+1$  are observed, as well as between  $i$  and  $i+2$ ,  $i+3$  or  $i+4$ . From this series, the most intense peaks are for  $i$  and  $i+1$  cross peaks and they should correspond to the distance of approximately 2.5 Å. Additionally, cross peaks between  $H_N$  and  $H_\alpha$  between amino acids  $i$  and  $i+1$ ,  $i+2$ ,  $i+3$  or  $i+4$  are characteristic. Among these signals, due to the nature of the  $\alpha$ -helix, the most intense signals arise from  $i+1$  and  $i+3$  and are less intense for  $i+2$  and  $i+4$ . Considering the side chain cross peaks, signals between  $H_\alpha$  and  $H_\beta$  of  $i$  and  $i+3$  residues are also distinct and can be observed as the distance between them is 2.5-4 Å apart. In the case of  $\beta$ -sheets, contacts are made between two pieces of the sequence that can be parallel or anti-parallel to each other. Assuming that one sequence is around amino acid  $i$  and another around residue  $j$ , the most intense signals should be observed between  $H_\alpha$  and  $H_N$  of  $i$  and  $i+1$  as well as  $H_\alpha$  and  $H_\alpha$  between  $i$  and  $j$  amino acids. The most distinguishing signature of amino acids from  $\beta$ -sheets is the NOE signal around the diagonal in the spectrum arising from close

proximity in space between amide protons of  $i$  and  $i+1$  ( $j$  and  $j+1$ ) along with amide protons of  $i-1$  and  $j+1$ . Where possible, all above mentioned cross peaks were assigned in the 2D and 3D NOESY experiments of Ddi1UBL.

Detailed analysis of HD exchange experiments and NOESY spectra allowed for preparation of an initial list of H-bonds used for structure calculation. Final hydrogen bond constraints used for the high resolution structure were made with support of information obtained from preliminary structure runs. In total, 25 hydrogen bonds were identified and used for structure calculation. For each bond the distance between  $H_N$  and O was set to be 1.8Å, whereas the distance between N and O was 2.8Å; for both values a deviation of 0.5Å distance was allowed.

### 2.3.5 Residual dipolar couplings

Residual dipolar couplings (RDC) are a type of NMR measured properties that provide structural information not local in nature. These dipolar couplings can be observed because molecules placed in proper media align partially to the static magnetic field, and as a result, dipolar couplings do not average out to zero. RDCs are a type of long range constraints and contain information about the orientation of the individual amide bonds with respect to the molecular alignment frame. For the Ddi1UBL structure calculation only one set of RDC was collected, in which the protein was in PEG/hexanol-based alignment medium<sup>40</sup>. After analysis of IPAP-HSQC experiments, a total 55 RDC constraints were used in the calculation<sup>73</sup>.

## 2.4 Structure calculations

Structure calculation was done using ARIA (Ambiguous Constraints for Iterative Assignment) software with the CNS engine and simulated annealing strategy<sup>74</sup><sup>76</sup>. ARIA allows for automative NOE assignment and structure calculation based on NMR constraints. The process of structure calculation was a cycle of multiple iterations. The ambiguous distance constraints from one run were used in the next run in order to improve results. In the last step of each calculation the refinement in explicit solvent was performed by molecular dynamic simulations.

The constraints used for final structure calculations were: the protein sequence, the list of proton chemical shifts, the NOESY peak list, and \*.tbl files with dihedral angels, hydrogen bonds, RDC, and the list of unambiguous assignments from the best previous run. The ARIA project was set with the standard setting. The structure calculation was done in 9 iterations (from 0 to 8), where each iteration had 100 structures out of which the 7 best were used for the next cycle. These iterations had different violation tolerances and thresholds, which guaranteed improvement in calculations. The last iteration was water refined and the 10 best lowest energy structures were identified as the final result.

## 2.5 Ddi1UBL structure

All 10 lowest energy structures from AIRA presented a good convergence. They had a backbone RMSD of  $0.39 \pm 0.05$  Å for the secondary structure elements and  $0.80 \pm 0.16$  Å for residues 2-76 (Figure 2-6). The difference between the RMSD reflects the fact that Ddi1UBL has a long flexible loop (residues 52-69) that connects strands β4

and  $\beta$ 5. The C-terminal residues 77-80 had no inter-residue NOE constraints and therefore are not included in this comparison.

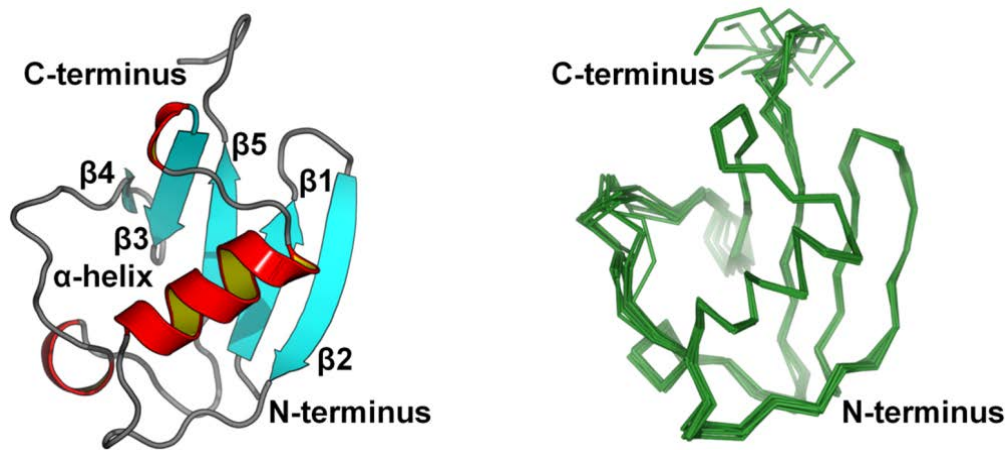


**Figure 2-6. Structure of Ddi1UBL.** Cartoon representation of backbone structure showing the secondary structure elements of Ddi1UBL (left) and overlay of 10 lowest-energy structures showed as backbone traces of Ddi1UBA (right).

The structure was evaluated by comparison of experimental RDC with back-calculated values. The correlation coefficient for this data was 0.987, while the quality factor was equal to 0.104 (Figure 2-7), confirming that the structure is correct. The refinement statistics including evaluation of distance and dihedral angles violation, and deviations from idealized geometry are summarized in Table 2-D. The R.M.S values reported are for 10 refined structures.

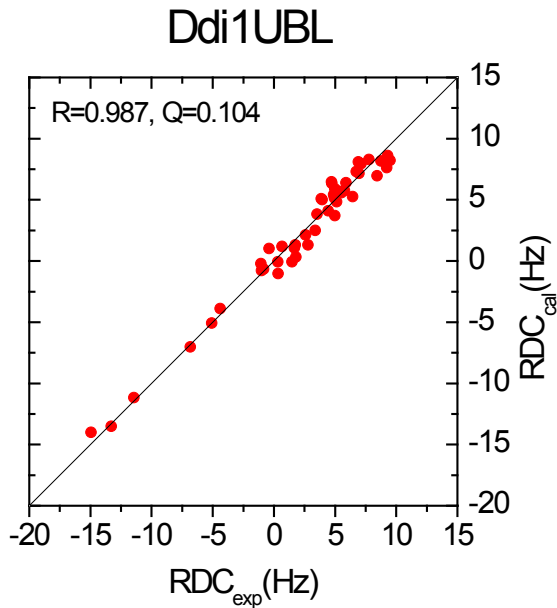


**Figure 2-7. Ddi1UBL structure evaluation based on RDC.** The correlation between the experimental RDCs and their back-calculated values from the derived structures for Ddi1UBL. The values of the Pearson's correlation coefficient ( $r$ ) and the quality factor ( $Q$ ) are indicated<sup>77</sup>.

Structure statistics	
Violations (mean and s.d.)	
Distance constraints (Å)	0.05 $\pm$ 0.05
Dihedral angle constraints (°)	3.57 $\pm$ 0.38
Max. dihedral angle violation (°)	6.70
Max. distance constraint violation (Å)	0.22
Deviations from idealized geometry	
Bond lengths (Å)	0.16 $\pm$ 0.01
Bond angles (°)	1.26 $\pm$ 0.04
Improper (°)	2.79 $\pm$ 0.17
Average pairwise r.m.s. deviation** (Å)	
Heavy	1.90 $\pm$ 0.35
Backbone	1.34 $\pm$ 0.32

**Table 2-D. NMR refinement statistics for Ddi1UBL structures.**

## 2.6 Ddi1UBL vs. Ubiquitin structure comparison

Interestingly, despite the low sequence identity to Ub, the N-terminal segment of Ddi1 has a domain with a Ub-like fold, in which the  $\beta$ -sheet is packed against the  $\alpha$ -helix, forming the hydrophobic core of the protein. Ddi1UBL has four full  $\beta$ -strands: antiparallel  $\beta_1$  and  $\beta_2$  strands connected through type I  $\beta$  turn, antiparallel  $\beta_3$  and  $\beta_5$  strands and a short  $\beta_4$  strand antiparallel to  $\beta_3$ . Lastly, strands  $\beta_1$  and  $\beta_5$  are oriented in a parallel manner, as in Ub. When the structure of Ddi1UBL is overlaid with the structure of Ub, it is observed that both Ddi1UBL and Ub have a 12 amino acid long  $\alpha$ -helix. However, the position of the Ddi1UBL helix is slightly different, as the helix is tilted such that its N-terminal end is farther away from the  $\beta$ -strands (Figure 2-8). Moreover, despite the same  $\beta$ -strand organization and packing against the  $\alpha$ -helix, the  $\beta$ -sheet in Ddi1UBL appears flatter and is not wrapped around the helix as much as in Ub.

When evaluating Ddi1 and Ub structure packing, most side chain contacts forming and stabilizing the hydrophobic core of Ub are preserved in Ddi1UBL (Figure 2-9). These amino acids are L40 and L44 (V26 and I30 in Ub) that “anchor” the  $\alpha$ -helix and L83 and I85 (L67 and L69 in Ub) that bring strand  $\beta_5$  to the core of the protein, as well as L45 and L52 (L43 and L50 in Ub) that are also conserved among Ub and several UBLs (see Figure 1-15).

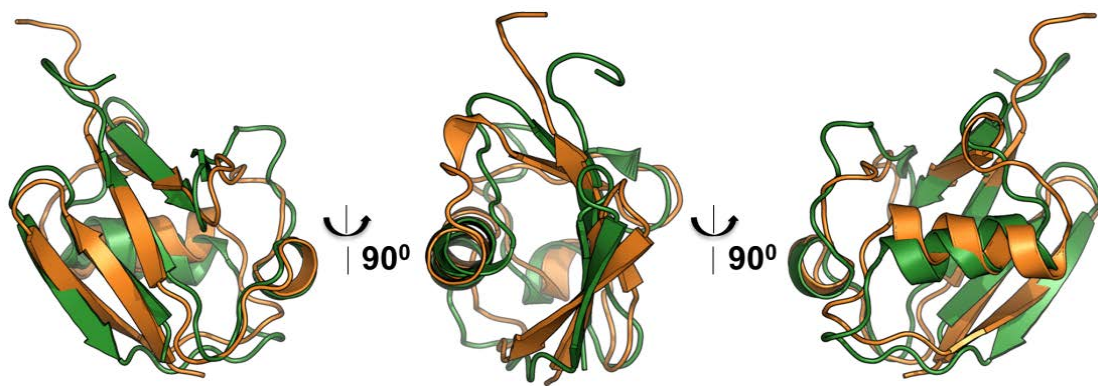


**Figure 2-8. Comparison of Ddi1UBL and Ub.** Cartoon representation of the overlay of Ub (orange) and Ddi1UBL (green) structures. Ub structure obtained from 1Ubq.pdb.

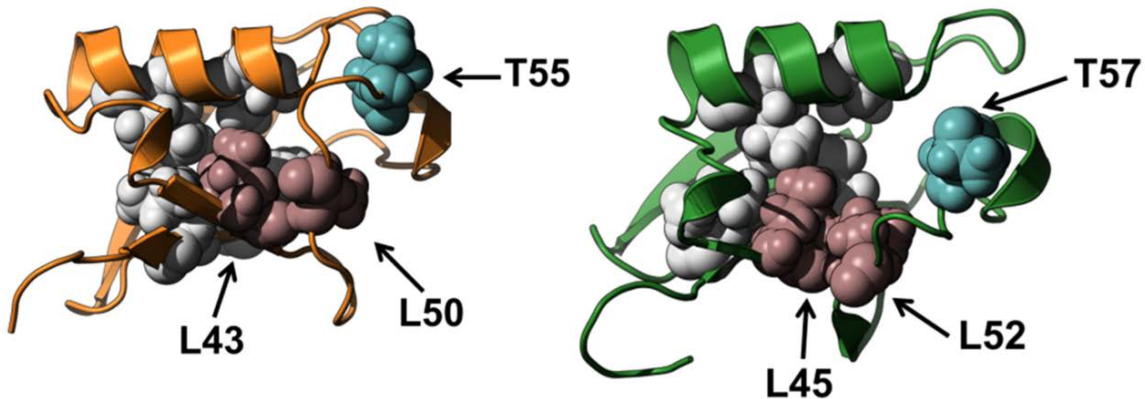


**Figure 2-9. Ddi1UBL and Ub structure packing.** Shown in pink and cyan are residues conserved among all the UBLs; L43, L50, T55 in Ub (left) and respectively L45, L52, T57 in Ddi1UBL (right). Several other residues that together with the abovementioned hydrophobic residues form the hydrophobic core in Ub (V26, I30, L67, L69) and Ddi1 UBL (L28, L32, L71, I73) are shown in white. Ub structure was taken from 1Ubq.pdb.

It is clear from the sequence and structure alignment with Ub that Ddi1UBL does not have the classical L8-I44-V70 hydrophobic patch which is characteristic for Ub (Figure 1-15 and 2-10)<sup>37</sup>. However, it has a few hydrophobic residues on the surface of the  $\beta$ -sheet that may be responsible for UBL's interactions with potential binding partners.

Surprisingly, in contrast to Ub (and the other UBLs shown in Figure 1-15), where the hydrophobic patch is surrounded by basic side chains, in Ddi1UBL the hydrophobic-patch surface contains several acidic residues.

Interestingly, amino acids D44 and D50 in Ddi1UBL are located in exactly the same position in the sequence as R42 and K48 are in Ub. Furthermore, E8 is very close to where K6 is in Ub. Such a distribution of acidic amino acids results in the opposite sign of the electrostatic potential of the  $\beta$ -sheet surface of Ddi1UBL compared to Ub and other UBLs (Figure 2-11).

The dissimilarity in the distribution of surface charges suggests that although Ddi1UBL has a Ub-like fold and both have a hydrophobic patch differences in electrostatic potential might dictate different binding preferences for Ddi1UBL when compared to Ub and the other UBLs.

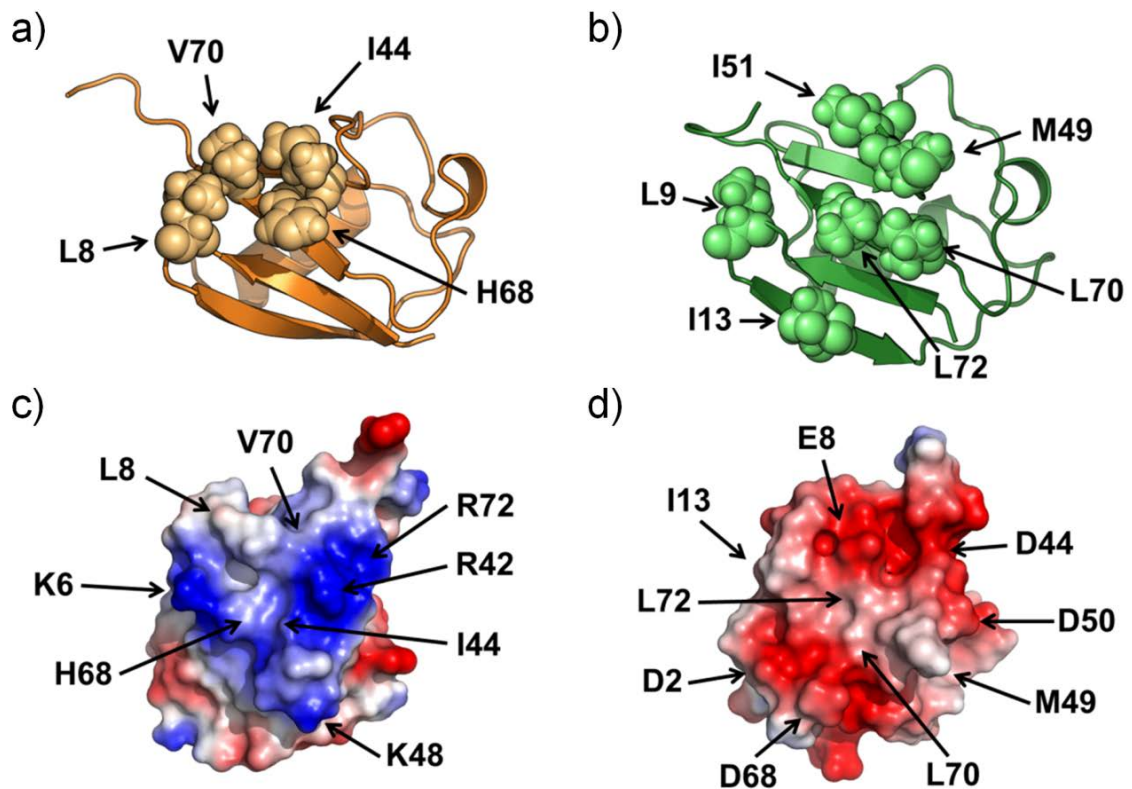


**Figure 2-10. Ddi1UBL and Ub structure comparison.** (a) Spherical representation of hydrophobic patch (L8, I44, V70) on Ub surface with additional indication of H68. (b) Hydrophobic amino acids: L9, I13, M49, I51, L70, L72 (spheres) on the surface of Ddi1UBL that can create alternative hydrophobic binding surface. Representation of electrostatic potential calculated using PyMol on the surface of Ub (c) and Ddi1UBL (d). Negatively charged amino acids (red) and positively charged (blue) are shown. Negatively charged side chains of D2, E8, D44, D50 and D68 in Ddi1UBL are highlighted by arrows. Similarly, positively charged K6, R42, K48 and R72 of Ub are indicated. Major hydrophobic residues are presented to help locate hydrophobic patches. Ub structure obtained from 1Ubq.pdb.

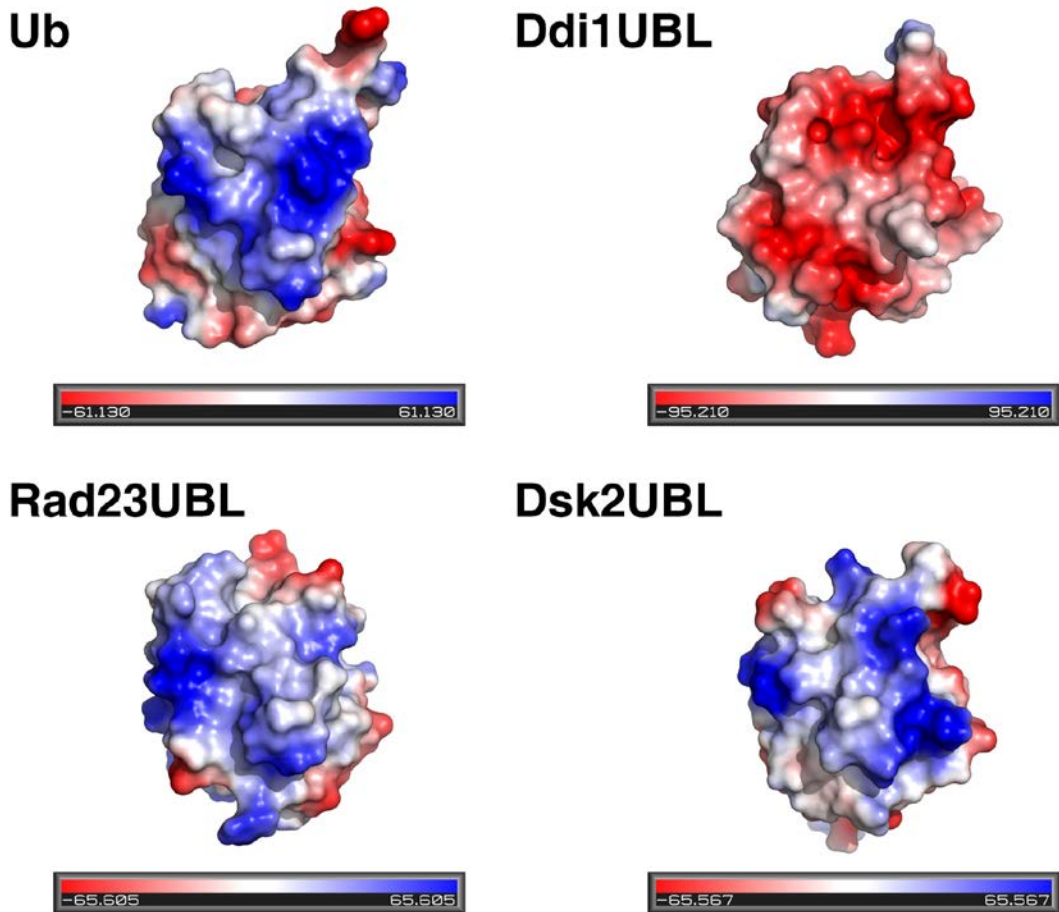


**Figure 2-11. Electrostatic potential of the surface of Ub and the UBL domains from shuttle proteins: Ddi1, Rad23, and Dsk2.** Positive values of the potential are colored blue while the negative values are red. All molecules are oriented similarly and such that the  $\beta$ -sheet surface faces the reader. The electrostatic potential map was generated using Pymol<sup>78</sup>. Pdb codes used for the illustration: 1Ubq.pdb for, 2WyQ.pdb for Rad23UBL and 2BWF.pdb for Dsk2UBL.

## 2.7 Dynamic properties of Ddi1UBL

Even though Ddi1UBL and Ub share the same fold, there are small dissimilarities between the two proteins. Comparison of the backbone dynamics will allow confirmation of the rigidity of secondary structure elements, the presence of the long  $\beta$ 4/ $\beta$ 5 loop that is more structured in Ub than in Ddi1UB and the unstructured C-terminus.

To address this,  $^{15}\text{N}$  spin-relaxation rates ( $T_1$  and  $T_2$ ) and steady-state heteronuclear  $^{15}\text{N}[^1\text{H}]$  NOEs (hetNOE) were measured since they are sensitive to the overall tumbling and backbone motions of a protein. Measured  $^{15}\text{N}$  relaxation for Ddi1UBL was compared to values for Ub (Figure 2-12).

The general pattern of R1 and R2 relaxation rates is similar between Ub and Ddi1UBL, however, the average  $^{15}\text{N}$   $T_1$  value for Ddi1UBL is  $^{15}\text{N} T_{1\text{ave}} = 601 \pm 37$  ms which is lower than the one for Ub ( $^{15}\text{N} T_{1\text{ave}} = 498 \pm 22$  ms). Consequently, the average Ddi1UBL  $^{15}\text{N} T_2$  is  $112 \pm 22$  ms, which is higher, than for Ub. This clearly indicates that Ddi1UBL tumbles slower than Ub (76 a.a.) under the same conditions, which can be a reflection of the larger size of the Ddi1UBL construct (95 a.a.) that was used in these studies. In order to quantify these observations, the  $^{15}\text{N}$  relaxation rates were analyzed to determine the overall rotational correlation time ( $\tau_c$ ) of the Ddi1UBL construct, which was determined to be  $6.77 \pm 0.24$  ns. This  $\tau_c$  is longer than for monoUb ( $\tau_c = 4.85$  ns) and approaches that reported for di-Ub, where the  $\tau_c$  varies from 7.85 ns to 8.92 ns depending on the Ub unit and linkage<sup>40,41,79,80</sup>.

Finally, the presence of the highly flexible C-terminus in Ddi1UBL was confirmed by particularly low hetNOE values for residues 76-80. Interestingly, residues

52-60 exhibited noticeably lower hetNOEs compared to the rest of the backbone (excluding the C-terminus). This indicates that the long  $\beta$ 4/ $\beta$ 5 loop in Ddi1UBL is more dynamic than a similar loop in Ub.

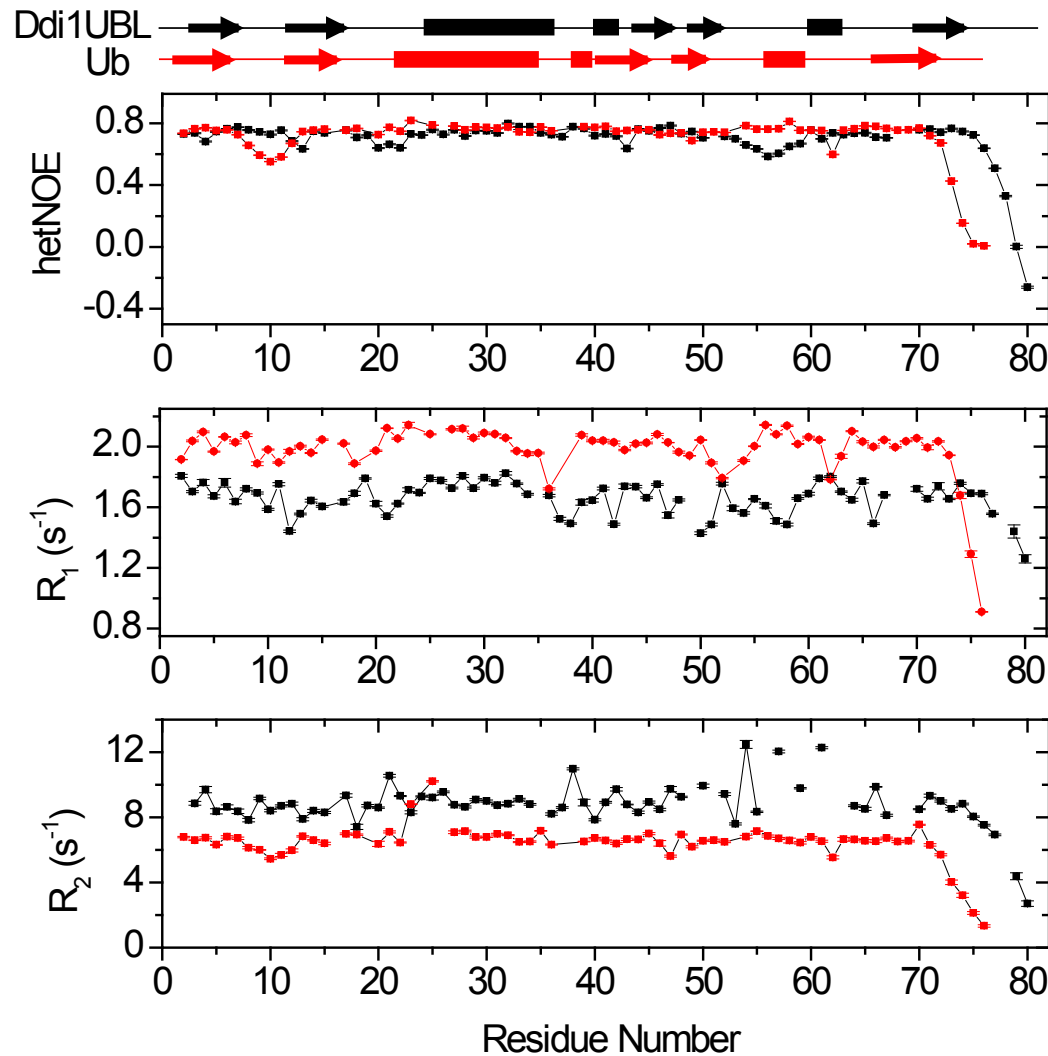


**Figure 2-12. Comparison of the  $^{15}\text{N}$  relaxation data in Ddi1UBL and Ub.** Shown are backbone amides in Ddi1UBL (black) and Ub (red): hetNOE and  $^{15}\text{N}$  longitudinal  $R_1 (=1/T_1)$  and transverse  $R_2 (=1/T_2)$  relaxation rates. The elements of secondary structure are indicated on the top.

## 2.8 Oligomeric state of Ddi1UBL

The slower tumbling of Ddi1UBL compared to Ub could also be interpreted as an indication of UBL's self-association. In order to determine the oligomeric state of the Ddi1UBL construct in solution, a sedimentation equilibrium experiment was performed at the same sample conditions as for the NMR studies (Figure 2-13). The results indicate that Ddi1UBL behaves as a monomeric species with a molecular mass of  $10508 \pm 406$  Da (10573.89 Da expected). The fact that Ddi1UBL does not dimerize (via disulfide bonds) was independently confirmed by electrospray mass spectrometry measurements that gave a molecular mass of 10574 Da (Figure 2-14).

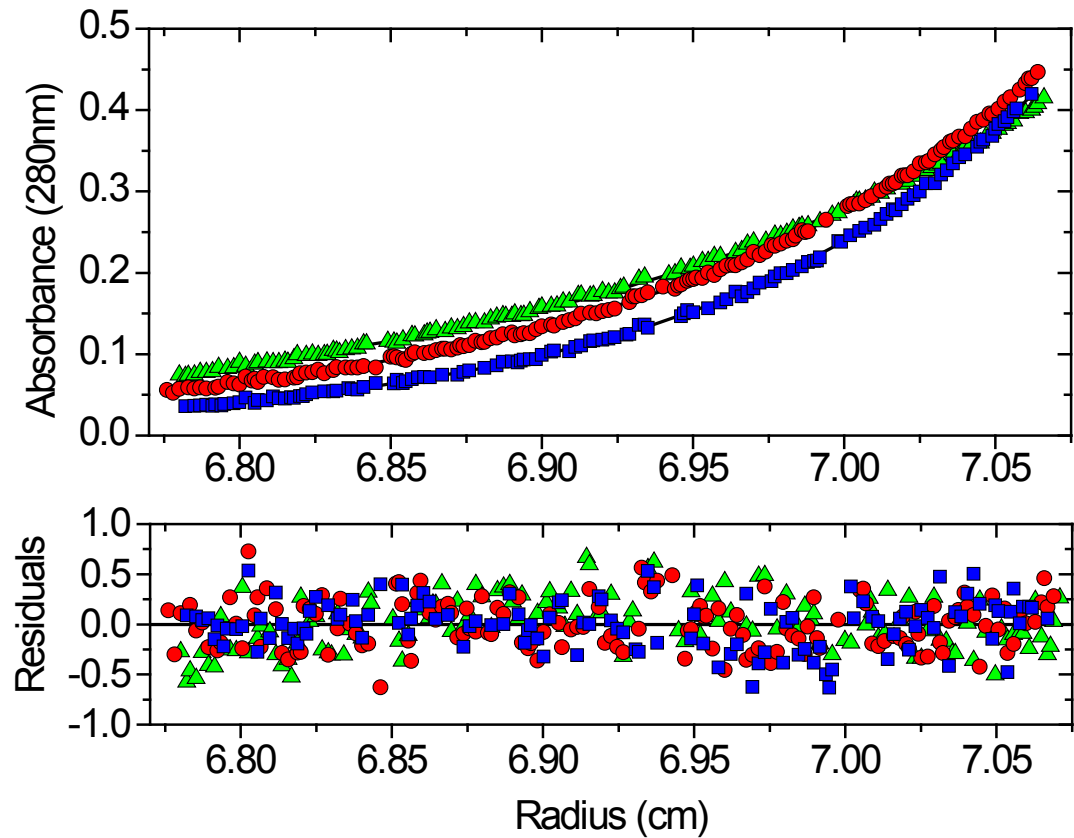


**Figure 2-13.** Sedimentation equilibrium analysis of Ddi1UBL. Shown in the top panel are absorbance-versus-radius profiles collected by analytical ultracentrifugation at three speeds: 26000 rpm (triangles), 29000 rpm (squares), and 32000 rpm (circles), for Ddi1UBL. The lines represent the best-fit curves obtained from global analysis of the data at all three speeds. The best fit of the data was obtained using a single-species model, which confirmed that Ddi1UBL indeed behaves as a monomer. The residuals of the fits are presented in the bottom panel. Based on the analysis the molecular mass of Ddi1UBL is  $10508 \pm 406$  Da, in excellent agreement with the expected molecular mass of 10573.89 Da. Data collections Urszula Nowicka and Poorni Adikaram, Department of Chemistry and Biochemistry, University of Maryland, College Park, USA. Data analysis Urszula Nowicka.

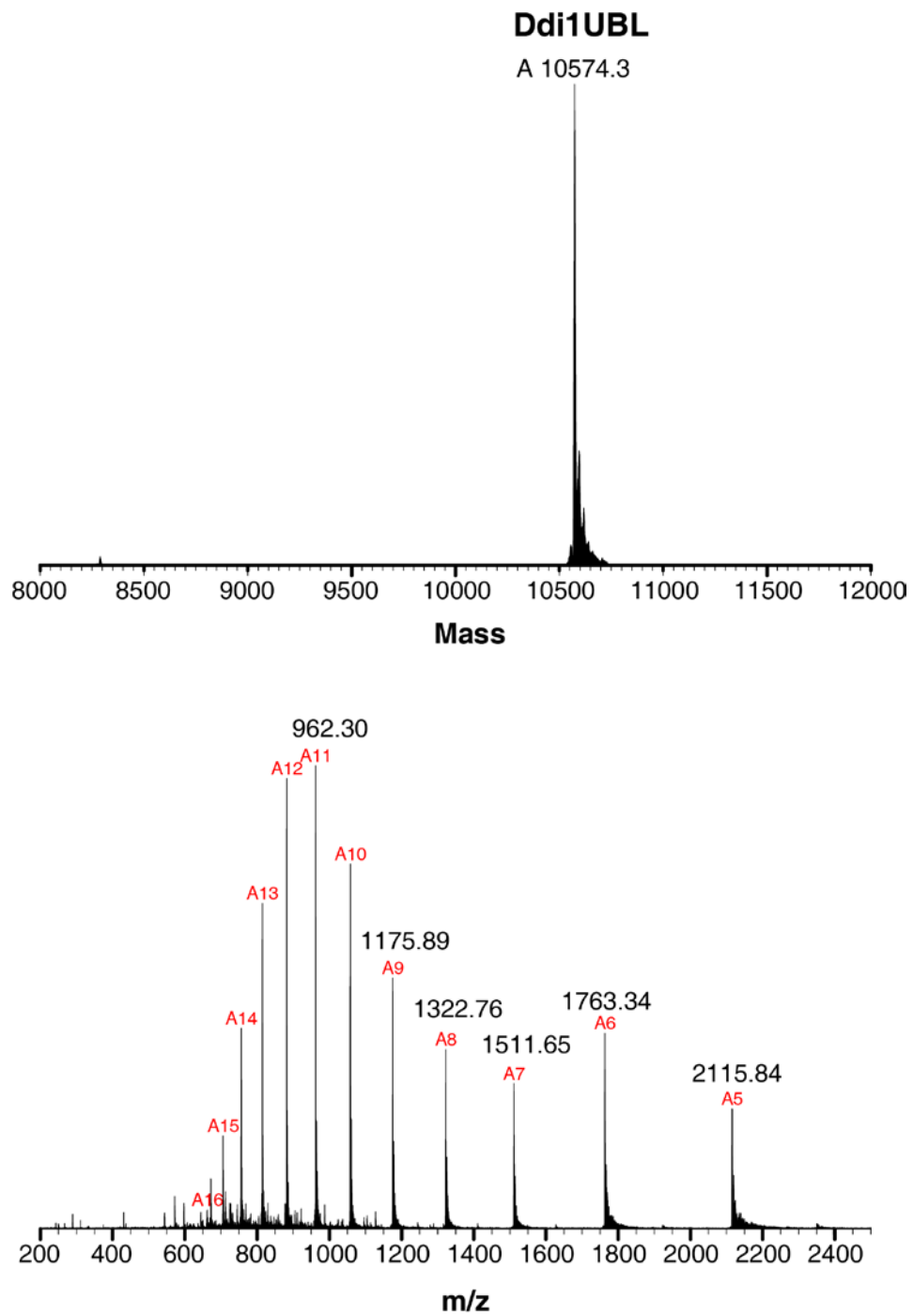


**Figure 2-14.** ESI-MS spectrum of DdiUBL. Ddi1UBL sample in 20mM NaP 3mM TCEP pH=6.8. Measured mass of Ddi1UBL was 10574.3Da (expected molecular weight is 10573.89 Da).

## **Chapter 3. Ddi1- novel ubiquitin receptor**

### **3.1 Ddi1 as a multidomain protein**

Previously it was shown that UBL-UBA proteins homodimerize through UBL and UBA domains<sup>61,62</sup>. In the case of Ddi1, the intra- and inter-molecular interaction between the UBL and UBA domains can be ruled out based on the spectrum of the full length Ddi1FL where peaks of UBL and UBA domains overlay perfectly with signals of individually expressed domains. All these results are consistent with previously published data that only the RVP domain is important for Ddi1 homodimerization<sup>59,61</sup>.

In the spectrum of the full length Ddi1, except for the peaks of UBL and UBA domains there are some additional peaks towards the middle of the spectrum. The number of peaks is less than expected for RVP domain. Moreover, in the hetNOE experiment negative peak intensities or near zero intensities are observed for these signals, indicating that they belong to some unstructured and/or flexible region of Ddi1 (Figure 3-1).RVP domain signal are probably broadened and therefore not visible in the Ddi1FL spectrum.

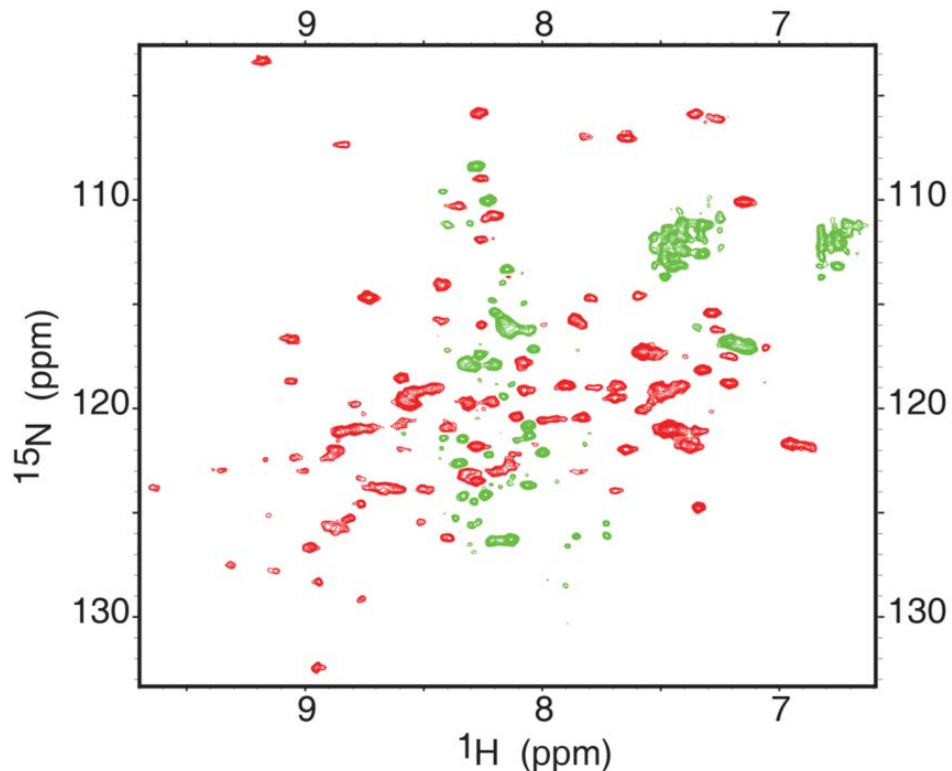


**Figure 3-1. Heteronuclear NOE spectrum of full length Ddi1.** Red contours show positive signal intensities, green contours correspond to negative intensities, indicating flexibility of the amide group.

Except for being responsible for homodimerization and for its involvement in *pds1-128* rescue, no other function for the RVP domain, especially in the UPS system, was reported<sup>58</sup>. We wanted to test whether this retroviral protease fold domain has any protease activity against Ub chains. For that purpose, we tested full length Ddi1 against deubiquitinase (DUB) activity for all seven lysines linked Ub<sub>2</sub>, we did not observe any chain cleavage even after extending the experimental time to 24 hours, indicating that Ddi1FL doesn't have DUB activity under these experimental conditions (Figure 3-2).

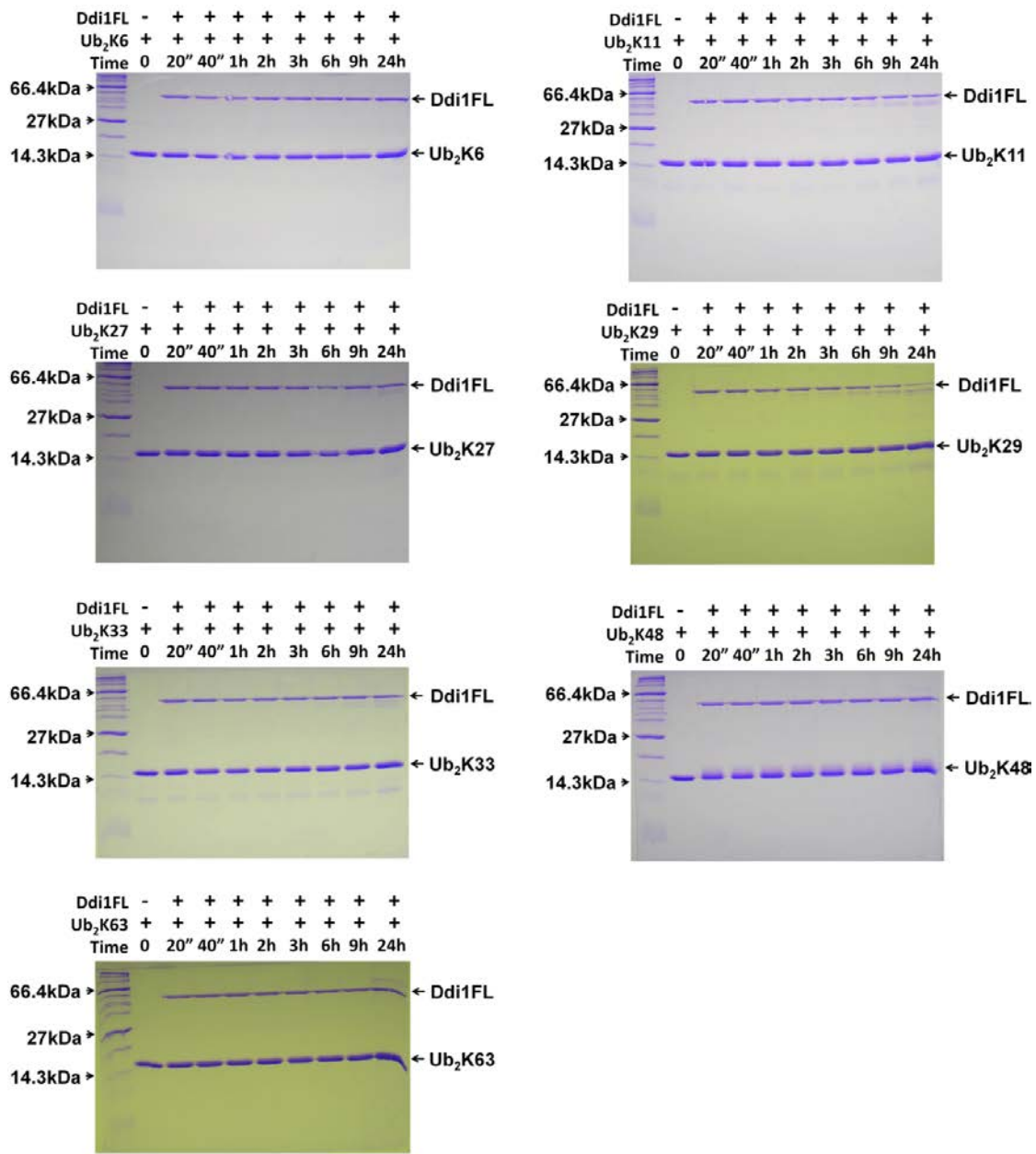


**Figure 3-2.** Time resolved deubiquitinating enzyme (DUB) activity assay, testing for Ddi1 protease activity against K6-, K11-, K27-, K29-, K33-, K48- and K63- $\text{Ub}_2$ s. Sample of each individual chain was incubated with Ddi1FL. Time points were collected as indicated on top of each gel. No Ddi1FL DUB activity was observed under experimental conditions.

Combining all the information mentioned above, including how UBL, RVP and UBA domains tumble independently from each other, as well as the fact that no interaction exists between UBA and UBL domains, and that the RVP domain is responsible for Ddi1 homodimerization allowed to propose a model of the FL Ddi1 structure, in which all three domains are connected through flexible linkers (Figure 3-3).

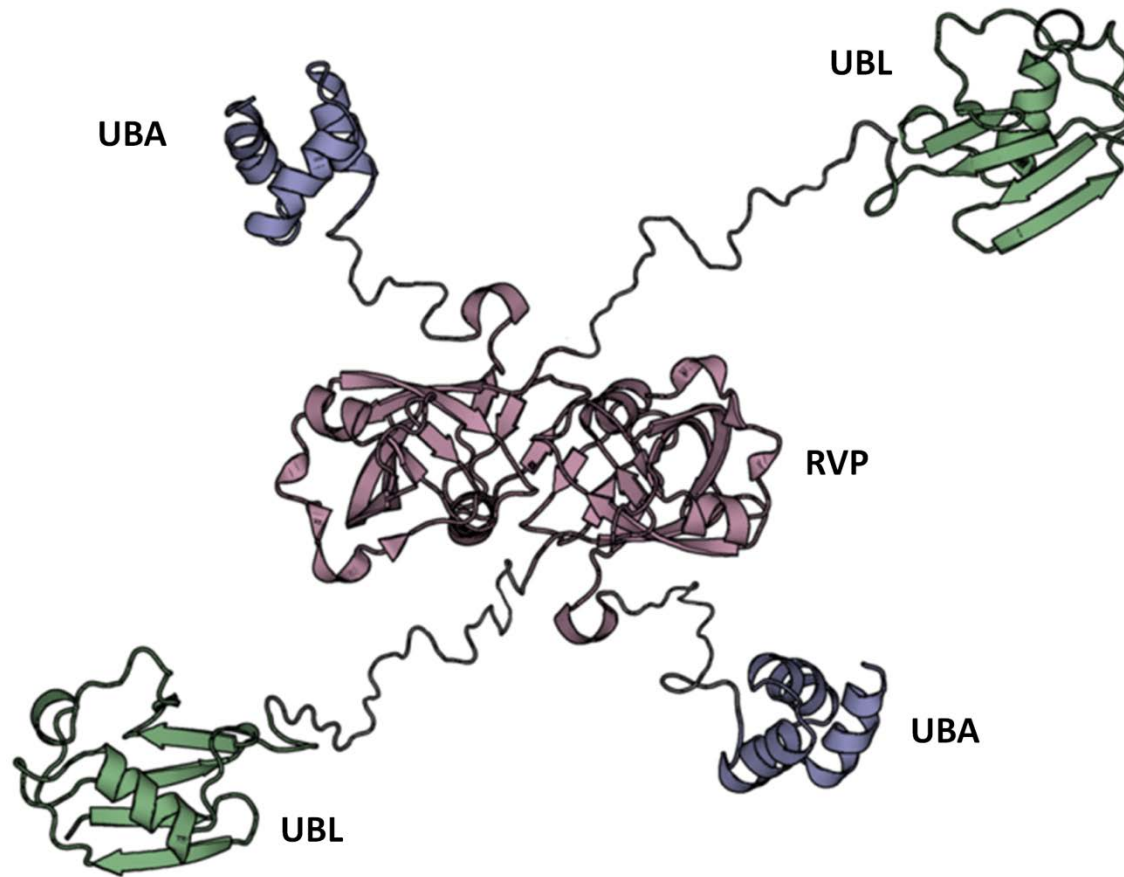


**Figure 3-3. Model structure of Ddi1FL. Model obtained based on NMR data with a use of Ddi1UBA (courtesy Daoning Zhang) and Ddi1UBL structures from these studies and RVP structure from 3S8I pdb record.**

### **3.2 Ddi1 interacts with ubiquitin not only through the UBA domain**

It was already shown that the UBA domain of Ddi1 binds Ub<sup>32</sup>. This phenomenon was also confirmed in detail using NMR studies performed by Daoning Zhang, who estimated that Ddi1UBA and Ub interacts with an equilibrium constant of  $150 \pm 16 \mu\text{M}$  (data not shown). While all NMR studies performed thus far were for the isolated UBA domain of Ddi1, we wanted to test whether these observations hold in the context of full-length Ddi1. For this, we performed NMR binding experiment with Ub and full length Ddi1. Two molar excess unlabeled Ub was added to <sup>15</sup>N labeled FL Ddi1 sample and <sup>1</sup>H-<sup>15</sup>N TROSY spectrum was collected and compared to the spectrum of Ddi1FL alone (Figure 3-4).

As expected, signals corresponding to the Ddi1UBA domain shifted with the same magnitude and direction as for the isolated UBA. Surprisingly, in addition to the shifts of Ddi1UBA domain signals, a greater change in signal positions and intensities for residues corresponding to the Ddi1UBL domain was observed. This entirely unexpected result indicates that Ddi1 interacts with Ub not only through the UBA domain but also through the UBL domain.

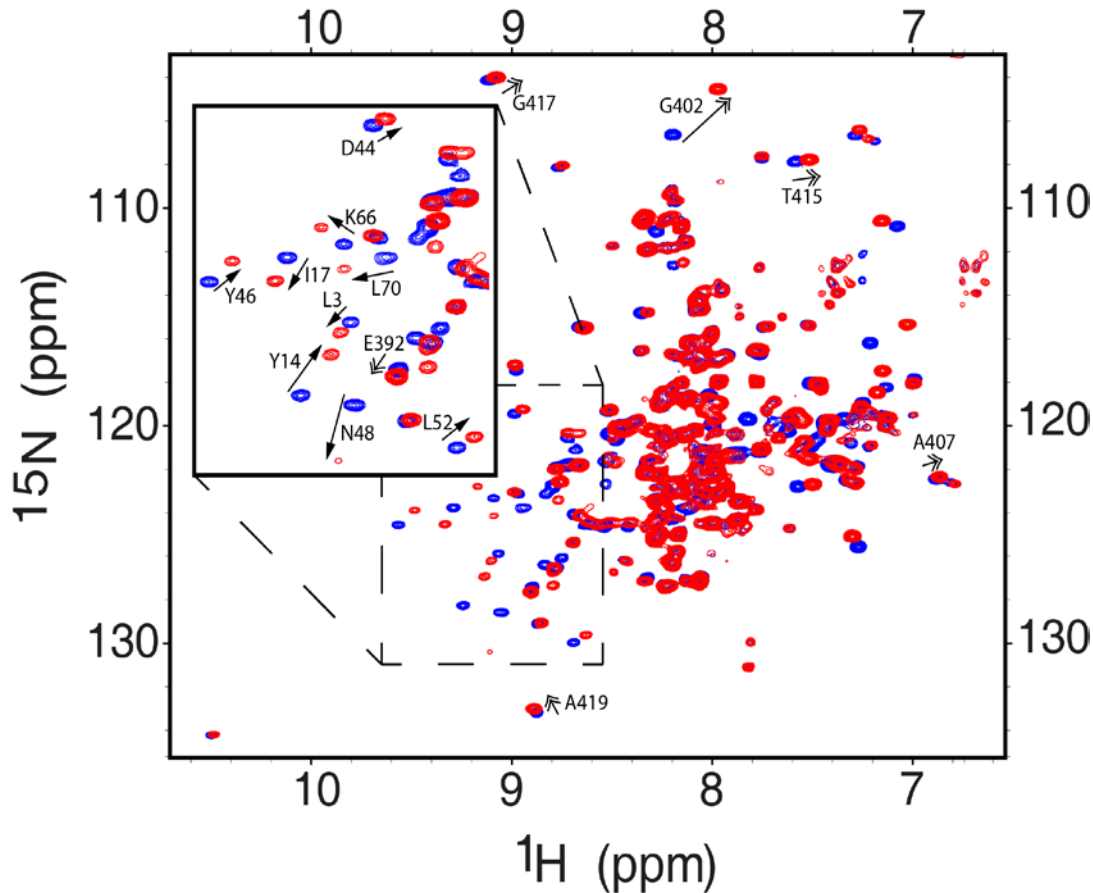


**Figure 3-4. Ddi1FL binding to Ub.** Overlay of the  $^1\text{H}$ - $^{15}\text{N}$  TROSY spectrum of FL Ddi1 alone (blue) and in the presence of Ub at 1:2 molar ratio (red). Single arrow represent shifts of UBL domain peaks, double arrow show shifts in UBA domain.

### 3.3 Ddi1UBL interacts with ubiquitin

UBL-domain signals in the FL Ddi1 spectrum were more affected by the presence of Ub than the signals of the UBA domain. The interaction of a UBL domain with Ub itself has never been reported; therefore we examined Ub binding to an isolated Ddi1UBL domain. When Ub was added to  $^{15}\text{N}$ -labeled Ddi1UBL, a number of residues showed strong chemical shifts perturbations, CSPs (Figure 3-5 and 3-6).

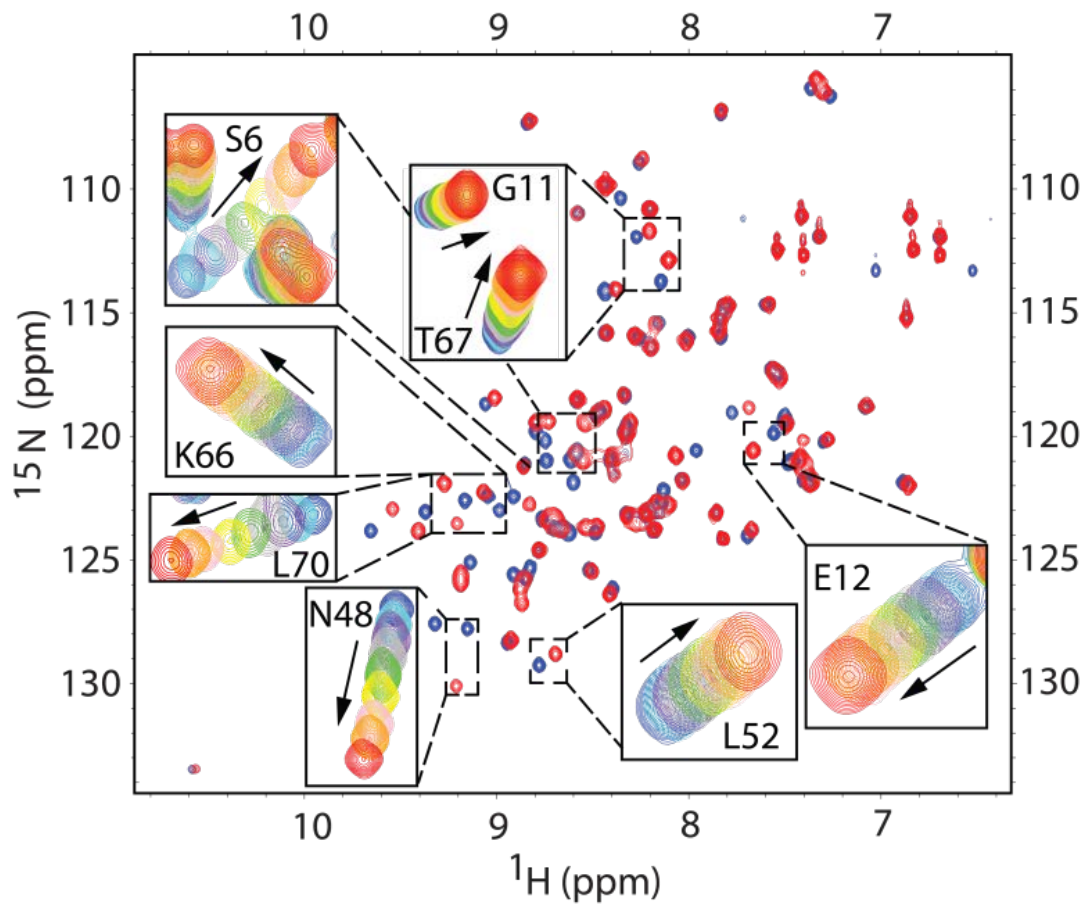


**Figure 3-5. Ub binding to Ddi1UBL. Overlay of the  $^1\text{H}$ - $^{15}\text{N}$  SOFAST-HMQC spectra of the free Ub (blue) and Ub bound to Ddi1UBL domain (red) at saturation (Ddi1UBL:Ub molar ratio 1:5.7). Insets show zoom on selected regions to illustrate gradual shifts in the peak position upon titration for representative residues.**

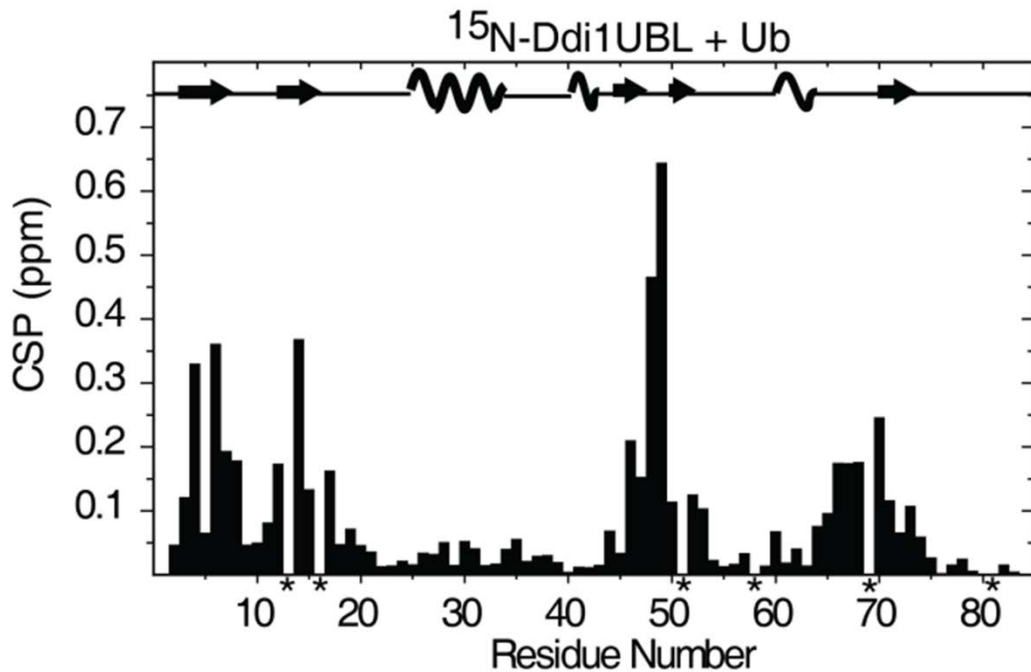


**Figure 3-6. Amide chemical shift differences in Ddi1UBL upon Ub binding.** CSP was obtained at the bound state at the endpoint of titration (molar ratio 1:5.7). Asterisks indicate P16 and those residues where N-H resonances cannot be followed in the spectra due to overlaps.

Mapping residues with CSPs > 0.075 ppm at the endpoint of titration, on the Ddi1UBL structure allowed for the identification of a putative binding site for Ub (Figure 3-7). Ub binding mostly affected residues located on all five  $\beta$ -strands of Ddi1UBL, thus forming a binding surface on the  $\beta$ -sheet side of the protein. It appears that the interaction with Ub is mediated through nonpolar and hydrophobic amino acids G11, L52, L70 but also by some polar and charged residues: T4, S6, E12, N48, K66 and T67. By contrast, the opposite ( $\alpha$ -helix) side of Ddi1UBL does not appear to be involved in Ub binding, as inferred from the almost negligible CSPs observed here. It should be emphasized that the location of the binding site on the  $\beta$ -sheet side of

Ddi1UBL is consistent with the location of the ligand-binding site on Ub and other UBL proteins<sup>36-38,81,82</sup>.

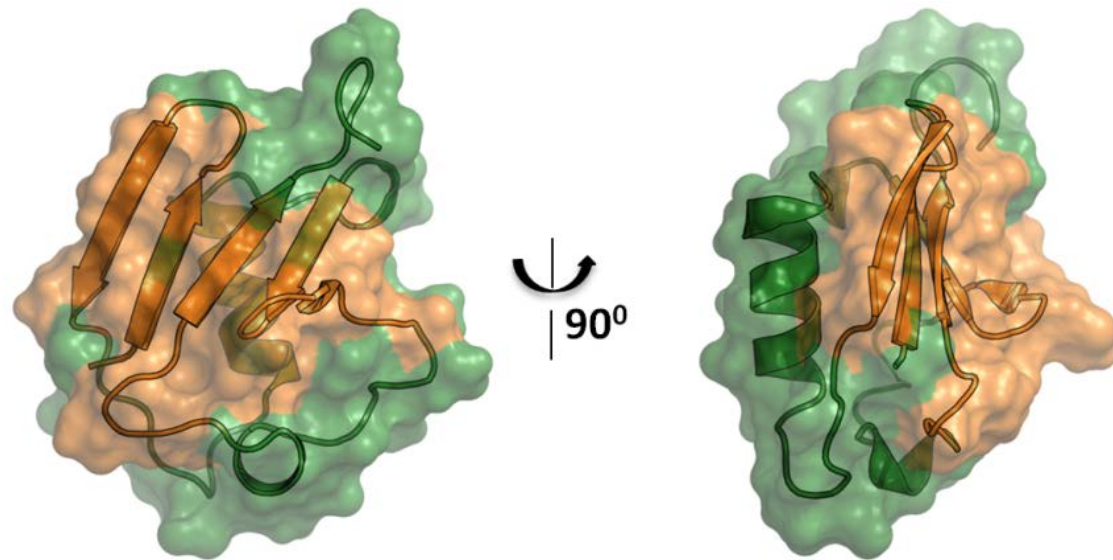


**Figure 3-7. Putative Ub-binding site on Ddi1UBL. Mapping the putative Ub-binding site (orange) on the Ddi1UBL surface (green). CSPs threshold >0.075 ppm was used for mapping in both cases.**

The best fit of titration curves was obtained for the 1:1 binding model and gave an average  $K_d$  value of  $45 \pm 15 \mu\text{M}$  (Figure 3-8). The 1:1 stoichiometry of binding is supported by the  $^{15}\text{N}$  T1 data where Ddi1UBL alone has an average T1 equal to  $601 \pm 37$  ms, while at the titration endpoint, the average T1 is  $951 \pm 52$  ms, which corresponds approximately to the rate that would be expected for moiety of the size of the Ub:Ddi1UBL complex.

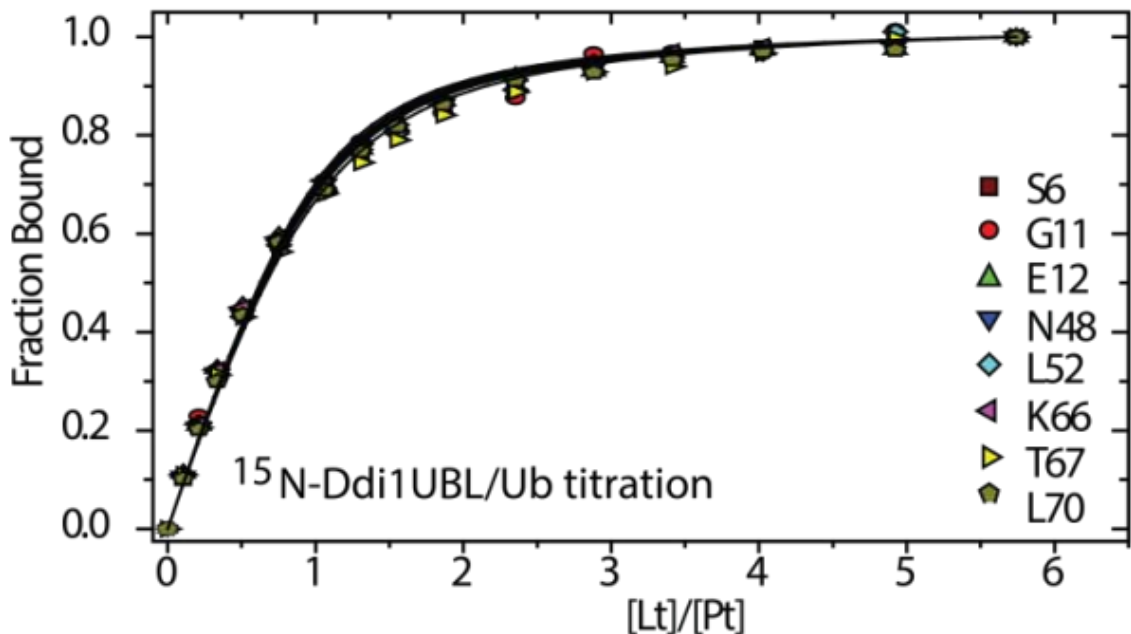


**Figure 3-8.** Titration curves for Ub binding to Ddi1UBL. Titration curves for representative residues from the  $\beta$ -sheet of  $^{15}\text{N}$ -Ddi1UBL involved in interaction with Ub. The lines show fits of the data to a 1:1 binding model.  $^{15}\text{N}$ -Ddi1UBL starting concentration was  $250\mu\text{M}$ .

### 3.4 Ubiquitin interacts with Ddi1UBL through the hydrophobic-patch residues

The unexpected interaction involving Ub raised the question as to whether Ub interacts with Ddi1UBL through the same (hydrophobic-patch) surface as other known Ub ligands, or through a different binding site. To address this question, we titrated  $^{15}\text{N}$ -labeled Ub with unlabeled Ddi1UBL. Upon addition of Ddi1UBL, a number of amide signals of Ub changed their resonance positions significantly (Figure 3-9). Moreover, signals of A46 and G47 disappeared and then reappeared in the course of titration,

which is consistent with slow exchange on the NMR chemical shift time scale, indicative of tight binding.

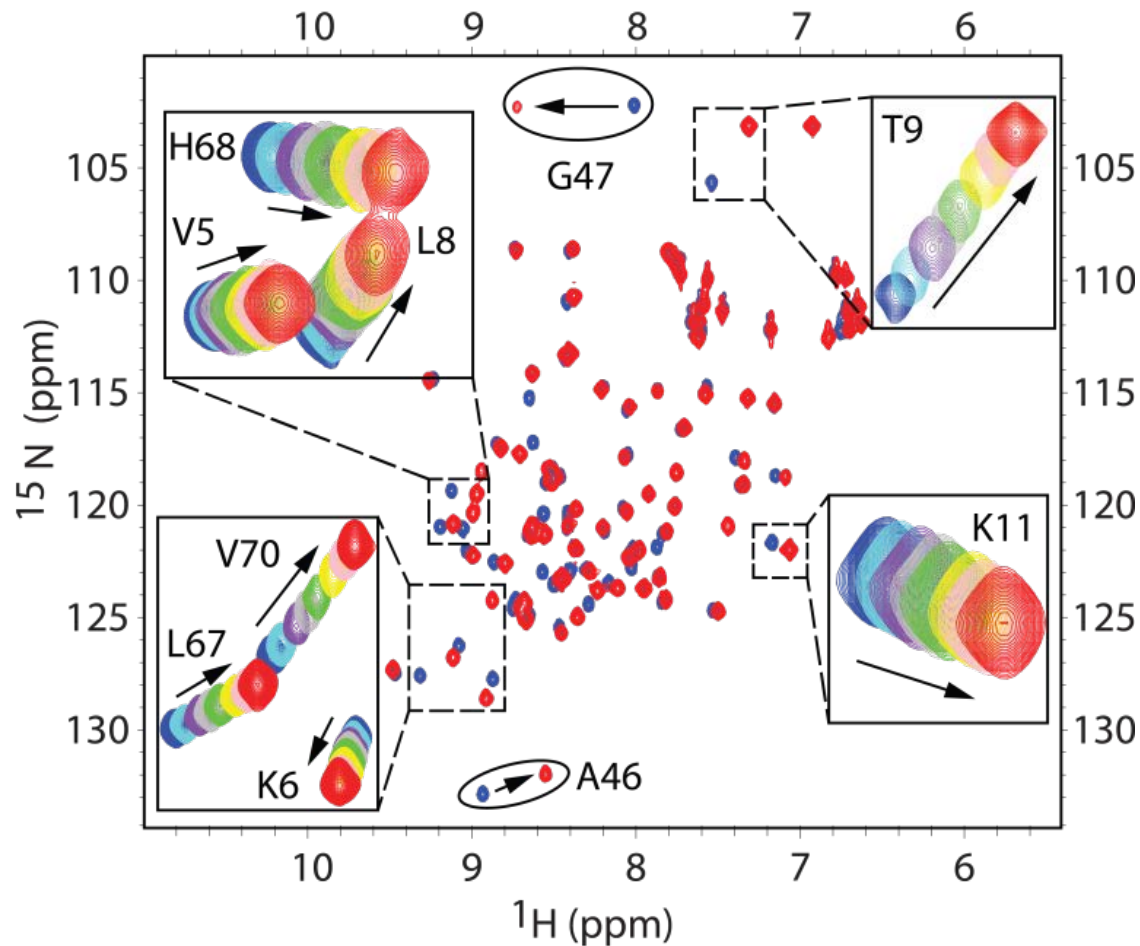


**Figure 3-9. Titration spectra of  $^{15}\text{N}$ -Ub with Ddi1UBL. Superposition of  $^1\text{H}$ - $^{15}\text{N}$  SOFAST-HMQC spectra of  $^{15}\text{N}$ -labeled Ub alone (blue) and saturated with Ddi1UBL (molar ratio 1:5). Signal shifts of the residues used for  $K_d$  estimation are shown in insets. A46 and G47 showing slow exchange upon ligand binding are marked with ovals.**

Interestingly, the overall magnitude of the observed CSPs is similar to that of  $^{15}\text{N}$  Ddi1UBL titrated with Ub (Figure 3-10).

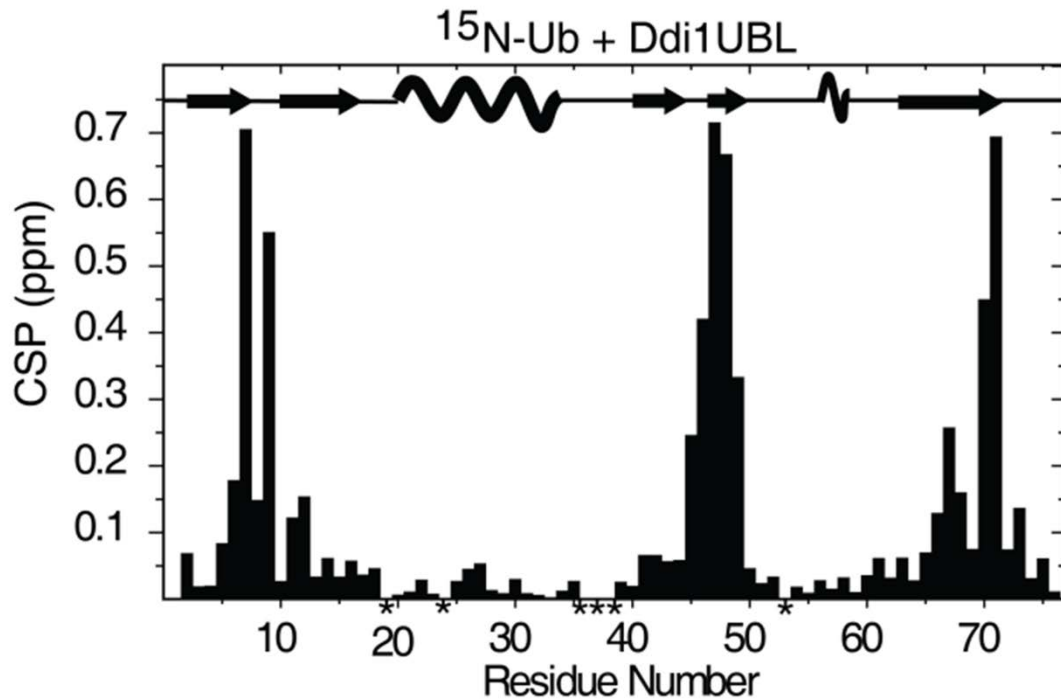


**Figure 3-10. CSP between free Ub and Ub upon saturation with Ddi1UBL.** Saturation was achieved at 1:5 molar ratio. P19, P37 and P38 are marked with asterisks; additionally E24 that is in fast exchange and I36 that does not appear in the SOFAST spectrum are marked with asterisks.

Mapping the observed CSPs on the structure of Ub confirmed that Ub interacts with Ddi1UBL through the same “canonical” hydrophobic patch (centered at residues L8-I44-V70) used to bind other known Ub-ligands (Figure 3-11)<sup>36-38</sup>. Finally, the analysis of titration curves gave the dissociation constant  $K_d=71\pm9 \mu\text{M}$  (averaged over residues with  $\text{CSP}>0.075 \text{ ppm}$ ), in good agreement with the results obtained when

looking at  $^{15}\text{N}$  Ddi1UBL and adding Ub (Figure 3-12). The  $^{15}\text{N}$  relaxation rates gave an average T1 equal to  $956\pm53$  ms, confirming the 1:1 stoichiometry of binding with support from the 1:1 model that gave the best fit of titration curves.

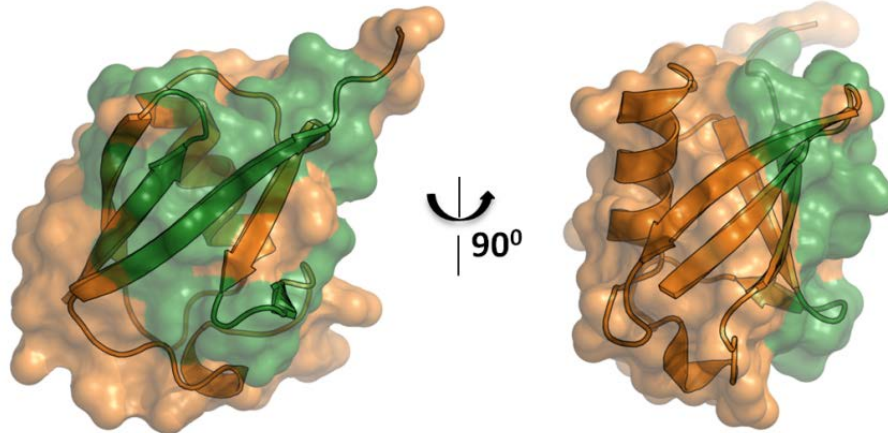


**Figure 3-11. Putative binding side for Ub on Ddi1UBL structure. Ddi1UBL binding site is shown in green on the surface of Ub (orange). Ub structure obtained from 1Ubq.pdb.**

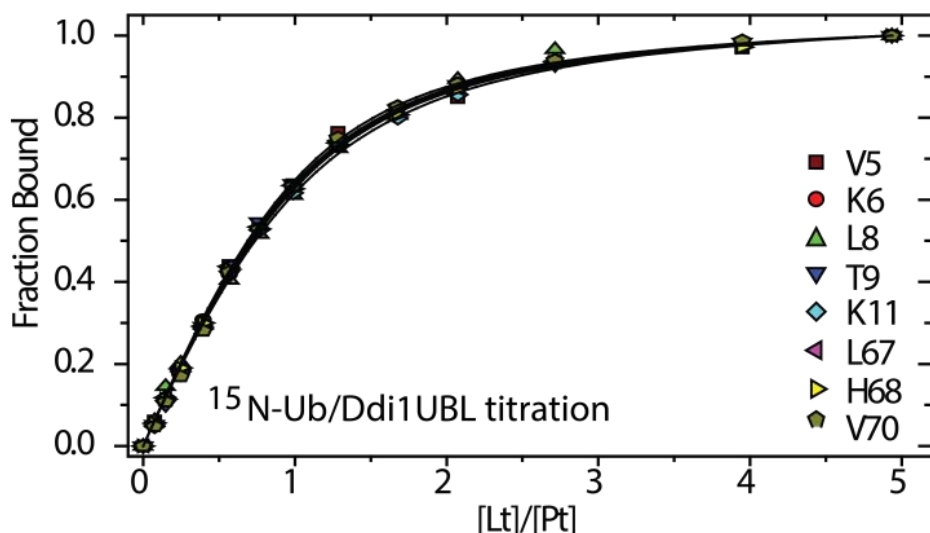


**Figure 3-12. Representative titration curves for  $^{15}\text{N}$ -Ub binding to Ddi1UBL. Data were fitted to 1:1 binding model.**

### 3.5 Ddi1 UBL pulls out ubiquitin conjugates from cell extract

The binding between Ddi1UBL and Ub was also independently verified by a pull-down/IP experiment (Figure 3-13), where immobilized 6xHis-Ub pulled down purified Ddi1UBL, thus providing additional evidence of a physical interaction between the two proteins and confirming the results of NMR studies.

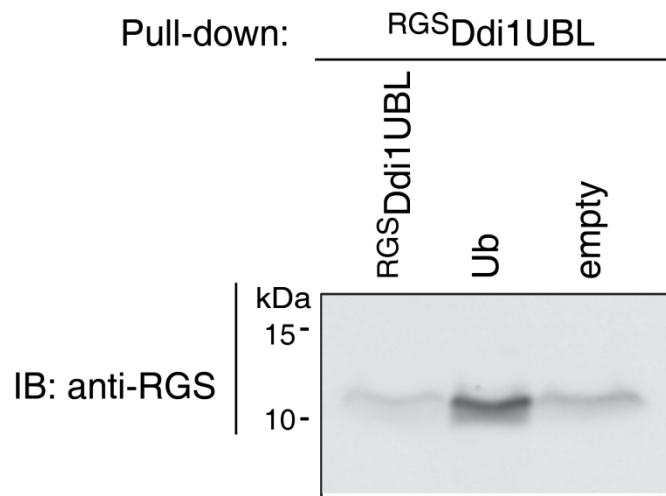


**Figure 3-13.**  $^{6\text{His}}$ Ub Co-immunoprecipitates Ddi1UBL. Purified  $^{6\text{His}}$ DDI1UBL or  $^{6\text{His}}$ Ub was incubated with activated CH-sepharose beads and then incubated with  $^{6\text{His}}$ Ub or  $^{6\text{His}}$ DDI1UBL respectively. Beads were boiled for elution. Data courtesy Daria Krutauz and Michael H. Glickman, Department of Biology, Technion–Israel Institute of Technology, 32000 Haifa, Israel.

Furthermore, 6xHis-Ddi1UBL was capable of pulling out Ub-conjugates from the yeast cell extract lacking Ddi1, DDI1 $\Delta$  (Figure 3-14). The latter result suggests that the unusual capability of the Ddi1 UBL domain to bind Ub could be utilized in the cell.

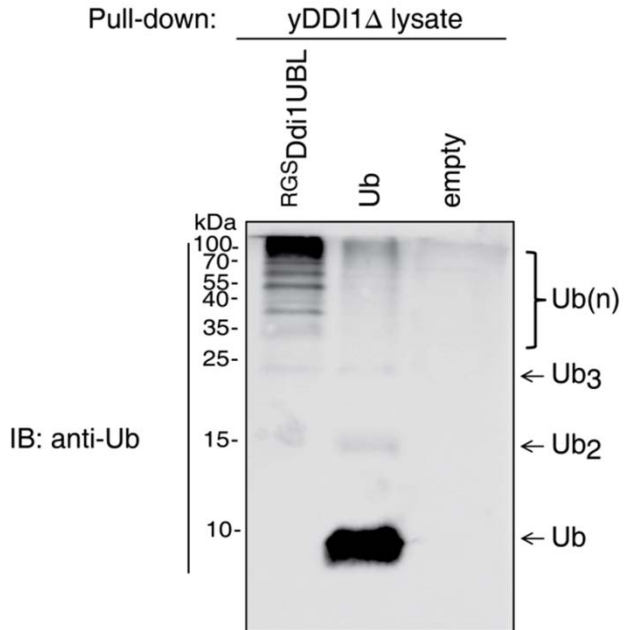


**Figure 3-14. Ddi1UBL pull out ubiquitin conjugates from cell extract.** As previously, purified  $^{6x}\text{His}$ DDI1UBL or  $^{6x}\text{His}$  Ub were incubated with activated CH-sepharose beads. Total protein extract was obtained from growing *DDI1Δ* yeast cells (strain lacking Ddi1 gene). Beads loaded with proteins were incubated with cell extract. Elution was performed by beads boiling. Data courtesy Daria Krutauz and Michael H. Glickman, Department of Biology, Technion–Israel Institute of Technology, 32000 Haifa, Israel.

### 3.6 Ub interacts with UBL domain of Ddi1 but not of Dsk2 or Rad23

Furthermore, we were interested in examining whether the UBL domains from other UBL-UBA shuttle proteins interact with Ub. To test it, the UBL domains of Rad23 and Dsk2 were titrated into  $^{15}\text{N}$ -labeled Ub. No changes in the Ub signal positions were observed, indicating that neither Rad23UBL nor Dsk2UBL interacts with Ub (Figure 3-15). These results confirm that the Ddi1UBL:Ub interaction is entirely unique among the shuttle protein family.

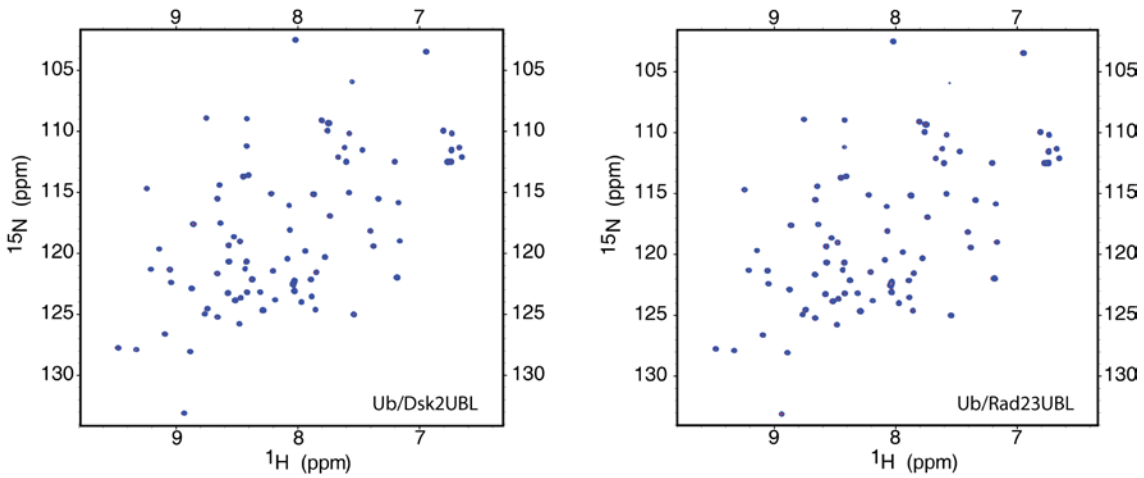


**Figure 3-15. NMR titration of Ub with the UBL domains from Dsk2 and Rad23.** On the left,  $^1\text{H}$ - $^{15}\text{N}$  SOFAST-HMQC spectra overlay of  $^{15}\text{N}$ -Ub alone (red) with the spectrum of  $^{15}\text{N}$ -Ub sample to which Dsk2UBL was added at 1:5 molar ratio (blue). A similar experiment is shown on the right, however, the spectrum of  $^{15}\text{N}$ -Ub (red) is overlaid with the spectrum of  $^{15}\text{N}$ -Ub mixed with Rad23UBL (blue) at 1:2 molar ratio. In both cases the spectra overlay perfectly indicating there is no interaction between Ub and Dsk2UBL as well as Ub and Rad23UBL.

### 3.7 Structure of the Ub:Ddi1UBL complex

As the interaction of Ub and Ddi1UBL is novel and has not been previously studied, we wanted to characterize the structure of this complex. The Ddi1UBL structure and Ub structure obtained from 1Ubq.pdb were used for docking. A structural model of the complex was obtained using the biomolecular docking software HADDOCK<sup>83-85</sup>, along with two sets of experimental intermolecular NMR constraints: (1) ambiguous constraints based on the observed CSPs (Table 3-A) and (2) long-distance constraints (Table 3-B) derived from paramagnetic relaxation enhancement

(PRE) detected in  $^{15}\text{N}$ -Ddi1UBL after attaching a nitroxide spin-label (MTSL) to residue 12 of Ub (UbT12C variant), in a 1:1 Ub: Ddi1UBL complex. The derived structure of the Ub:Ddi1UBL complex is shown in Figure 3-16. The backbone RMSD between 8 lowest energy structures from this cluster was  $0.94 \pm 0.33$  Å.

<b>Ub:Ddi1UBL Complex</b>		
<b>Ubiquitin</b>	<b>Active Residues</b>	<b>6,8,9,12,46,47,49,68,71,72,73</b>
	<b>Passive Residues</b>	<b>2,10,14,39,44,48,51,52,64,74,75,76</b>
<b>Ddi1UBL</b>	<b>Active Residues</b>	<b>4,8,11,12,15,17,48,49,50,53,66,67,68</b>
	<b>Passive Residues</b>	<b>1,2,6,9,10,13,16,21,44,46,51,54,55,56,58,64,70,72,74,75</b>

**Table 3-A.** Active and passive residues used for docking of Ub-Ddi1UBL complexes. Docking was performed with HADDOCK software. Identification of active and passive residues was done based on the information from titration data with support of NACCESS analysis that allows for quantification of individual amino acids accessibility<sup>86</sup>.

## Ub:Ddi1UBL Complex Constraints

<b>Distance ID #</b>	<b>Protein</b>	<b>Residue</b>	<b>Atom</b>	<b>Protein</b>	<b>Residue</b>	<b>Atom</b>	<b>Distance [Å]</b>
1	Ubiquitin	CYM	OAH	Ddi1UBL	2	H <sub>N</sub>	15.84
2		CYM	OAH		3	H <sub>N</sub>	16.07
3		CYM	OAH		4	H <sub>N</sub>	15.39
4		CYM	OAH		17	H <sub>N</sub>	17.75
5		CYM	CYM		48	H <sub>N</sub>	14.51
6		CYM	OAH		49	H <sub>N</sub>	15.02
7		CYM	OAH		50	H <sub>N</sub>	16.71
8		CYM	OAH		64	H <sub>N</sub>	15.97
9		CYM	OAH		65	H <sub>N</sub>	12.84
10		CYM	OAH		66	H <sub>N</sub>	11.14
11		CYM	OAH		67	H <sub>N</sub>	9.95
12		CYM	OAH		68	H <sub>N</sub>	9.12
13		CYM	OAH		69	H <sub>N</sub>	11.3
14		CYM	OAH		70	H <sub>N</sub>	14.2

**Table 3-B. Distance constraints for Ub:Ddi1UBL complex based on MTS defense studies.**  
The spin label was attached to residue 12 in Ub (UbT12CD77) and signal attenuation was observed on <sup>15</sup>N-Ddi1UBL. The MTS defense attached to Cys12 is denoted as CYM residue.

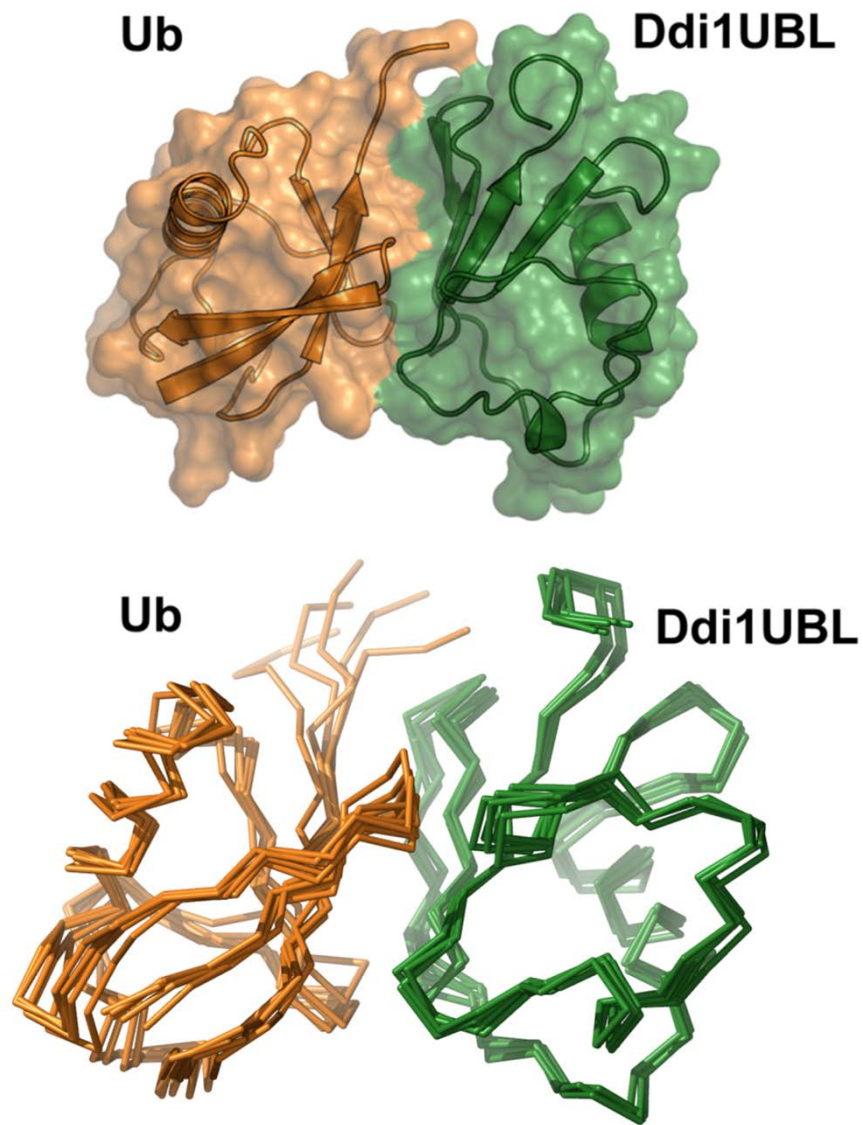


**Figure 3-16. Haddock derived structure of the Ub:Ddi1UBL complex. Ddi1UBL is shown in green while and Ub is shown in orange. Overlay of five structures of Ub:Ddi1UBL complex from the top cluster generated by HADDOCK. Shown are backbone traces for Ub (orange) and UBL (green), superimposed by secondary structure elements; the backbone RMSD was  $0.94 \pm 0.33 \text{ \AA}$ . Complex was obtained with help of Olivier Walker, Institut des Sciences Analytiques, UMR5280-Université de Lyon, 69100 Villeurbanne, France.**

To further examine the structure, the coordinates of Ddi1UBL in the complex were used to reconstruct the position of the spin label on Ub from the complex structure. The calculated position matched almost ideally the position of the ubiquitin cysteine residue to which MTSL was attached (Figure 3-17a). To independently validate the structure of the Ub:Ddi1UBL complex, we used two separate sets of site-specific spin labeling/PRE data that was not used for the docking. Specifically, as a positive control, we attached MTSL to residue 75 in Ub (Ub G75C), and, in a separate experiment, to residue 63 (UbK63C), as a negative control. The experimental data showed a strong site-specific PRE effect on Ddi1UBL when MTSL was placed on Cys75 of Ub. When the complex structure was used to reconstruct the spin label's position, the back-calculated attenuations in signal intensities matched those observed experimentally. Furthermore, the reconstruction placed the MTSL in close proximity as well, thus confirming that the Ub/Ddi1UBL structure is correct (Figure 3-17b). Finally, we did not detect any major/systematic PRE effects in Ddi1UBL when MTSL was attached to UbK63C. In the complex structure the distance between residue 63 of Ub to amides of Ddi1UBL is about 25Å, which is the MTSL's PRE range, hence is too far to cause significant PRE effects (Figure 3-17c).

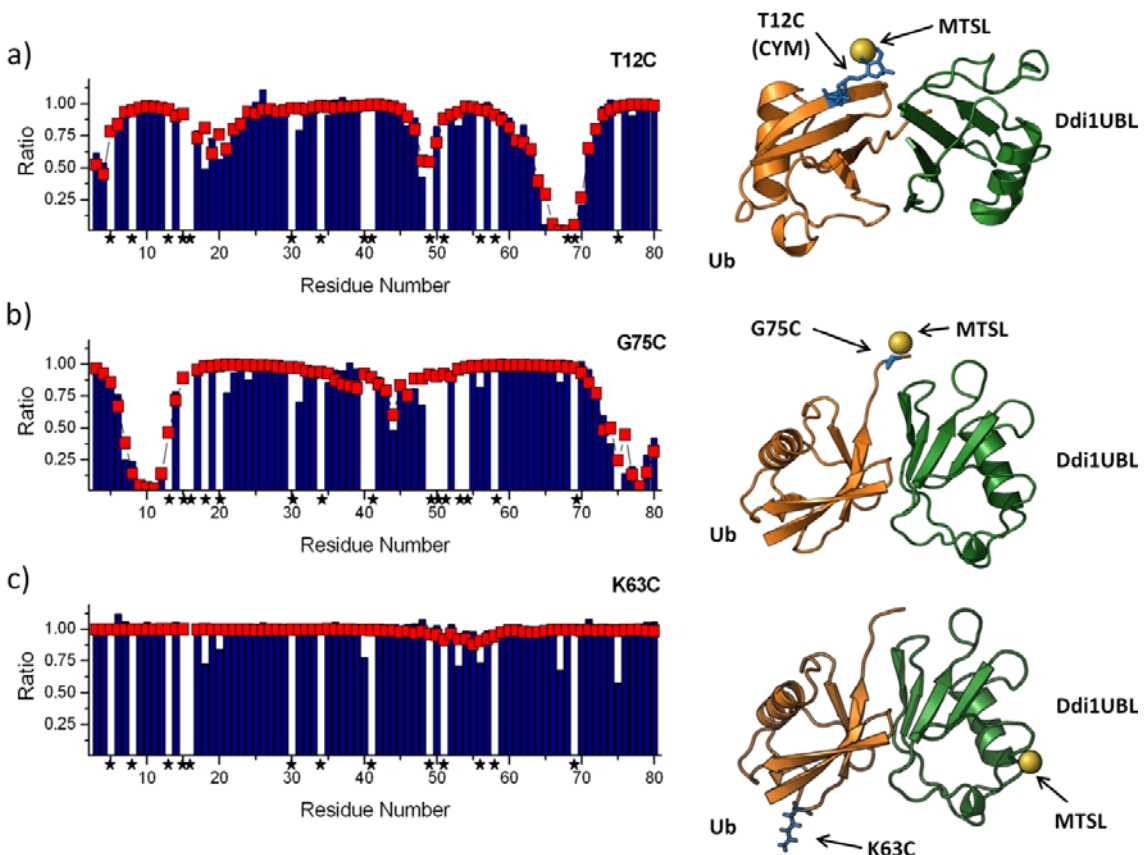


**Figure 3-17. Validation of the NMR-derived (HADDOCK) structure of Ub:Ddi1UBL complex using site-specific paramagnetic spin-labeling.** Signal attenuations in Ddi1UBL caused by MTS defense system attached to the proper cysteine mutant, T12C (a), G75C (b) and K63C (c). On the left, signal attenuations in Ddi1UBL from experimental data (blue bars) and calculated based on the complex structure (red squares), overlapping signals are marked with asterisks. The positions of the spin label's unpaired electron reconstructed from experimental data in the complex structure for each of the mutant are shown as spheres. Locations of the amino acids that were muted to Cys are indicated as sticks. Ub structure is presented in orange, Ddi1UBL structure is shown in green.

When studying the Ud:Ddi1UBL complex interface in detail it can be noticed that the interaction between the two proteins is mainly mediated through side chains of hydrophobic amino acids (Figure 3-18 and 3-19). Ub exploits its classical hydrophobic patch: L8-I44-V70, whereas Ddi1UBL utilizes I13, L70, and L72 that corresponds to the analogous hydrophobic patch on the UBL surface. The total buried surface area due to the created interface was estimated to be around  $1500 \text{ \AA}^2$ .

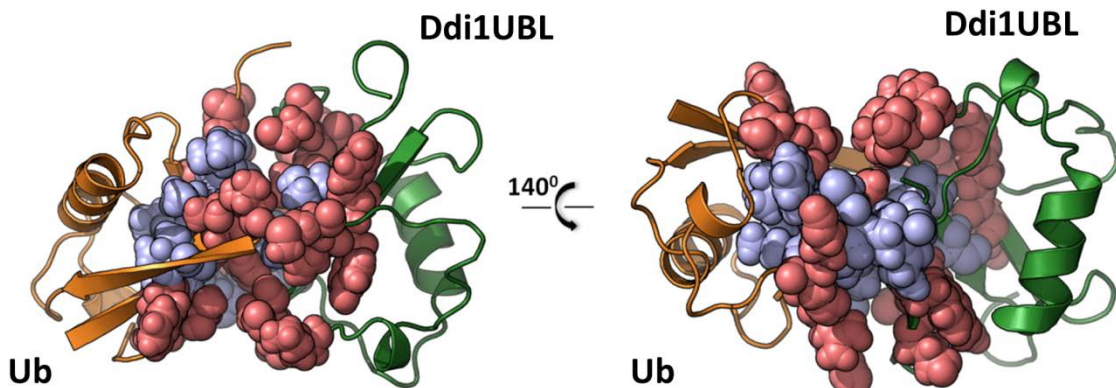


**Figure 3-18. Interface between Ddi1UBL and Ub.** Hydrophobic amino acids are shown as blue spheres, polar and charged amino acids are in salmon. Ribbon colors Ub (orange), Ddi1UBL (green).

As shown the hydrophobic interaction is stabilized by several electrostatic and polar contacts surrounding hydrophobic amino acids of both complex components. An example of such a pair of contacts is the interaction of K6 (Ub) with D68 (Ddi1), R42 (Ub) and R72 (Ub) with E8 (Ddi1), as well as H68 (Ub) and D2 (Ddi1) (Figure 3-19).

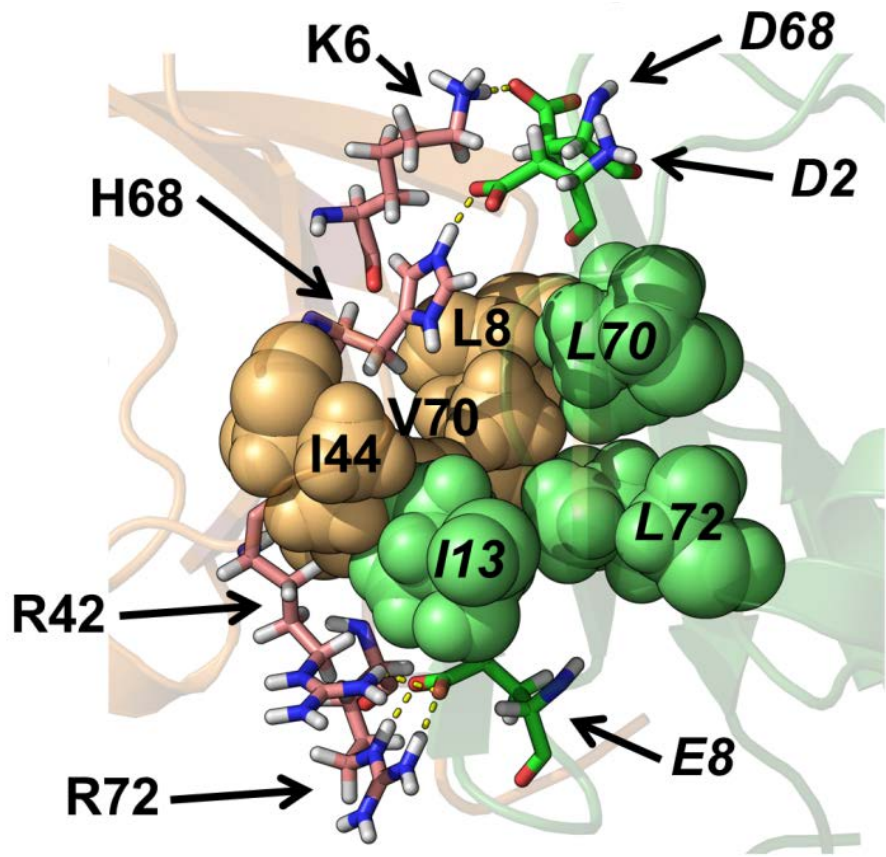


**Figure 3-19.** Side chains contacts at the interface of the Ub:Ddi1UBL complex. Hydrophobic amino acids of Ub: L8, I44, V70 (orange) and Ddi1: I13, L70, L72 (green) are shown as spheres. In sticks are shown amino acids of Ub: K6, R42, H68, R72 (pink) and Ddi1UBL: D2, E8, D68 (green) that create polar contacts (yellow dash lines).

### 3.8 Ufo1UIMs interact with ubiquitin but not with Ddi1

As mentioned above, Ufo1 was the only identified binding partner that interacted with Ddi1UBL<sup>56</sup>. Therefore, we wanted to study Ddi1 binding to the UIM domains of Ufo1 (Ufo1UIMs). For this purpose, we titrated <sup>15</sup>N-Ddi1UBL with the

unlabeled Ufo1UIMs construct containing three UIM domains (Figure 3-20a). Surprisingly, despite reaching a very high saturation, even at the Ufo1UIMs:Ddi1UBL molar ratio of 10:1 no significant changes in the Ddi1 spectrum were detected (Figure 3-20b).

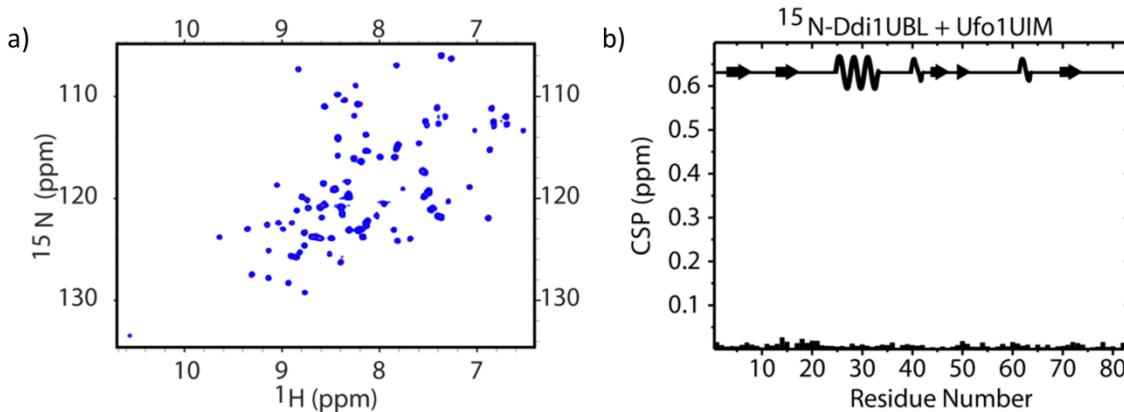


**Figure 3-20. Ufo1UIMs binding to Ddi1UBL.** (a) Demonstration of lack of changes in the Ddi1UBL spectrum (red) under presence of Ufo1UIM in the sample (blue) at 1:10 molar ratio. (b) CSP quantification of Ddi1UBL interaction with Ufo1UIMs at saturation.

To verify the lack of binding between the two proteins, a reverse titration was performed, by adding unlabeled Ddi1UBL to  $^{15}\text{N}$ -labeled Ufo1UIMs; the Ufo1UIMs signals also did not show any perturbations even at 10-fold excess of Ddi1UBL (Figure 3-21a). A similar lack of binding was observed in FL Ddi1 when titrating it with Ufo1UIMs up to 10:1 molar ratio (Figure 3-21b). Combined, all these results indicate that Ddi1 does not interact directly with Ufo1UIMs.

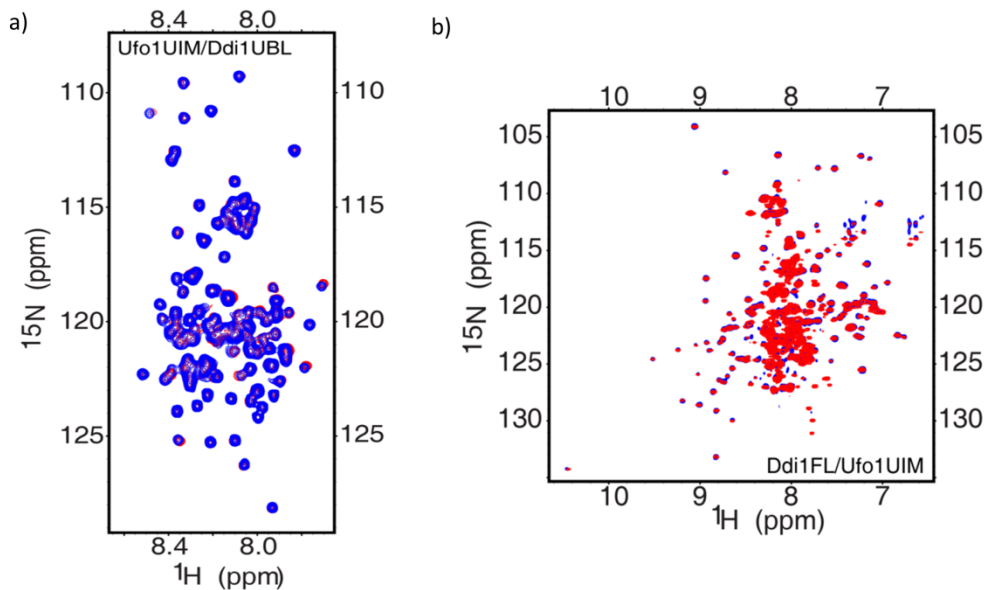


**Figure 3-21. Lack of interaction of Ufo1UIM with Ddi1UBL and Ddi1FL.** (a) Overlay of the <sup>1</sup>H-<sup>15</sup>N SOFAST-HMQC spectrum of Ufo1UIM (red) upon saturation (blue) with Ddi1UBL. (b) Overlay of the <sup>1</sup>H-<sup>15</sup>N TROSY spectrum of <sup>15</sup>N-Ddi1FL alone (red) and saturated with Ufo1UIM (blue), also at 1:10 molar ratio.

Since it was known that the Ddi1FL and Ddi1UBL protein samples were active, we wanted to confirm that the Ufo1UIMs protein is in its folded state after expression and purification and therefore capable of performing its function. The CD spectrum of Ufo1UIMs confirms the presence of  $\alpha$ -helical and some random coil elements, which matches prediction that Ufo1 has UIM helices connected through unstructured linkers (Figure 3-22).

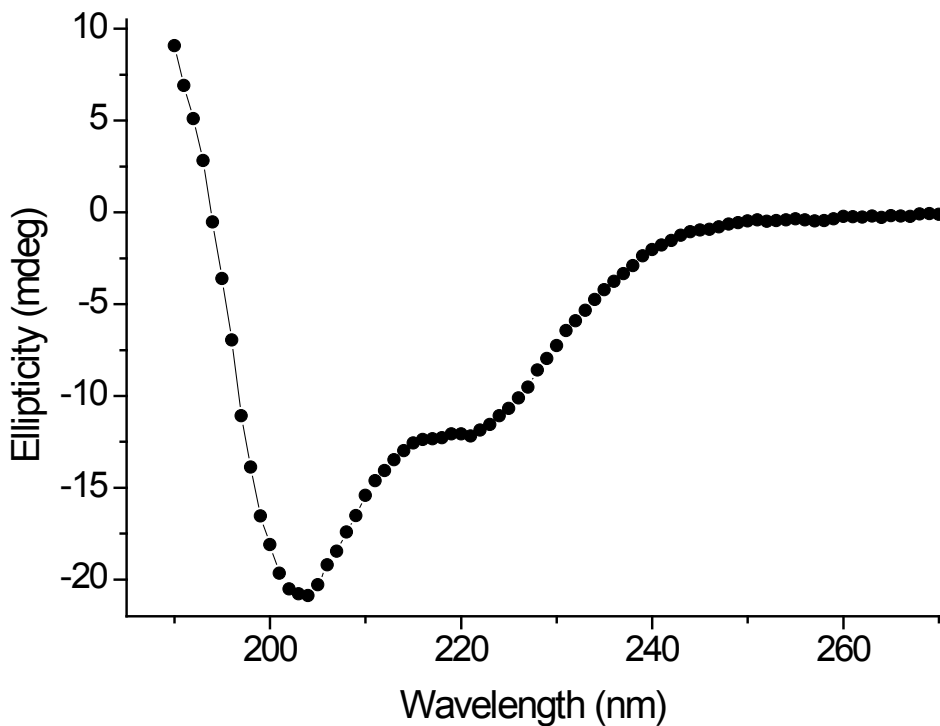


**Figure 3-22. CD spectrum of Ufo1UIM. The CD spectrum was measured in 20mM NaP buffer pH 6.8.**

If a protein that has three UIM domains is active, the addition of Ub should promote changes in the Ufo1UIMs' spectrum. As expected, when the  $^{15}\text{N}$  Ufo1UIMs sample was mixed with Ub at a 1:1 ratio, shifts and signal attenuations several residues were observed (Figure 3-23a). Confirmation of binding was also observed when  $^{15}\text{N}$  Ub sample was mixed with Ufo1UIMs (Figure 3-23b).

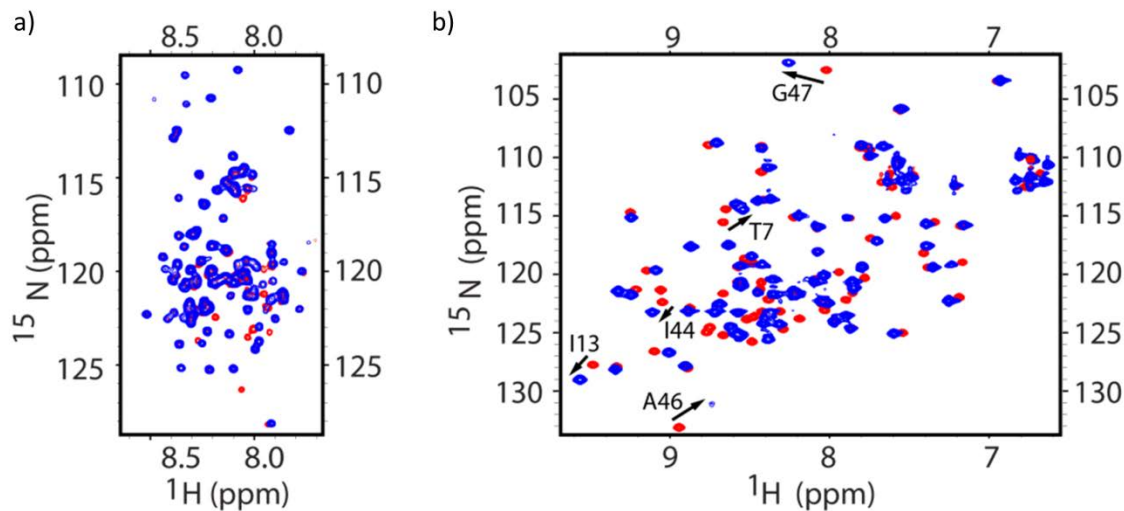


**Figure 3-23. Ufo1UIMs recognize Ub.** (a) Comparison of the peaks position in the spectrum of Ufo1UIM alone (red) and upon addition of Ub (blue), ratio 1:1. (b) Reference <sup>1</sup>H-<sup>15</sup>N spectrum of Ub (red) overlaid with the spectrum of Ub mixed with Ufo1UIM at 1:1 ratio (blue). Some of the major shifts in the peak positions are indicated with arrows.

A full titration of <sup>15</sup>N Ub with Ufo1UIMs was performed until saturation was reached (at 5:1 molar ratio) which allowed quantification of changes in the Ub spectrum using CSP (Figure 3-24a). As above, residues with significant CSPs allowed the identification of the hydrophobic patch as being the site for Ufo1UIMs binding (Figure 3-24b).

Taking into account the presence of three UIMs in Ufo1UIMs, the average dissociation constant for UIM/Ub interaction was estimated to be  $\sim 237 \pm 52 \mu\text{M}$  (Figure 3-25).

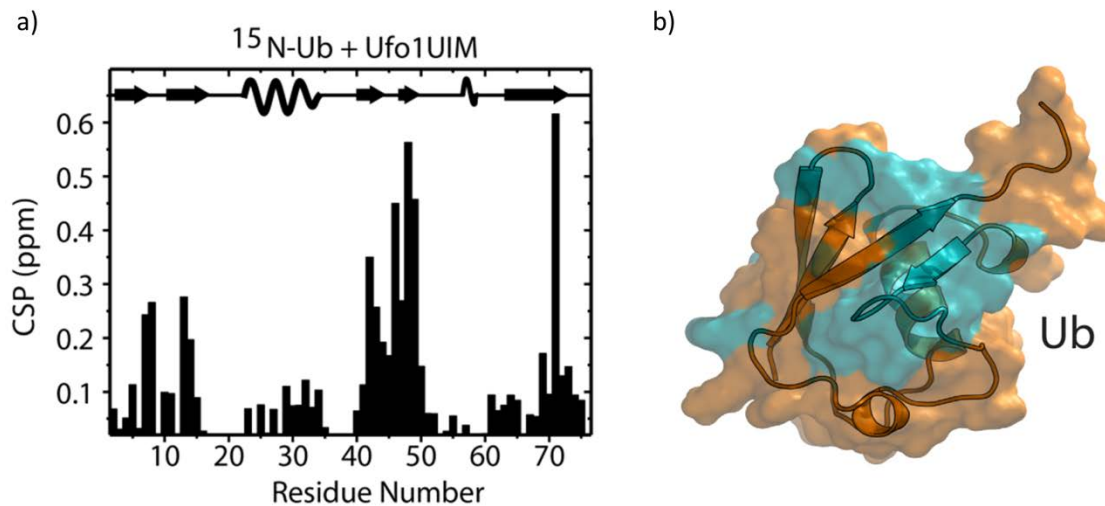


**Figure 3-24.** Ub recognizes Ufo1UIMs through the hydrophobic patch. (a) CSP plot for Ub at titration endpoint (Ub:Ufo1UIM ratio = 1:5). (b) Illustration of position where UIM domains of Ufo1 bind to Ub (cyan), Ub showed in orange. Ub structure was taken from 1Ubq.pdb.

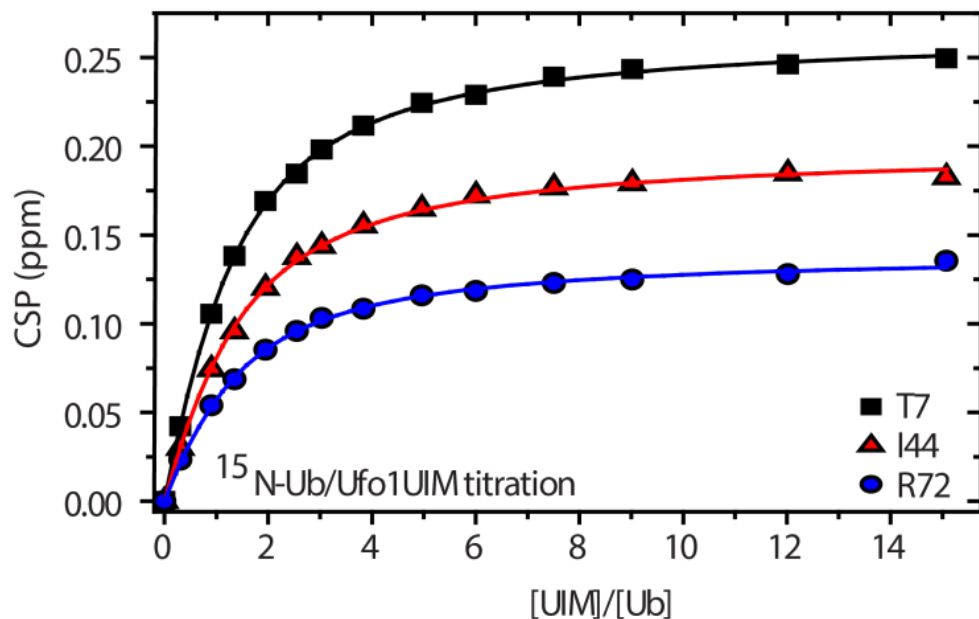


**Figure 3-25.** Representative titration curves for Ufo1UIMs binding to Ub. Shown are titration curves of Ub T7, I44, and R72 residues that are close to hydrophobic patch.

### **3.9 Ddi1UBL and Ub:Ddi1UBL complex crystallization**

To further understand the protein structures and interactions, Ddi1UBL as well as the Ub:Ddi1UBL complex can be crystallized. For the purpose of crystallization both samples were kept in 20mM HEPES buffer at pH 7.5. For screening crystallization conditions, the following types of screening suites were used: Index (Hampton), Wizard I and II (Emerald), PEG Suite (Qiagen), Cryo Suite (Qiagen), Natrix (Hampton). For Ddi1UBL, a concentration of 22mg/ $\mu$ L was used, while the complex sample concentration was 52 mg/ $\mu$ L. Precipitant was present in a number of conditions in PEG, Index, Wizard I and II and Natrix suites both for Ddi1UBL alone as well as for the complex. The Cryo suite had only a few hits with precipitation for Ddi1UBL but not for the complex. The crystals were only observed for the Ub:Ddi1UBL complex in the INDEX suite and the most promising results were in the following conditions (Figure 3-26):

- INDEX 3: 0.1 M BIS-TRIS pH 5.5, 2.0 M ammonium sulfate
- INDEX 6: 0.1 M Tris pH 8.5, 2.0 M ammonium sulfate
- INDEX 20: 0.1 M HEPES pH 7.5, 1.4 M sodium citrate tribasic dehydrate
- INDEX 21: 1.8 M ammonium citrate tribasic pH 7.0
- INDEX 27: 2.4 M sodium malonate pH 7.0
- INDEX 29: 60% v/v Tacsimate TM pH 7.0

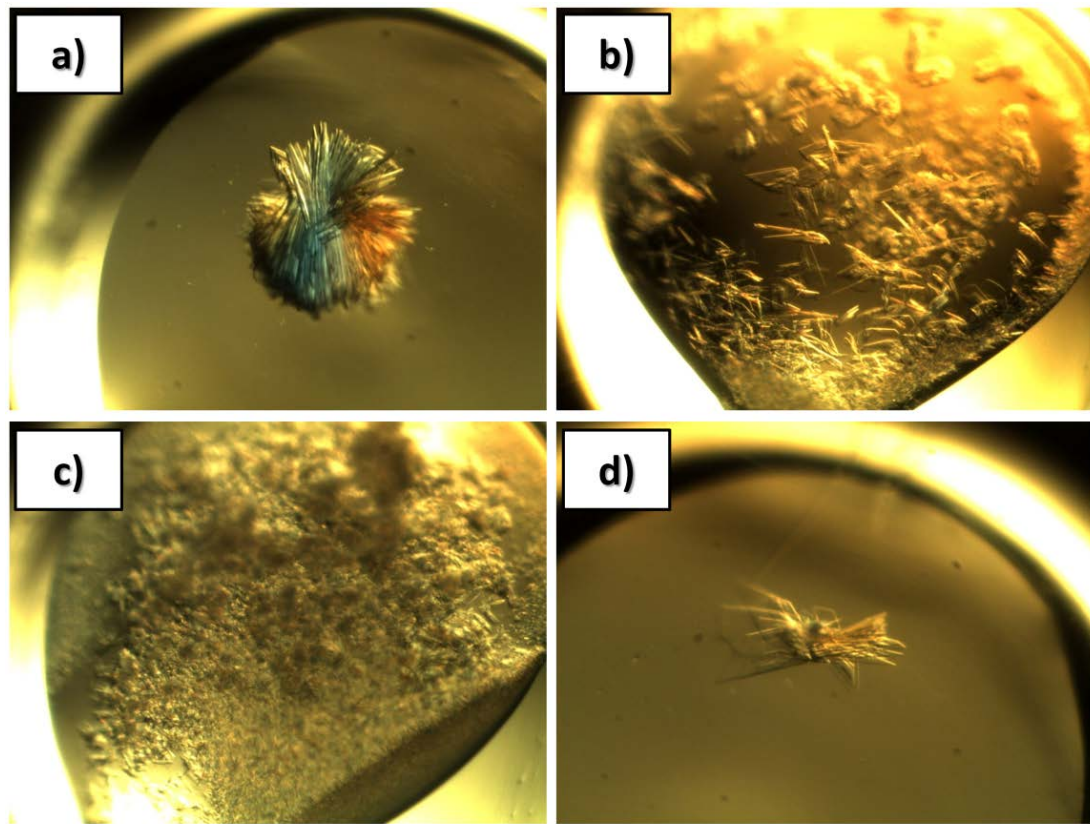


**Figure 3-26. Potential crystal hits of Ub:Ddi1UBL complex from the INDEX screening suite. a) INDEX 6: 0.1 M Tris pH 8.5, 2.0 M ammonium sulfate; b) INDEX 20: 0.1 M HEPES pH 7.5, 1.4 M sodium citrate tribasic dehydrate; c) INDEX 27: 2.4 M sodium malonate pH 7.0; d) INDEX 29: 60% v/v Tacsimate TM pH 7.0.**

# **Chapter 4. Ddi1UBL, first known ubiquitin like domain with a UIM motif**

## **4.1 Ddi1 heterodimerization with other shuttle proteins**

As previously mentioned, it is common for the shuttle proteins to homo- and hetero-dimerize. Till now, it was thought that these interactions were mediated through the classical binding of UBA to UBL domains. It is unclear whether and how Ddi1 is involved in heterodimerization with Dsk2 and Rad23. Due to this reason, and because of the unusual properties of Ddi1UBL, we wanted to study the interactions between the shuttles in detail, with the main focus on Ddi1<sup>29,30,61</sup>. Ideally both UBA and UBL domains can be used for interactions with Dsk2 and Rad23; therefore first we tested interactions between FL Ddi1 and the UBL domains of Rad23 and Dsk2 (Figure 4-1). As shown, Ddi1 binds differently to Dsk2UBL and Rad23UBL. Upon addition of Rad23UBL to Ddi1FL only a limited number of changes are observed, in the case of Dsk2UBL the changes in the spectrum are significant. Moreover, signals arising from the Ddi1UBL are very often invisible, while signals of the UBA domain of Ddi1 show just small shifts. This indicates that there is significant interaction between Ddi1UBL and Dsk2UBL.

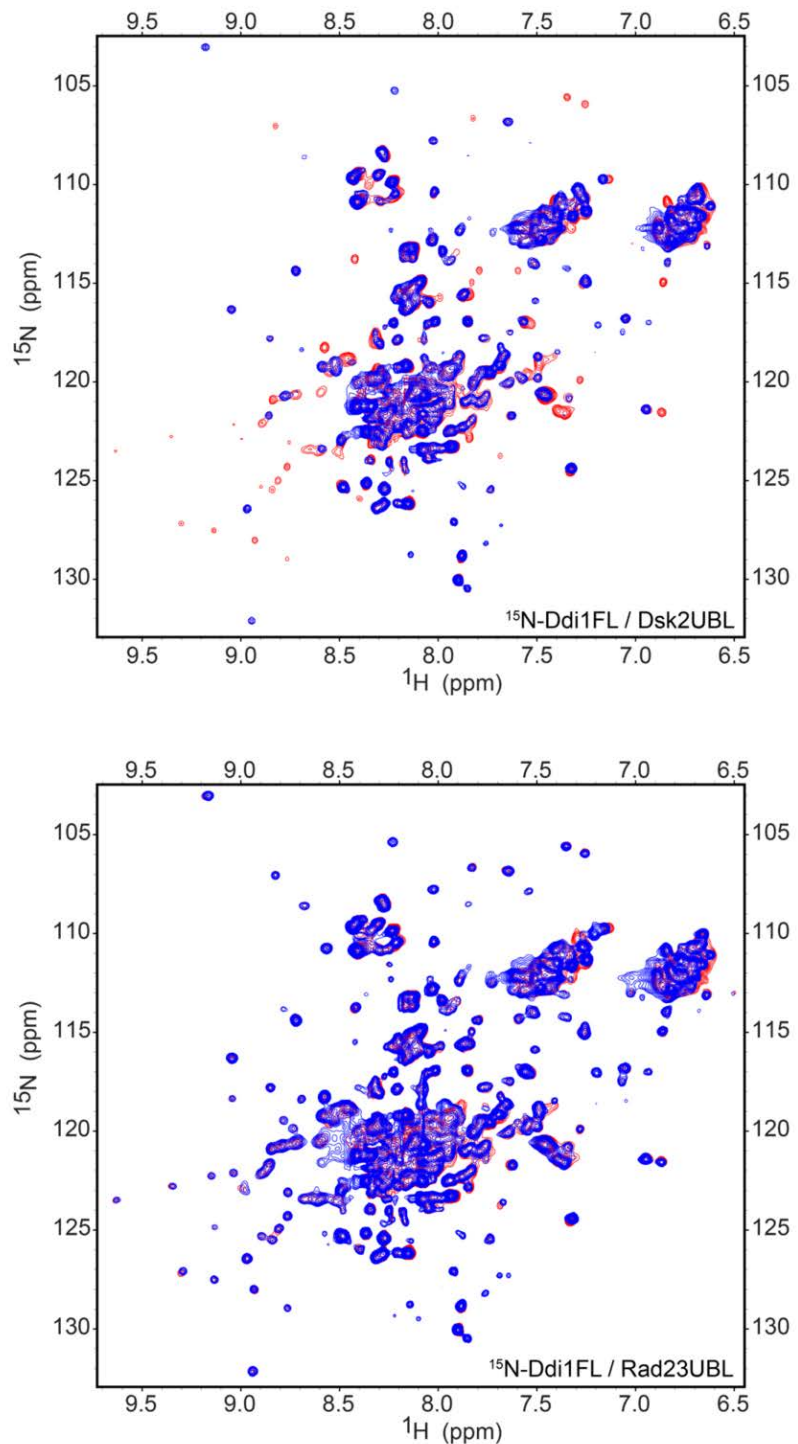


**Figure 4-1. Binding of UBL domains of Dsk2 and Rad23 to full length Ddi1.** The spectrum of FL Ddi1 is shown in red, and the spectrum obtained upon binding is shown in blue. Top, 250 $\mu$ M  $^{15}\text{N}$ -Ddi1FL at 1:3 ratio with the UBL domain of Dsk2. Bottom, 250 $\mu$ M  $^{15}\text{N}$ -Ddi1FL at 1:2 ratio with Rad23UBL.

We also wanted to check how the spectrum of full length Dsk2 and Rad23 would be affected in the presence of the Dd1iUBL domain (Figure 4-2). When Dsk2FL is titrated with Ddi1UBL, signals that correspond to the Dsk2UBL domain either attenuate or show shifts that complement results from previously observed binding experiments. As expected, in the case of Rad23 there are no easily noticed differences between spectra.

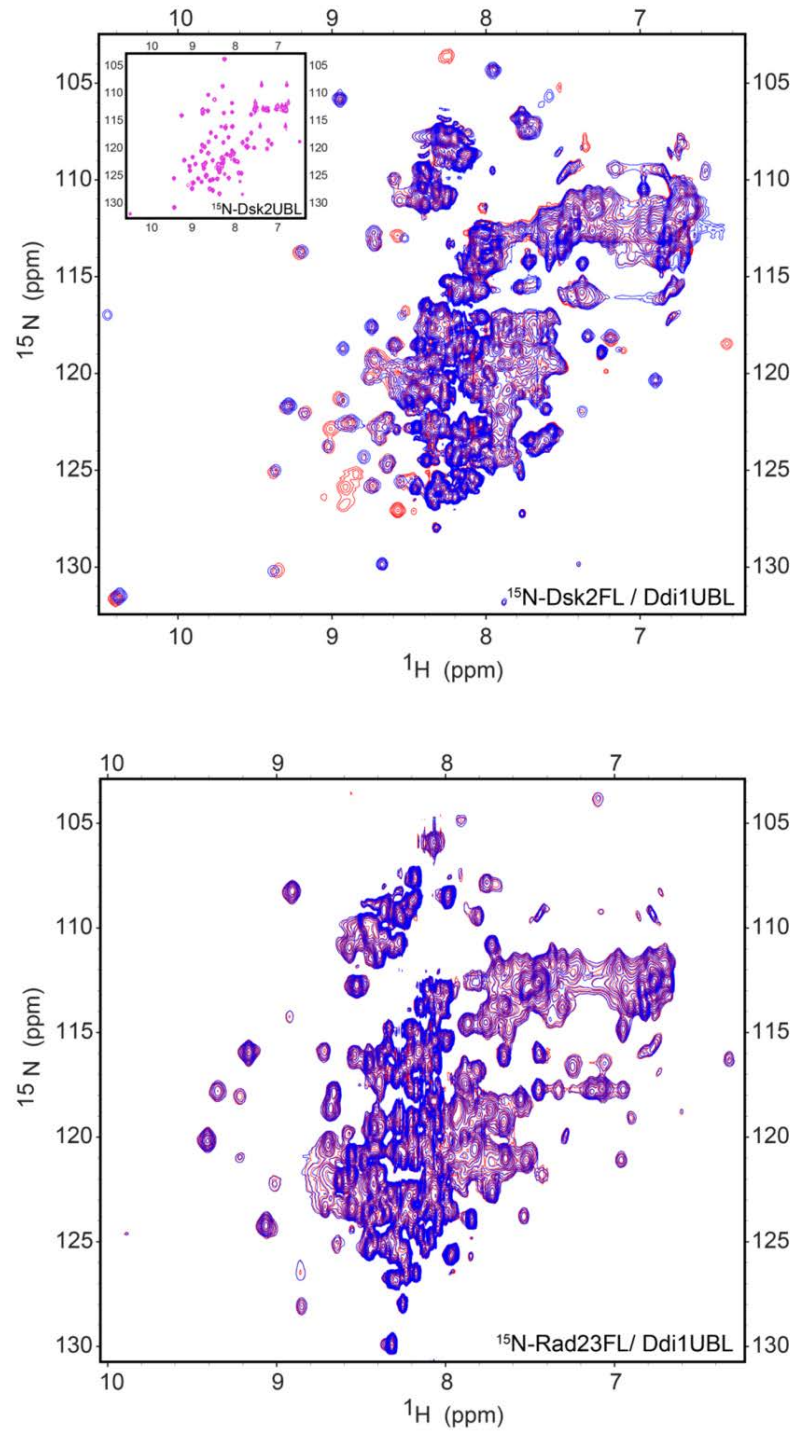


**Figure 4-2. Binding of UBL domain of Ddi1UBL to full length Dsk2 and Rad23. The spectra of FL constructs are shown in red, while the spectra obtained upon binding are shown in blue. Top, 165 $\mu$ M <sup>15</sup>N-Dsk2FL at 1:1 ratio with Ddi1UBL. Insert shows the spectrum of 250 $\mu$ M <sup>15</sup>N-Dsk2UBL in magenta. Bottom, 610 $\mu$ M <sup>15</sup>N-Rad23FL also at 1:1 upon binding of UBL domain of Ddi1.**

As a final confirmation that a significant interaction between Rad23UBL and Ddi1UBL does not exist, similar studies were performed using construct with only the UBL domain of Rad23 (Figure 4-3). Only a limited number of peaks changed position in the presence of Ddi1UBL, and these changes were not as drastic as in the case of Dsk2UBL, indicating that Ddi1UBL interacts stronger with Dsk2UBL than with Rad23UBL.

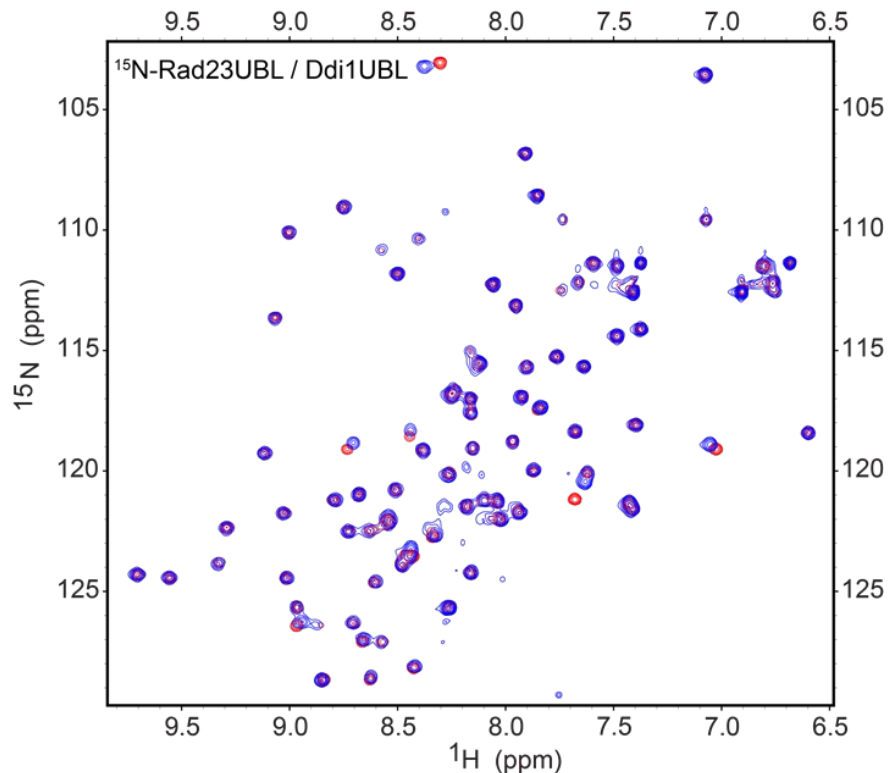


**Figure 4-3. Ddi1UBL binding to Rad23UBL.  $250\mu\text{M}^{15}\text{N}$ -Rad23UBL (red) in the presence of Ddi1UBL at 1:2 ratio (blue).**

Lastly, the absence of interactions between the UBA domain from Rad23 and Ddi1UBL was confirmed by individual titration of Ddi1UBL with the UBA2 domain of hHR23A, the human homolog of Rad23 (hRad23) and the UBA domain of UBQLN1, the human homolog of Dsk2 (Figure 4-4). There were no changes in the spectrum of Ddi1UBL upon addition of each of the ligands. These human homologs share on average sequence similarity of 70% and 60%, respectively, with yeast sequences. Based on the above results, it can be assumed that despite the fact that both constructs were obtained from the *Homo sapiens*, Ddi1UBL doesn't interact with the UBA2 domain of Rad23 as well as the UBA domain of Dsk2. The interaction between Ddi1UBL and the UBA1 of Rad23 was not tested. It is worth mentioning that this interaction was indicated to be responsible for dimerization of Ddi1UBL and Rad23 in previous studies<sup>61</sup>.

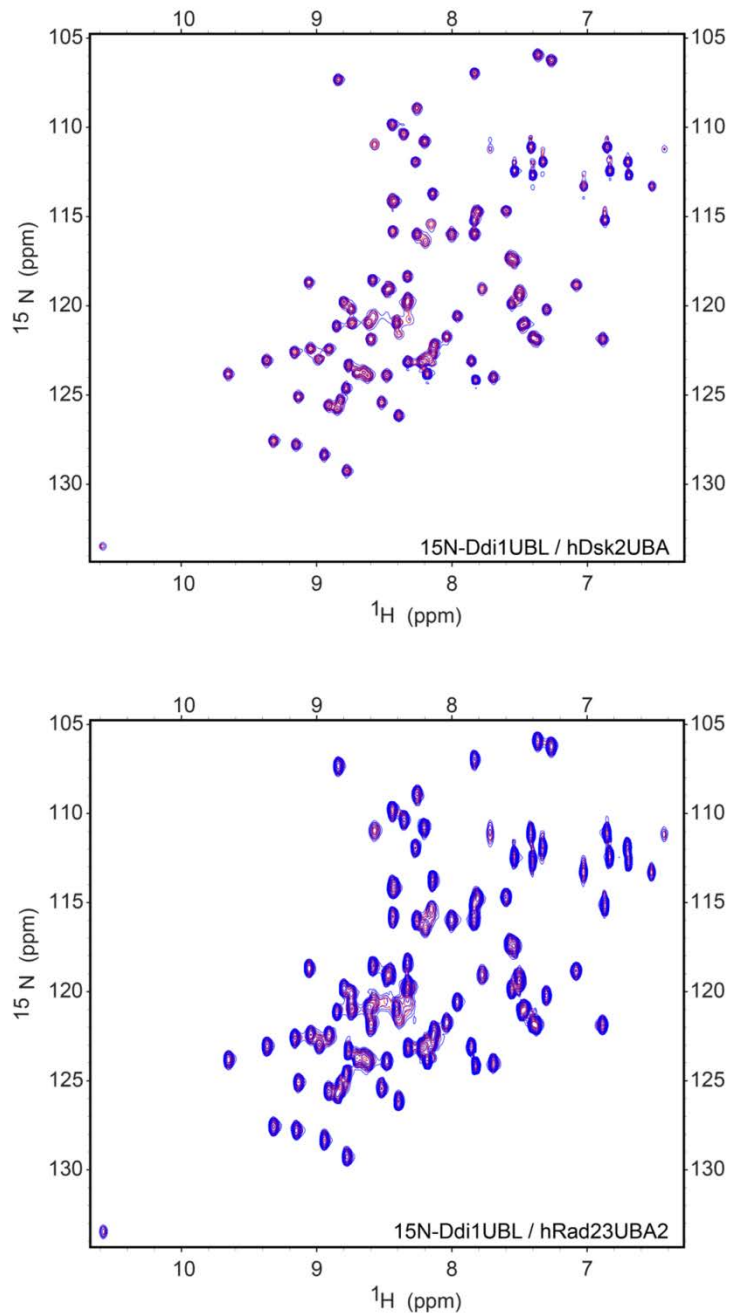


**Figure 4-4. Ddi1UBL interaction with hDsk2UBA and hRad23UBA2.** The spectra of the UBL domains of Ddi1 alone are shown in red, and the spectra upon binding are in blue. Top, 250 $\mu$ M <sup>15</sup>N-Ddi1UBL was mixed with a sample of *H.sapiens* UBA domain from Dsk2 at 1:2 ratio (this construct had additionally introduced Tyr for easier estimation of concentration). Bottom, 250 $\mu$ M <sup>15</sup>N-Ddi1UBL titrated with UBA2 domain of Rad23 from *H.sapiens* at 1:3 ratio.

## 4.2 Dsk2UBL binding to Ddi1UBL

The fact that a number of peaks belonging to Dsk2UBL either disappeared or shifted in the spectrum of Dsk2FL in the presence of Ddi1UBL motivated us to study the interaction between Dsk2UBL and Ddi1UBL in more detail. For that purpose, a full titration was performed by adding increasing amounts of unlabeled Ddi1UBL to a 250 $\mu$ M sample of Dsk2UBL. Saturation, the point at which no more changes in the spectrum was observed, was achieved when Dsk2UBL and the UBL domain of Ddi1 were mixed in 1:4.5 ratio (Figure 4-5). Consistent with results obtained from full length Dsk2, a number of peaks significantly changed their position.

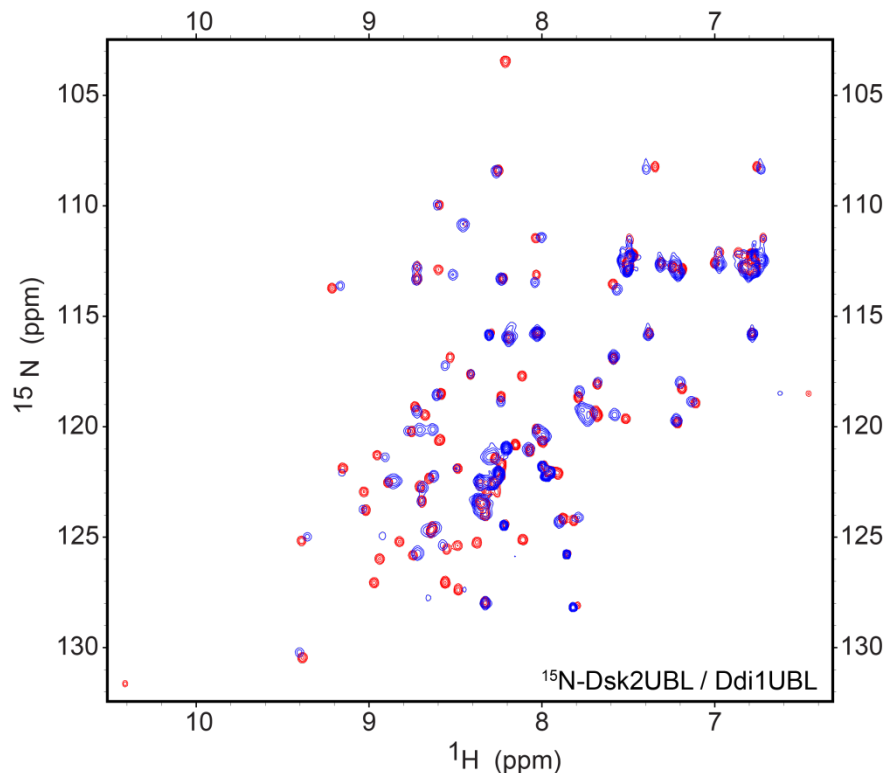


**Figure 4-5. Interaction of UBL domains from Dsk2 and Ddi1. In red, the spectrum of 250 $\mu$ M Dsk2UBL, while in blue is the spectrum of Dsk2UBL saturated with Ddi1UBL (ratio 1:4.5).**

Changes in the spectrum were quantified as CSP (Figure 4-6) and were used to identify putative binding sites on the structure of Dsk2UBL (Figure 4-7). A number of residues involved in the interaction showed attenuation, and therefore could not be used for Kd estimation.

Residues that showed significant chemical shift perturbations ( $CSP > 0.1$ ) were used to obtain the affinity of this interaction. The best fit was obtained for the 1:1 binding with an affinity of  $16 \pm 10 \mu\text{M}$ . The  $^{15}\text{N}$  relaxation rates gave an average T1 equal to  $\sim 1170\text{ms}$ , slightly greater than for Ddi1UBL:Ub. Further estimation of the binding affinity and stoichiometry of this interaction will require additional experimentation, preferably from another technique that is not residue specific.

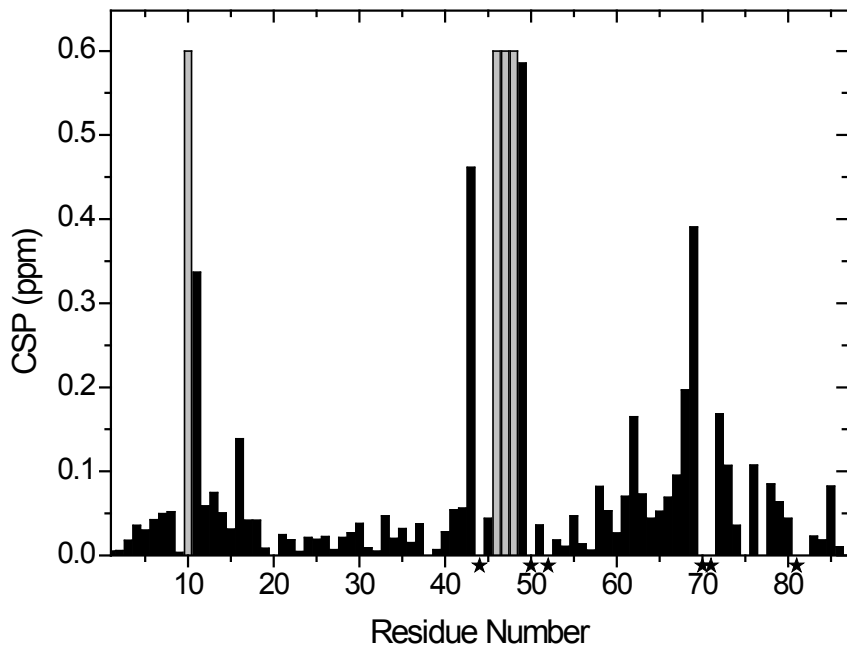


**Figure 4-6. Chemical shift perturbations of Ddi1UBL binding to Dsk2UBL. CSP obtained at saturation (ratio 4:5). Light gray bars represent peaks that attenuated. Overlapping peaks are indicated with asterisks.**

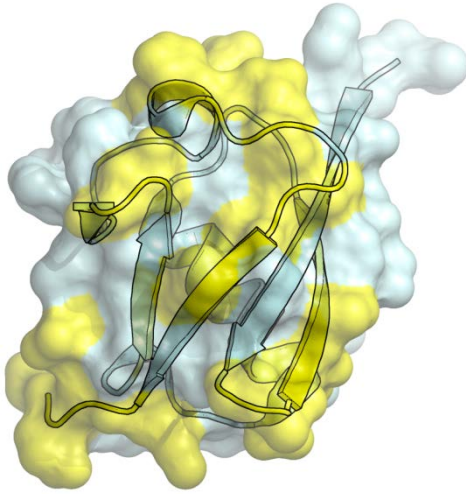


**Figure 4-7. Putative Ddi1UBL binding site on the surface of Dsk2UBL. Amino acids showing CSP>0.05 at saturation are mapped in yellow on the Dsk2UBL model (2BWF.pdb) shown in light blue color.**

### 4.3 Ddi1UBL has an additional binding site for Dsk2UBL

Having observed significant differences for the UBL domain in the spectrum of the full length Ddi1, it was important to determine whether Ddi1UBL uses the same binding site for the UBL domain of Dsk2 as it does for Ub. The above titration demonstrated that the number of Ddi1UBL peaks change position; however, because the Ddi1FL spectrum is very crowded, further characterization was performed using individual domains. A number of shifts can be observed when comparing the spectrum of Ddi1UBL alone and in the presence of Dsk2UBL at a ratio as high as 1:5 (Figure 4-8).

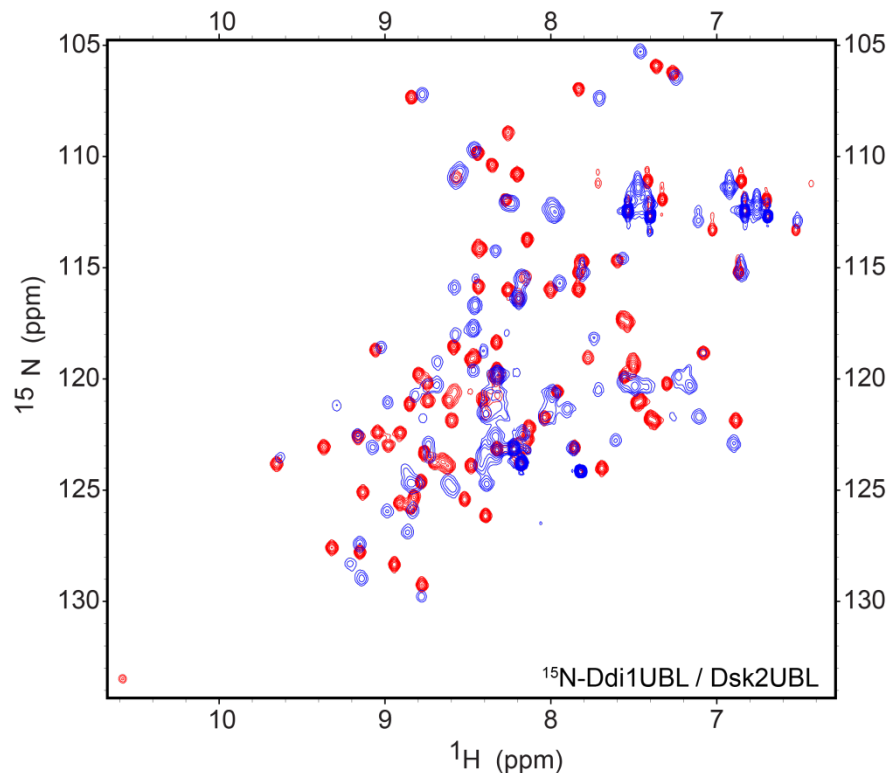


**Figure 4-8. Dsk2UBL binding to Ddi1UBL. Spectra of 250 $\mu$ M  $^{15}\text{N}$ -Ddi1UBL alone (red) and in the presence of Dsk2UBL at 1:5 ratio (blue).**

Detailed analysis of the full titration is very complicated as a number of peaks overlap, rendering it difficult to estimate their final position. For the purpose of illustration, at a 1:1 ratio of proteins, the amino acids affected by binding can be identified (Figure 4-9). Chemical shift perturbations of peaks observed at 1:1 ratio reveal that most of the amide groups in Ddi1UBL were affected by binding of Dsk2UBL, with two amino acids even attenuated.

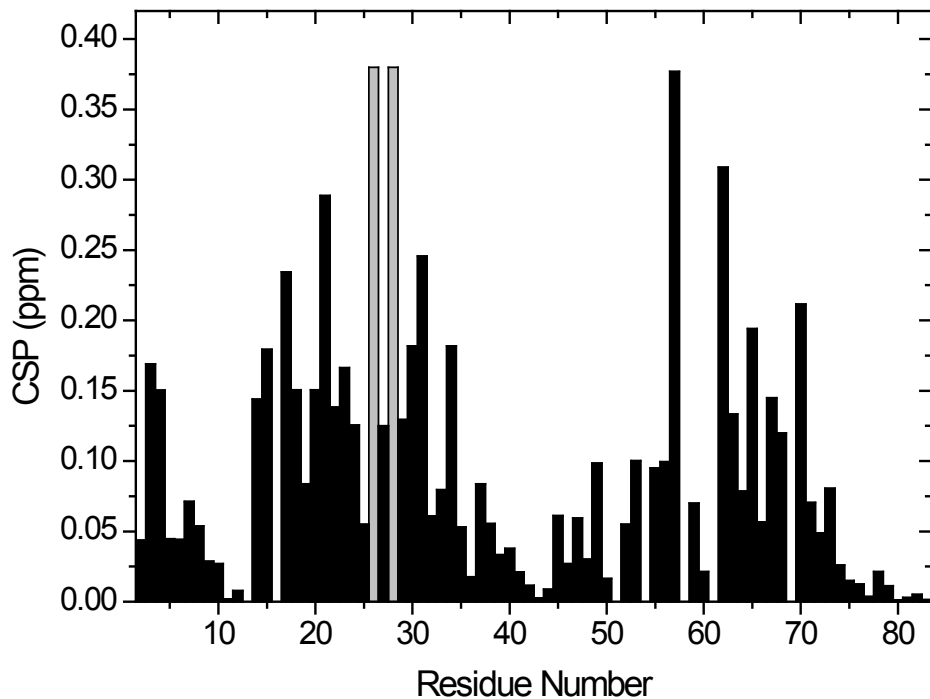


**Figure 4-9. Chemical shift perturbations upon Dsk2UBL binding to <sup>15</sup>N-Ddi1UBL. CSP obtained between peak positions in spectrum of Ddi1UBL and spectrum of Ddi1UBL in the presence of Dsk2UBL at 1:1 ratio. Light gray bars highlight residues with peaks attenuated.**

When CSPs at this ratio were mapped on the structure of Ddi1UBL, it was observed that in addition to the binding site that was utilized for Ub binding, Dsk2UBL also interacts with the long loop of Ddi1UBL and, more importantly, with the  $\alpha$ -helix of the UBL domain of Ddi1 (Figure 4-10). The <sup>15</sup>N relaxation rates yielded an average T1 equal to  $\sim$ 1300ms, which is higher than what was observed for Ddi1UBL:Ub binding (956ms).

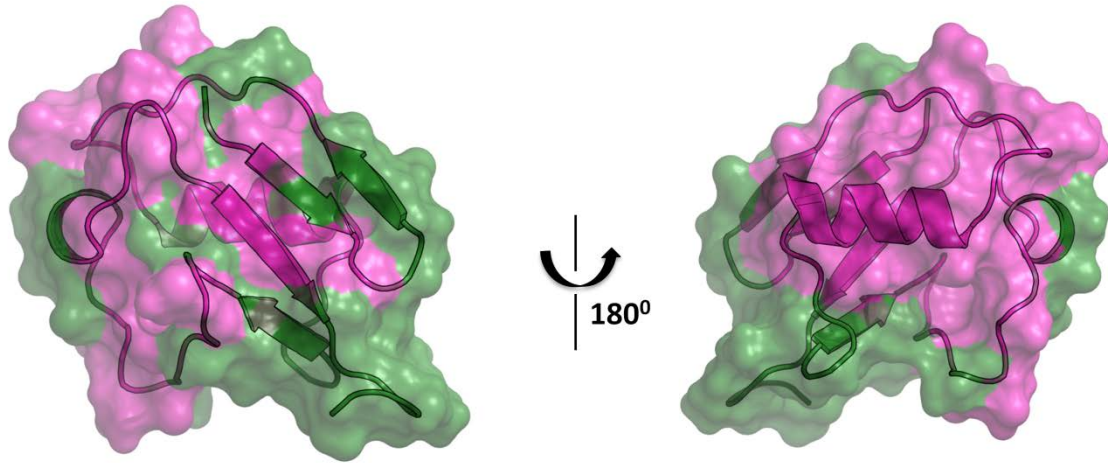


**Figure 4-10. Putative Dsk2UBL binding site on the surface of Ddi1UBL. Ddi1UBL is shown in green. Amino acids with CSP>0.05 at 1:1 ratio are used to indicate Dsk2UBL binding site and are colored in magenta.**

Finally, we wanted to determine whether Dsk2UBL competes with Ub for binding to Ddi1UBL. The experiment was designed to first observe binding of Ddi1UBL to  $^{15}\text{N}$ -Ub, then take advantage of the fact that Dsk2UBL does not bind Ub (as shown in Chapter 3.6) and add Dsk2UBL to the same sample. If binding between Dsk2UBL and Ddi1UBL is stronger than Ddi1UBL to  $^{15}\text{N}$ -Ub, upon addition of Dsk2UBL the spectrum should resemble the spectrum of  $^{15}\text{N}$ -Ub in its unbound state, since only signals from Ub are visible.  $^{15}\text{N}$ -Ub and Ddi1UBL were mixed in a 1:1 ratio. Since, Dsk2UBL can have two binding sites for the UBL domain of Ddi1, a double molar amount of Dsk2UBL was added to the tube to compensate for this. When the three spectra were overlaid with each other:  $^{15}\text{N}$ -Ub alone (red),  $^{15}\text{N}$ -Ub / Ddi1UBL mixed at 1:1 ratio (blue) and  $^{15}\text{N}$ -Ub / Ddi1UBL /Dsk2UBL mixed at ratio 1:1:2 (cyan) it was observed that Dsk2UBL did not fully outcompete Ub (Figure 4-11). However,

considering the trajectories of the peak shifts, it can be assumed that some Ub was released from the Ddi1UBL since the peaks shifted back to their original positions in the unbound state. This result suggests that both Ub and Dsk2UBL display similar ranges of affinity towards Ddi1UBL.

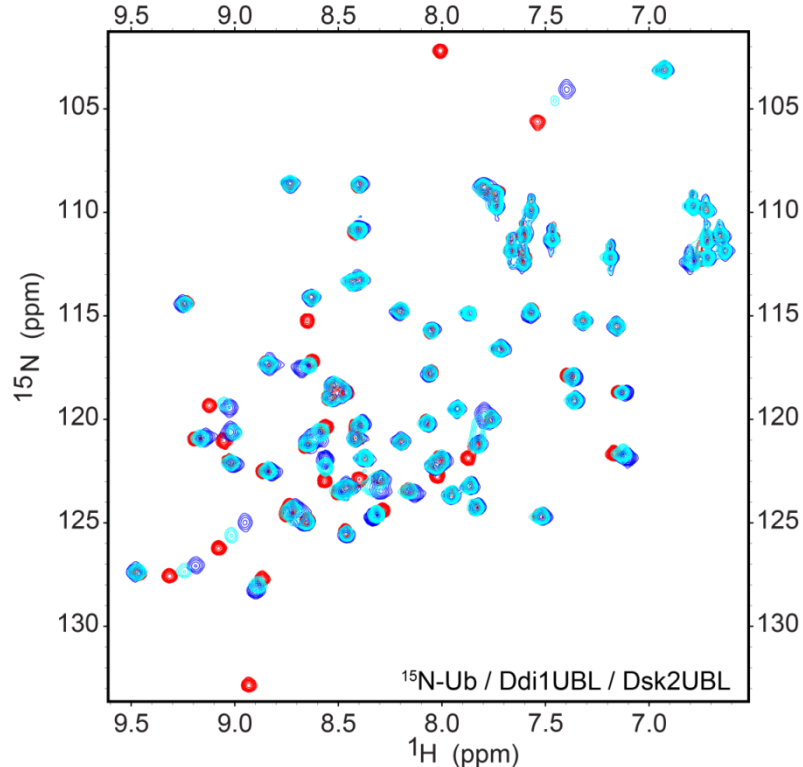


**Figure 4-11. Competition assay between Ub, Ddi1UBL and Dsk2UBL. In red, spectrum of  $250\mu\text{M}$  sample of Ub. In blue, spectrum of  $250\mu\text{M}$  Ub with unlabeled Ddi1UBL sample added in equal molar amount. In cyan, spectrum of the above mentioned sample to which double molar excess of Dsk2UBL sample was added (cyan). Final stoichiometry  $^{15}\text{N-Ub} / \text{Ddi1UBL} / \text{Dsk2UBL}$  is 1:1:2.**

#### **4.4 Ddi1UBL differentiates between different linkages of Ub<sub>2</sub>**

Research performed up to now indicated that Ddi1UBL binds not only Ub but also UBL domains such as Dsk2UBL. We wanted to determine whether Ddi1UBL also binds diUBs, two Ub that are connected through an isopeptide bond, in the same manner as mono Ub. We tested the interaction between Ddi1UBL and Ub<sub>2</sub>, where Ub are linked through K48 (K48-Ub<sub>2</sub>) and through K63 (K63-Ub<sub>2</sub>). These two linkages are particularly interesting because they display two distinguishing open and close conformations of Ub<sub>2</sub> that dictate the orientation and accessibility of hydrophobic patches on the Ub surface. When the spectrum of Ddi1UBL alone is compared with the spectrum of Ddi1UBL in the presence of each of these dimers, it can be observed that a number of peaks were affected in both cases (Figure 4-12). Furthermore, in the case of K48-Ub<sub>2</sub> binding, a number of peaks shift, but there are also peaks that disappear (attenuated) from the spectrum, while in the case of K63-Ub<sub>2</sub> binding, peaks mainly shift.

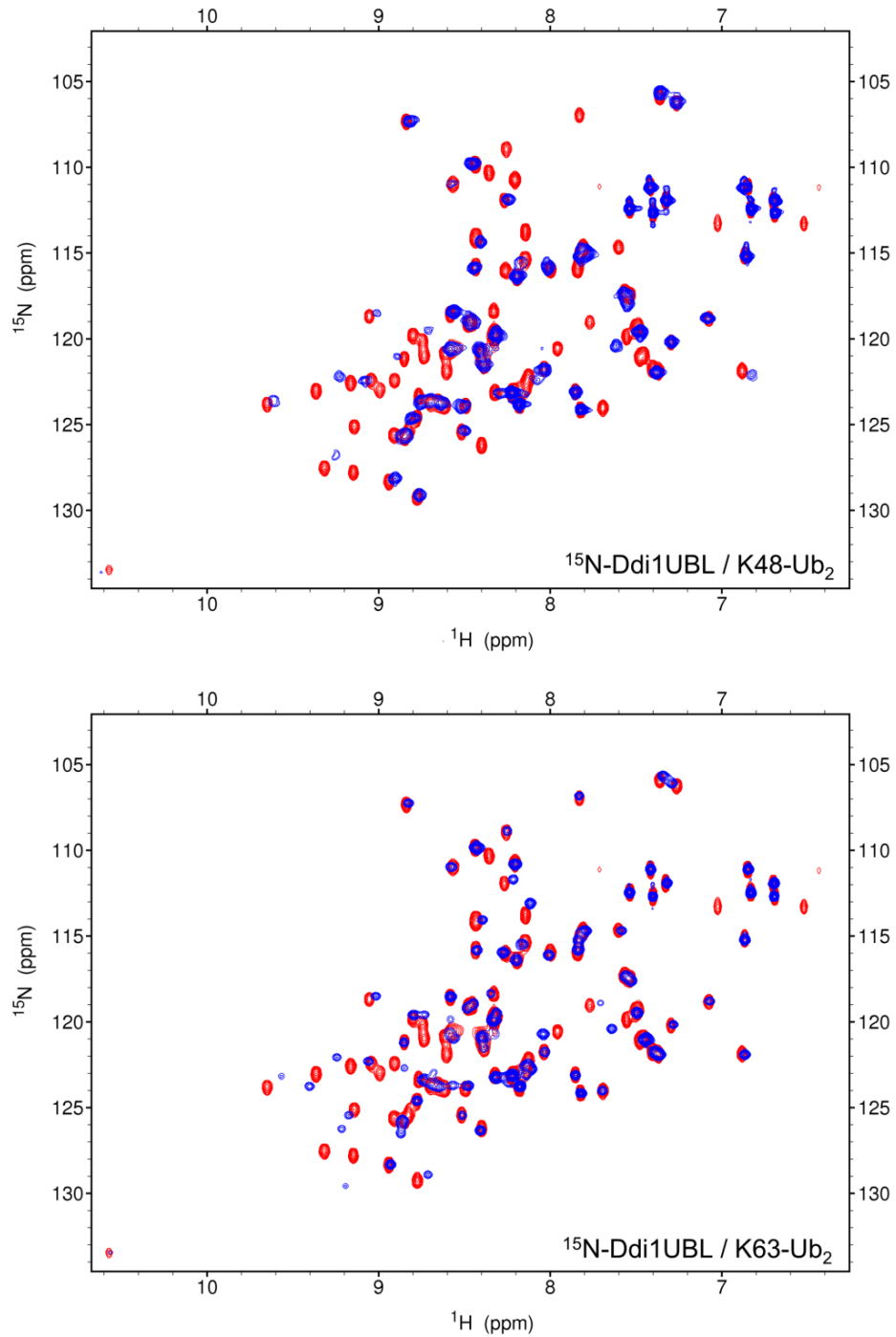


**Figure 4-12. Comparison of K48-Ub<sub>2</sub> and K63-Ub<sub>2</sub> binding to Ddi1UBL.** Spectra of 250  $\mu$ M <sup>15</sup>N-Ddi1UBL are shown in red. Top, spectrum of <sup>15</sup>N-Ddi1UBL in the presence of K48-Ub<sub>2</sub> at 1:0.5 ratio is shown in blue. Bottom, in blue spectrum of <sup>15</sup>N-Ddi1UBL mixed with K63-Ub<sub>2</sub> also at 1:1 ratio.

More interestingly, we wanted to determine whether there were any similarities between peak positions in the spectrum of Ddi1UBL bound to Ub, with the spectra of Ddi1UBL bound to each of these dimers (Figure 4-13). For consistency all Ub<sub>2</sub> bound states were compared with appropriate ratios between Ddi1UBL and Ub. Fascinatingly, the spectrum of the UBL domain of Ddi1 bound to K63-Ub<sub>2</sub> is almost the same as the spectrum of Ddi1UBL bound to Ub at the same ratio. On the contrary, the spectrum of Ddi1UBL bound to K48-Ub<sub>2</sub> does not fully match the spectrum of Ddi1UBL to Ub. These results indicate that the UBL domain of Ddi1 distinguishes between K48-Ub<sub>2</sub> and K63-Ub<sub>2</sub> and that they have different conformations. K63-Ub<sub>2</sub>, which is more open enables each Ub moiety to bind DdiUBL in the same way as mono Ub does, therefore no difference in the spectra of the bound states is observed. K48-Ub<sub>2</sub>, on the other hand, has Ub moieties that interact with each other and are in closer proximity, and as a result might increase local concentration of Ub that is available for Ddi1UBL, allowing simultaneous binding of both K48-Ub<sub>2</sub> domains.

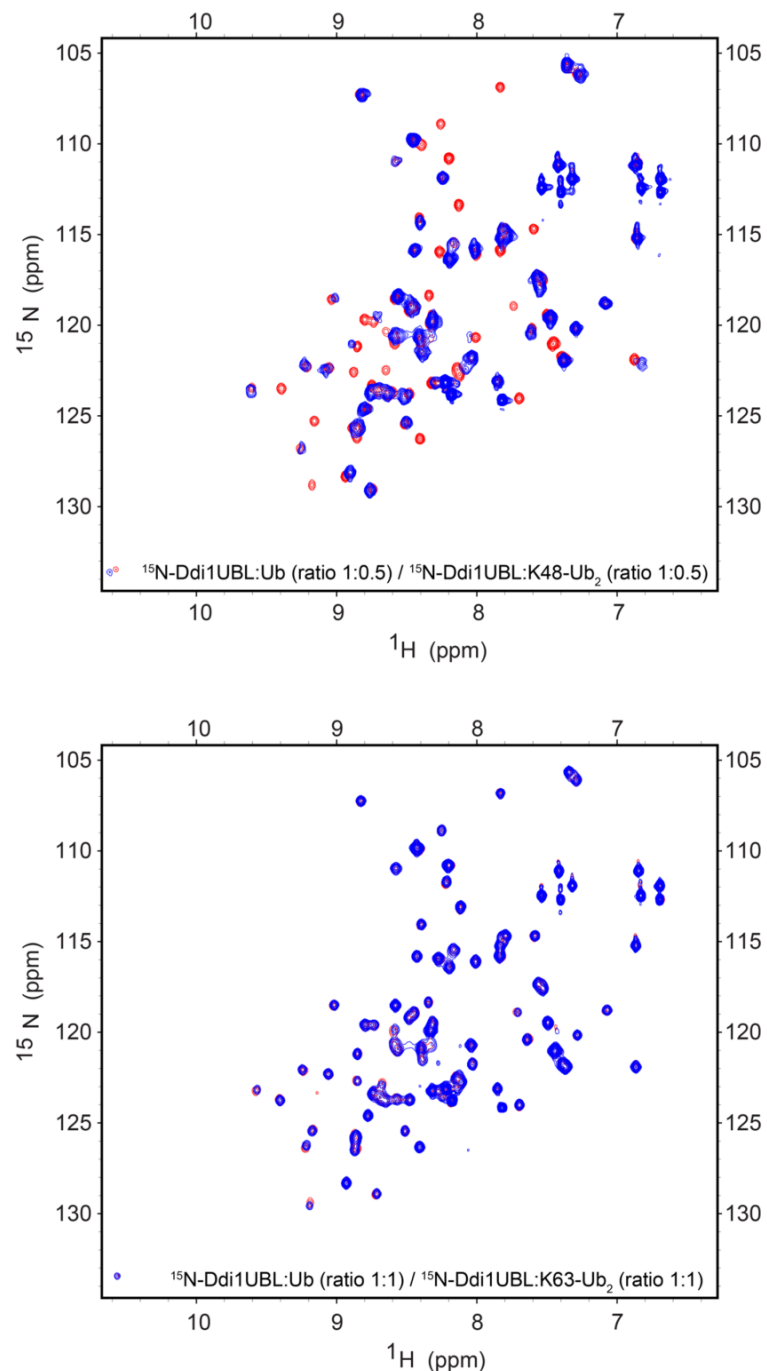


**Figure 4-13. Ddi1UBL differentiates between K48-Ub<sub>2</sub> and K63-Ub<sub>2</sub>.** On top, comparison of bound states of Ddi1UBL in the presence of monoUb (red) and in the presence of K48-Ub<sub>2</sub>(blue). Both bound states are at the same ratio, 1:0.5. On bottom, a similar type of comparison but Ddi1UBL:monoUb spectrum at 1:1 ratio (red) is overlaid with spectrum of Ddi1UBL mixed with K63-Ub<sub>2</sub> at 1:1 ratio (blue).

It was also interesting to observe how the chemical shift perturbations were distributed when reported as a function of the residue number (Figure 4-14). The CSP plot of Ddi1UBL binding to K63-Ub<sub>2</sub>, despite being at a different ratio than the plot in Figure 3.6 resembles it very closely. This indicates that the binding of K63-Ub<sub>2</sub> comprises the same binding site as binding of mono Ub. In the case of K48-Ub<sub>2</sub>, it seems that perturbations are distributed throughout the sequence, including the  $\alpha$ -helix.

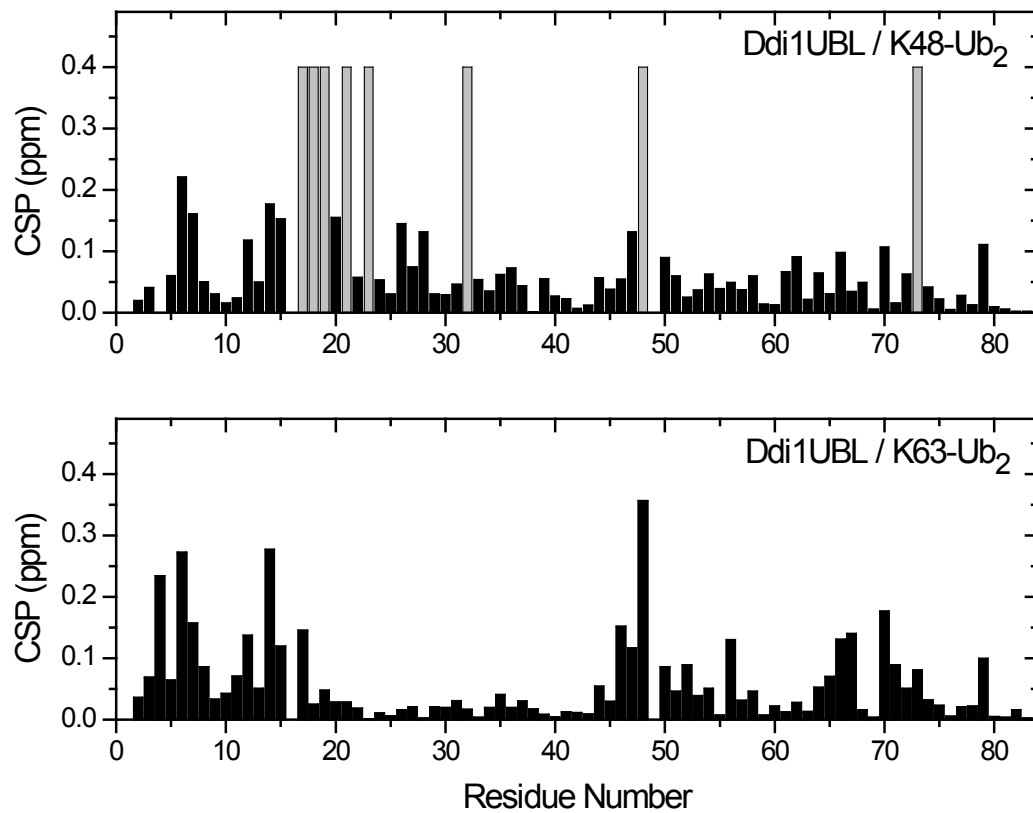


**Figure 4-14. CSP between free Ddi1UBL and Ddi1UBL bound to K48-Ub<sub>2</sub> and K63-Ub<sub>2</sub> at equal molar ratio. Gray bars show residues that attenuated upon binding.**

## 4.5 Ddi1UBL has UIM-like motif sequence in its $\alpha$ -helix

The surprising result, that both Dsk2UBL and K48-Ub<sub>2</sub> interact with the  $\alpha$ -helix of Ddi1UBL, was the main reason to further investigate this part of the Ddi1UBL amino acid sequence. After close analysis, we found that within the  $\alpha$ -helix sequence there is a stretch of hydrophobic amino acids that is not present in the  $\alpha$ -helix of Ub and UBL domains of other shuttle proteins (Figure 4-15).

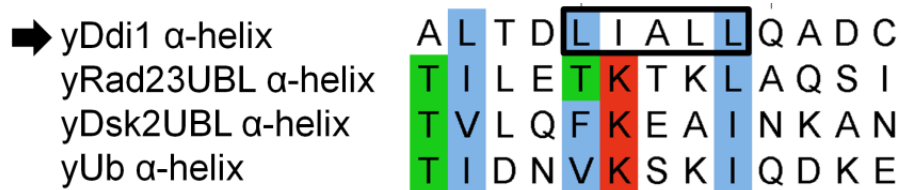


**Figure 4-15. Sequence alignment of the  $\alpha$ -helix amino acids of Ddi1UBL and  $\alpha$ -helix sequence in Ub, Dks2UBL and Rad23UBL.**

The presence of these hydrophobic amino acids resembles the sequence of the UIM motifs that is known to interact with Ub. The traditional UIM sequence is a series of hydrophobic residues such as LALAL or LAMAL that is terminated by the conserved Ser residue. For the purpose of analysis the sequence of the Ddi1UBL  $\alpha$ -helix was compared with the sequence of known UIM motifs (Figure 4-16). Despite the fact that Ddi1UBL doesn't have a Ser residue at the end of the sequence it does have a LIALL sequence that is very similar to the sequence characteristic for UIM motif. It will be interesting to see if introducing mutations at this part of the  $\alpha$ -helix will affect Ddi1UBL binding to Dsk2UBL or K48-Ub<sub>2</sub>.

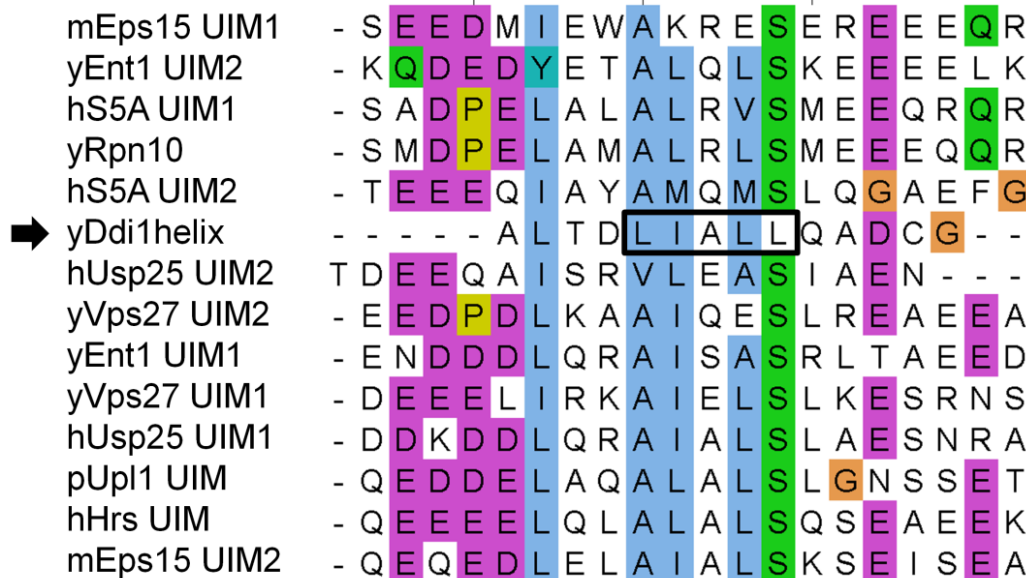


**Figure 4-16. Sequence alignment of the  $\alpha$ -helix amino acids of Ddi1UBL and other known UIM motif sequences.**

#### 4.6 Ddi1UBL mutants with altered UIM-like motif sequence

Since both Dsk2UBL and K48-Ub<sub>2</sub> interact with the Ddi1UBL  $\alpha$ -helix and the hydrophobic amino acids within it, the goal was to determine whether the UIM-like motif is responsible for recognitions of binding partners on the second binding site. To test this hypothesis three mutants were made: Ddi1UBL\_S, Ddi1UBL\_SK and Ddi1UBL\_KSK (Figure 4-17).

<i>Ub</i>	TIDNVVKSKIQDKEG
<i>Ddi1UBL WT</i>	ALTDLIALLQADCG
<i>Ddi1UBL_S</i>	ALTDLISLLQADCG
<i>Ddi1UBL_SK</i>	ALTDLISKLQADCG
<i>Ddi1UBL_KSK</i>	ALTDLKSKLQADCG

**Figure 4-17. Ddi1UBL mutants design. Three mutations were made to resemble  $\alpha$ -helix in Ub: Ddi1UBL\_S, Ddi1UBL\_SK and Ddi1UBL\_KSK.**

It was important to design mutations in such a way that they keep the proper fold but will introduce amino acids with different types of side chains that will not allow hydrophobic interactions. Since Ddi1UBL has the same fold as Ub,  $\alpha$ -helix sequence of Ub was used as a template for mutations, which should ensure that mutants will still have the  $\alpha$ -helix, but with different properties. All of the designed mutants expressed and were purified. All of them, with exception of Ddi1UBL\_KSK, showed well-dispersed signals on the  $^1\text{H}$ - $^{15}\text{N}$  correlation spectrum (Figure 4-18).

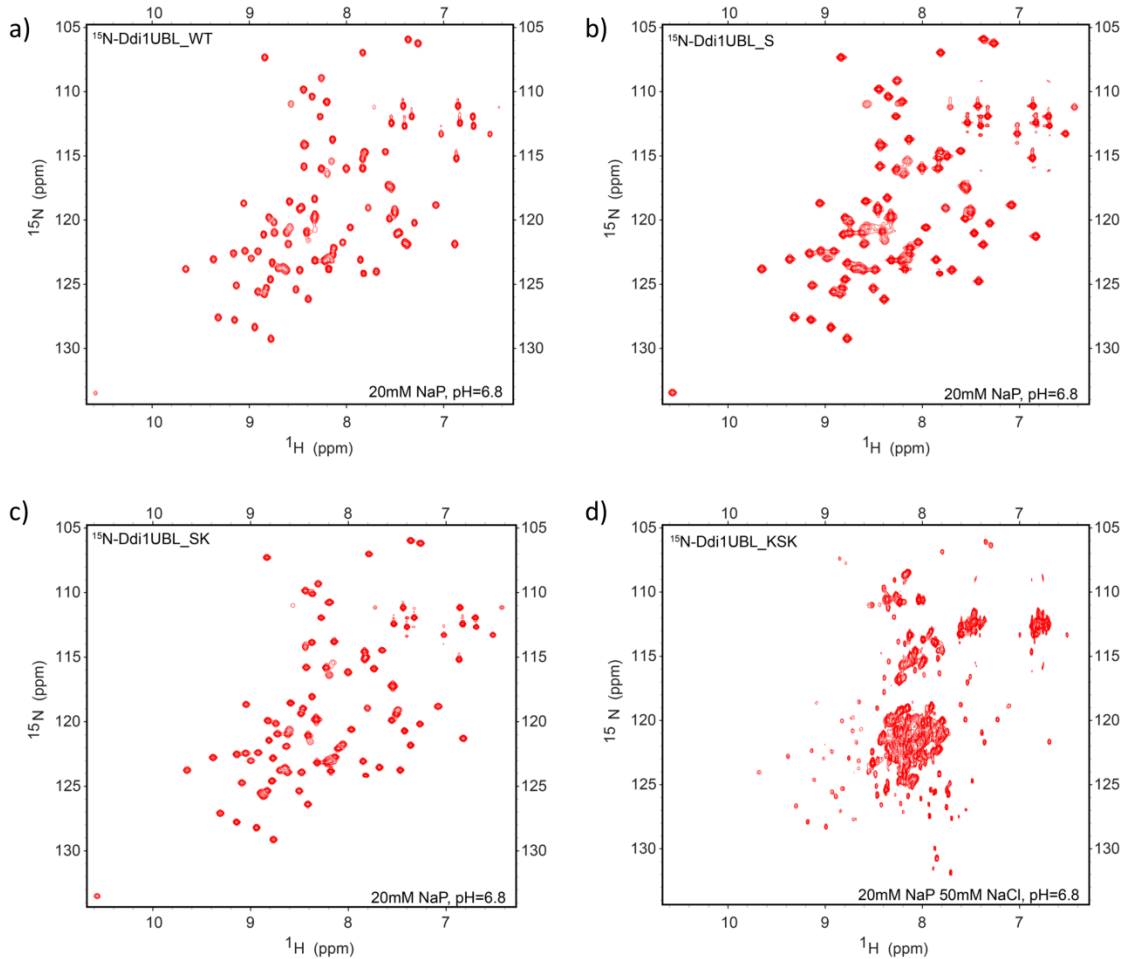


**Figure 4-18.  $^1\text{H}$ - $^{15}\text{N}$  SOFAST-HMQC spectra of Ddi1UBL\_WT and its mutants. (a) Ddi1UBL\_WT, (b) Ddi1UBL\_S and (c) Ddi1UBL\_SK are in 20mM NaP buffer at pH=6.8 and in 3mM TCEP; (d) Ddi1UBL\_KSK mutant is in the 20mM NaP buffer at pH=6.8 with 50mM NaCl in the presence of 3mM TCEP.**

Moreover, positions of the signals in the spectra of Ddi1UBL\_S and Ddi1UBL\_SK match positions of the signals in the Ddi1UBL WT spectrum, assuring that the structures of these two Ddi1UBL mutants were not affected upon substitution of amino acids (Figure 4-19).

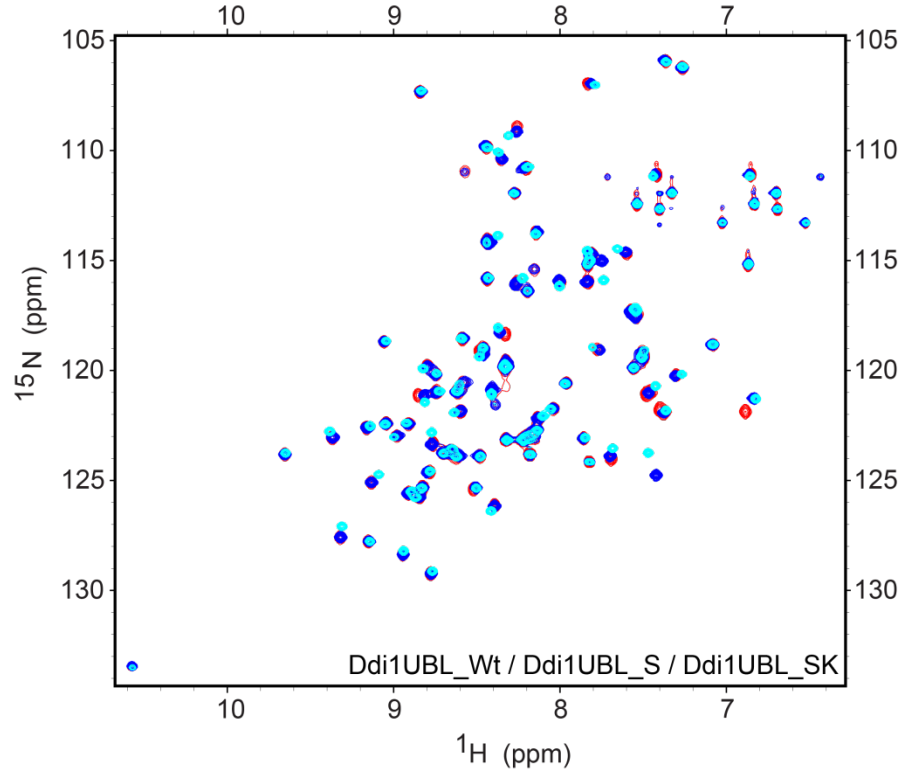


**Figure 4-19. Overlay of the spectra of Ddi1UBL\_WT, Ddi1UBL\_S and Ddi1UBL\_SK.** All proteins were in 20mM NaP buffer at pH=6.8 with 3mM TCEP. Ddi1UBL\_WT is shown as red peaks, Ddi1UBL\_S in blue and Ddi1UBL\_SK peaks are presented in cyan.

The Ddi1UBL\_KSK mutant showed very low stability during sample purification and preparation. It also precipitates from the 20mM sodium phosphate (NaP) buffer at pH 6.8. A number of buffering conditions were tested and some solubility was achieved in PBS at pH=7.4. Change of the pH from 7.4 to 6.8 did not affect the protein, therefore the amount of salt was further optimized. Finally, 20mM NaP buffer at pH=6.8 but in the presence of 50mM NaCl was chosen as the optimal conditions that ensured protein solubility and were as close as possible to buffering conditions used for all other studies. There were few spectral differences for the Ddi1UBL\_KSK in PBS and in 20mM NaP buffer with 50mM NaCl (Figure 4-20 a-c). Such low stability is probably caused by the fact that the mutated Ile amino acid is used to ensure a UBL like fold and anchors the  $\alpha$ -helix against its  $\beta$ -sheet. Introducing a longer and charged amino acid instead of it probably made the protein less stable. The significant amount of signals clustered in the middle of the spectrum is indicative of the presence of unfolded polypeptides. Only small portions of signals with lower intensities are spread in the spectrum. The final question was whether Ddi1UBL\_KSK had some structured and unstructured elements within the same polypeptide chain, or if some part of the sample was unfolded and only some small percentage was folded. A hetNOE experiment helped filter some of the signals (Figure 4-20d). Positive intensity signals are well dispersed all over spectrum and only negative signals are clustered in the middle. Moreover, the number of positive signals and their position indicate that it is very likely that there is some amount of Ddi1UBL\_KSK in the sample that is folded and functional.

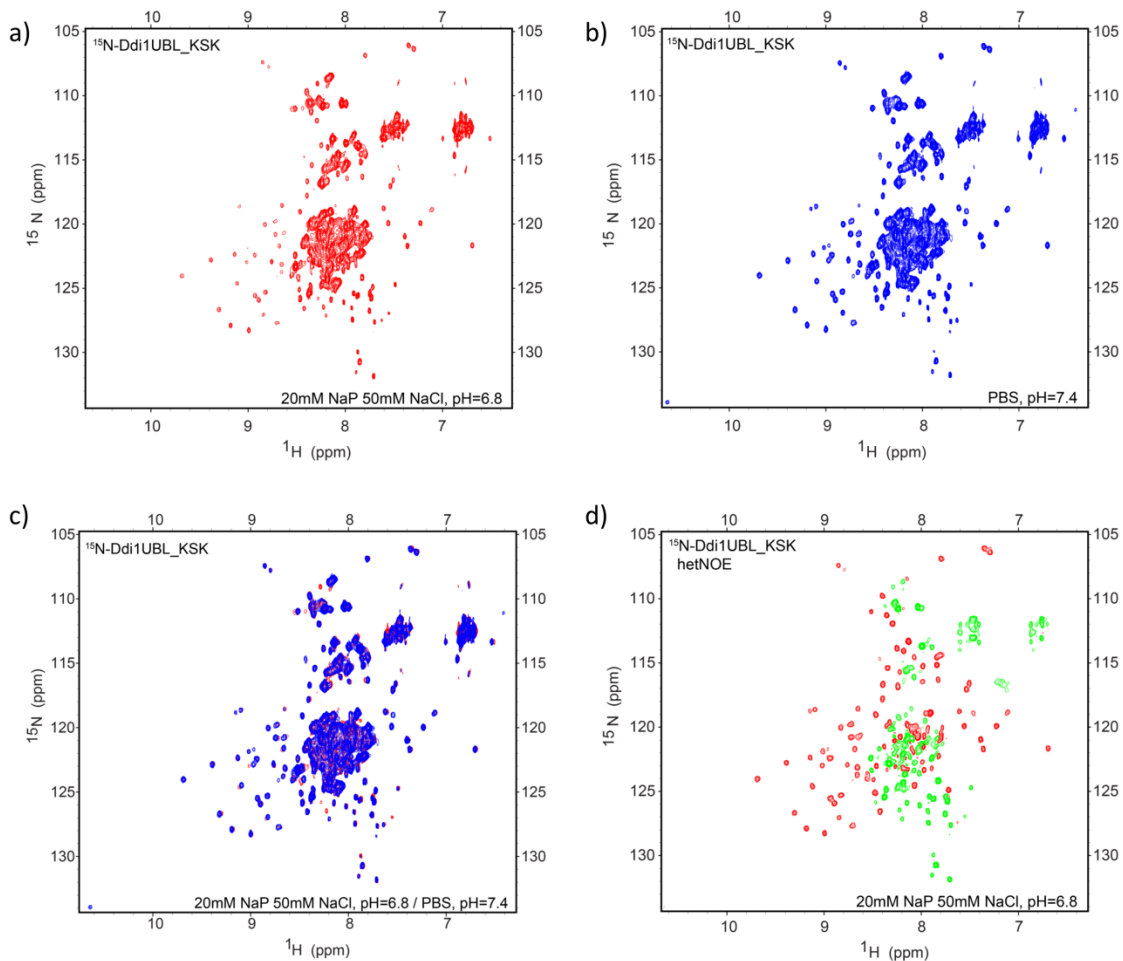


**Figure 4-20. Spectra of Ddi1UBL\_KSK mutant.** (a)  $^1\text{H}$ - $^{15}\text{N}$  SOFAST-HMQC Ddi1UBL\_KSK in  $20\text{mM NaP}$  buffer in the presence of  $50\text{mM NaCl}$  at pH 6.8 with  $3\text{mM TCEP}$ . (b)  $^1\text{H}$ - $^{15}\text{N}$  SOFAST-HMQC Ddi1UBL\_KSK in PBS buffer in the presence of  $5\text{mM DTT}$  at pH 7.4. (c) Overlay of the spectra and two different buffers:  $20\text{mM NaP}, 50\text{mM NaCl}, 3\text{mM TCEP}$  at pH 6.8 in red and PBS with  $5\text{mM DTT}$  at pH 7.4 in blue. (d) HetNOE spectrum of Ddi1UBL\_KSK; red peaks show positive signal intensities, green peaks represent negative signal intensities.

#### **4.7 Effects of mutations on binding to Ub, Dsk2UBL, K48-Ub<sub>2</sub> and K63-Ub<sub>2</sub>**

Firstly, it was important to determine whether the introduced mutations affected the general properties of recognizing binding partners. Since the proteins were mutated on the  $\alpha$ -helix site of the structure any changes should not affect recognition of Ub which interacts through the  $\beta$ -sheet. To confirm that this binding site is still active, we tested interactions of Ddi1UBL\_SK and Ddi1UBL\_KSK with Ub. Indeed when spectra of both samples were collected in the presence of Ub at 1:1 molar ratio and compared to spectra of each of the proteins alone, a number of peaks had shifted indicating that regardless of mutations, both constructs still interact with Ub (Figure 4-21). Following chemical shifts perturbation was very complicated for Ddi1UBL\_KSK mutant, however, when such analysis was performed for the Ddi1UBL\_SK mutant it can be easily noticed that the same residues are involved in binding as for the Ddi1UBL WT (Figure 4-22). Moreover, the general pattern and distribution of CSP along the sequence are very similar, what means that both WT and Ddi1UBL\_SK recognize the ligand in the same way.

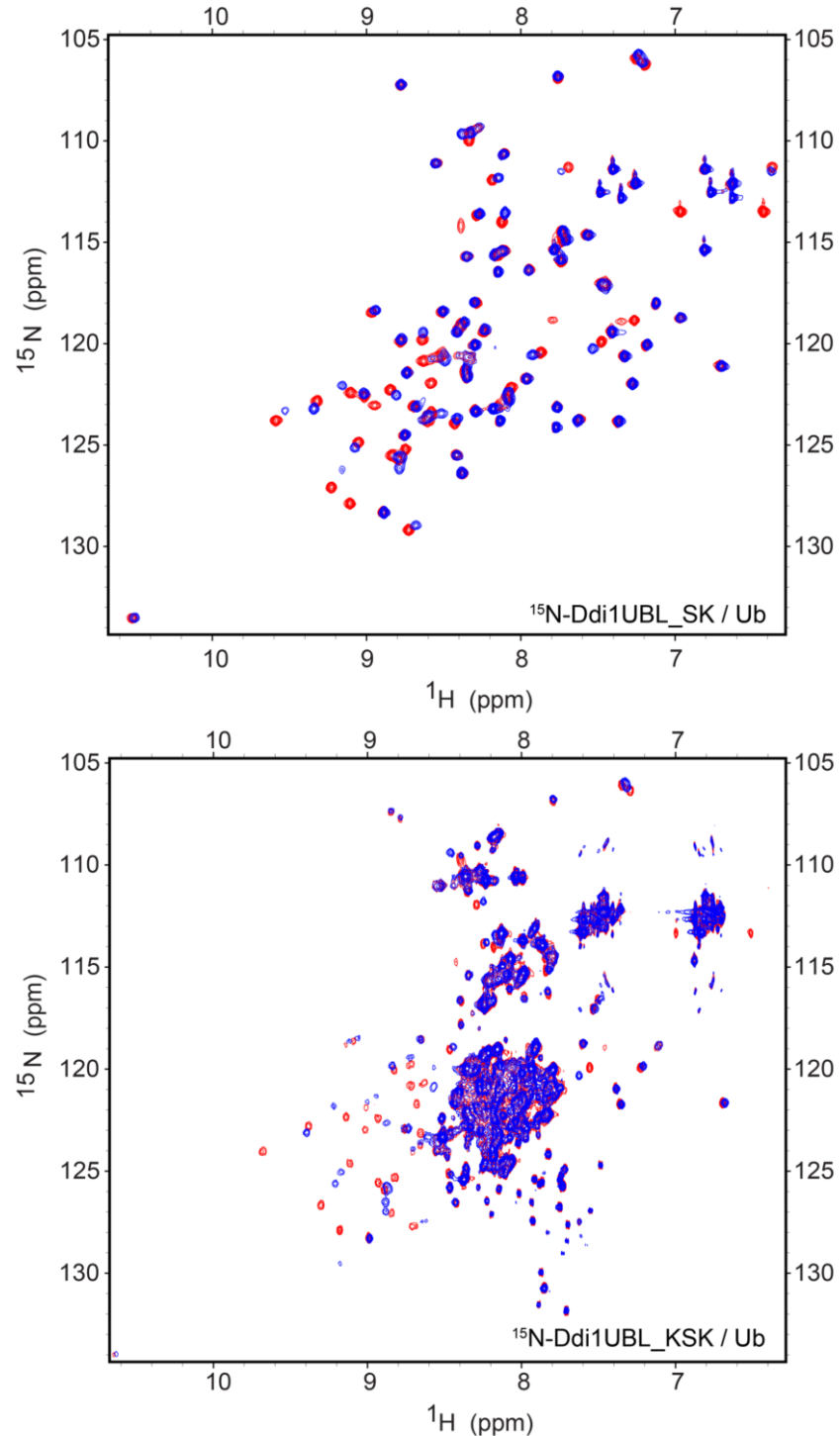


**Figure 4-21. Ddi1UBL\_SK and Ddi1UBL\_KSK binding to mono Ub.** Top, overlay of the spectrum of  $150\mu\text{M}$  Ddi1UBL\_SK (red) and in the presence of Ub mixed at 1:1 ratio (blue). Bottom,  $250\mu\text{M}$  Ddi1UBL\_KSK (red) binding to Ub at 1:1 ratio (blue).

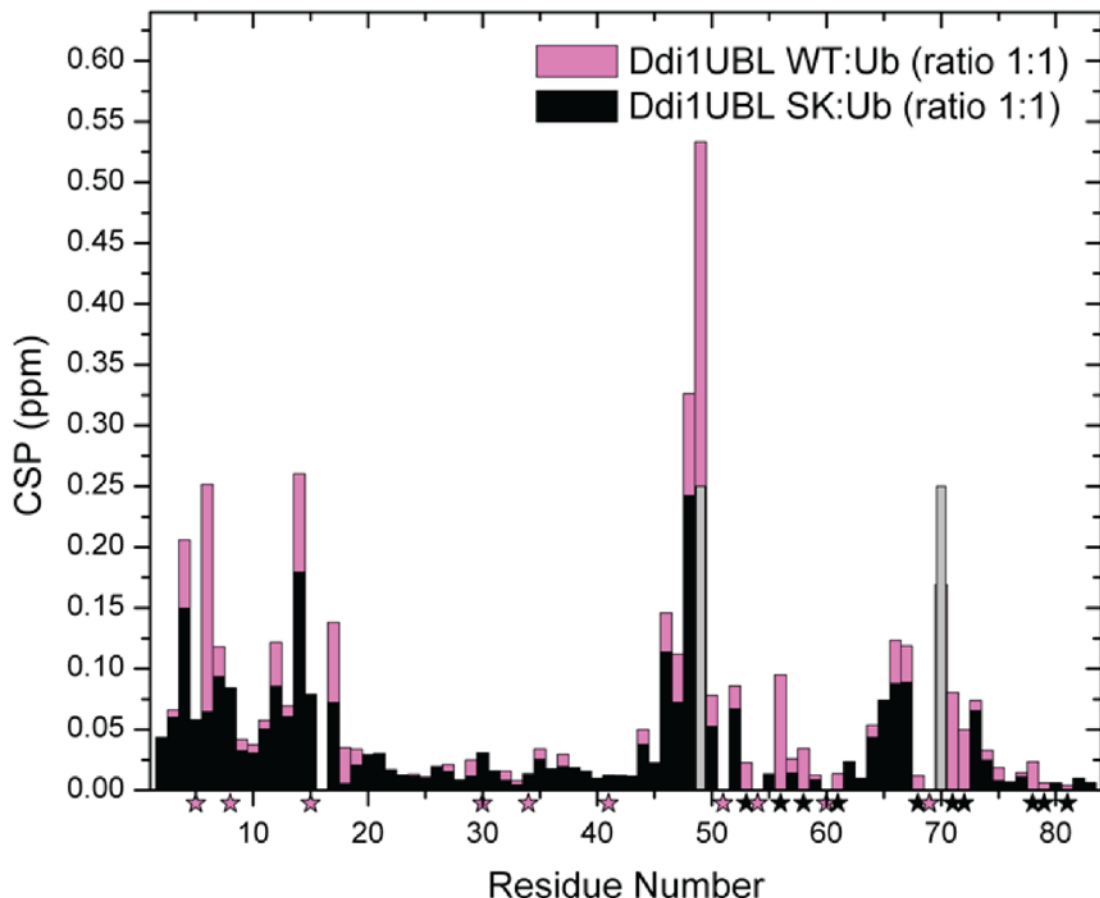


**Figure 4-22. Chemical shift perturbations of Ddi1UBL WT and Ddi1UBL\_SK binding to Ub. Ddi1UBL WT and Ddi1UBL\_SK are in 1:1 ratio with Ub. Gray bars show Ddi1UBL\_SK signals that attenuated upon Ub binding. Stars indicate residues for which data interpretation was impossible due to peak overlapping. Stars are colored in the same manner as in the legend.**

Despite the complicated nature of the Ddi1UBL\_KSK spectra for detailed interpretation, a portion of this sample that was properly folded was still capable of Ub recognition. Unfortunately, the unfolded part of Ddi1UBL\_KSK, did not fold upon Ub binding, since in the hetNOE experiment there are still a number of signals with negative intensities indicating unstructured elements (Figure 4-23).

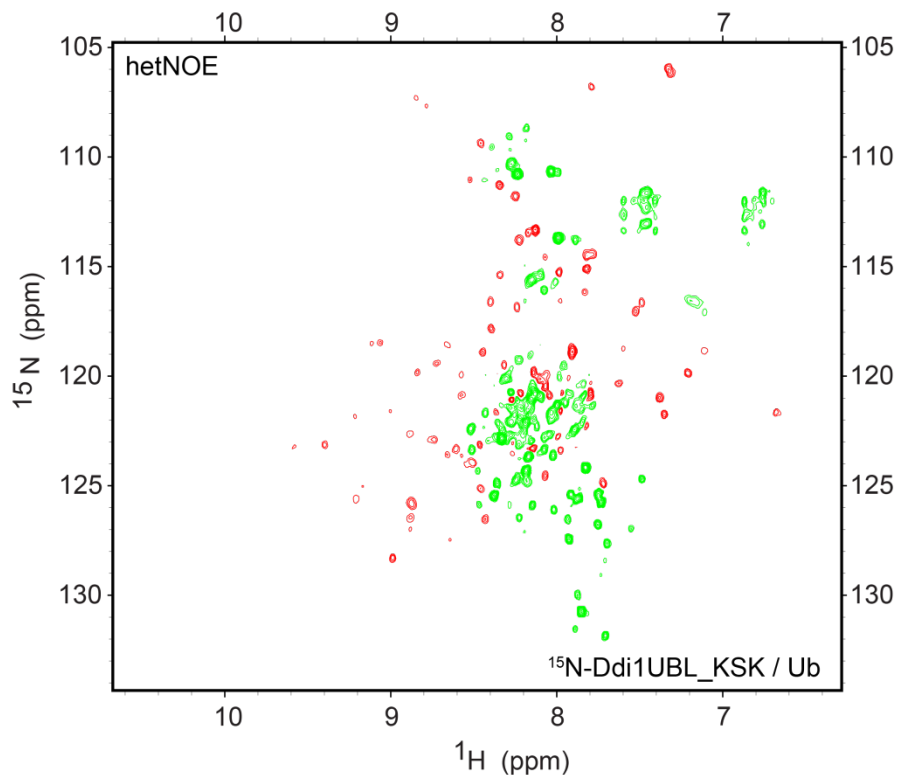


**Figure 4-23. HetNOE spectrum of  $^{15}\text{N}$ -Ddi1UBL\_KSK mutant in the presence of Ub. Both proteins are at 1:1 molar ratio. Red peaks show positive intensities, green peaks show negative intensities.**

Furthermore, we wanted to test how the mutations affect recognition of the Dsk2UBL domain. Binding was again monitored by NMR and spectra were collected when both mutant and ligand where at 1:1 stoichiometry. Each mutant was capable of recognizing the ligand (Figure 4-24). It seems that the changes in the spectrum of Ddi1UBL\_SK are smaller than in the case of Ddi1UBL\_S (Figure 4-24 a-b). As for Ddi1UBL\_KSK, the signals of structured elements upon binding could not be observed as already weak signals could become broaden upon binding and as a consequence disappear from the spectrum (Figure 24c). Unfortunately, nothing about the strength of Ddi1UBL\_KSK and Dsk2UBL interaction can be concluded. As in the case of Ub

binding, Dsk2UBL binding did not help in folding of unstructured Ddi1UBL\_KSK (Figure 4-24d).

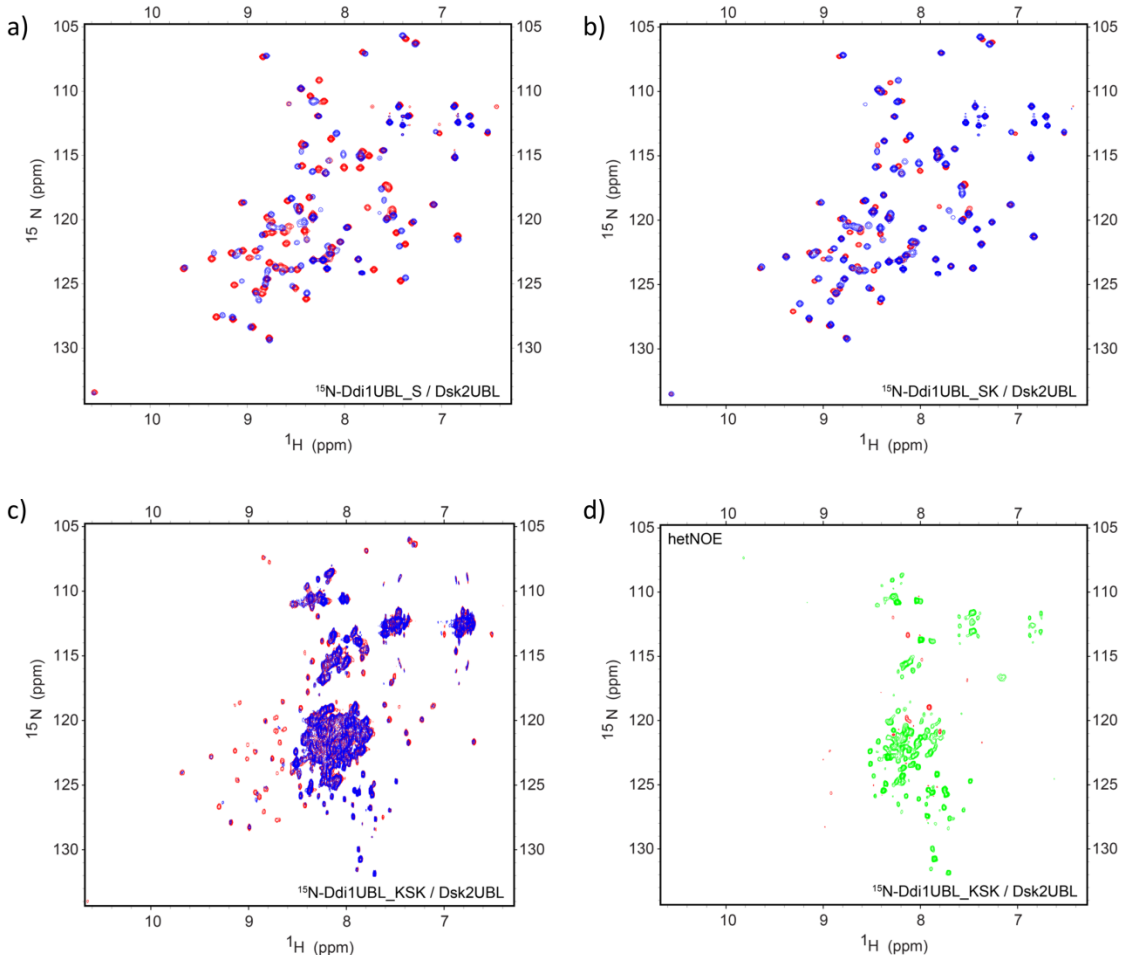


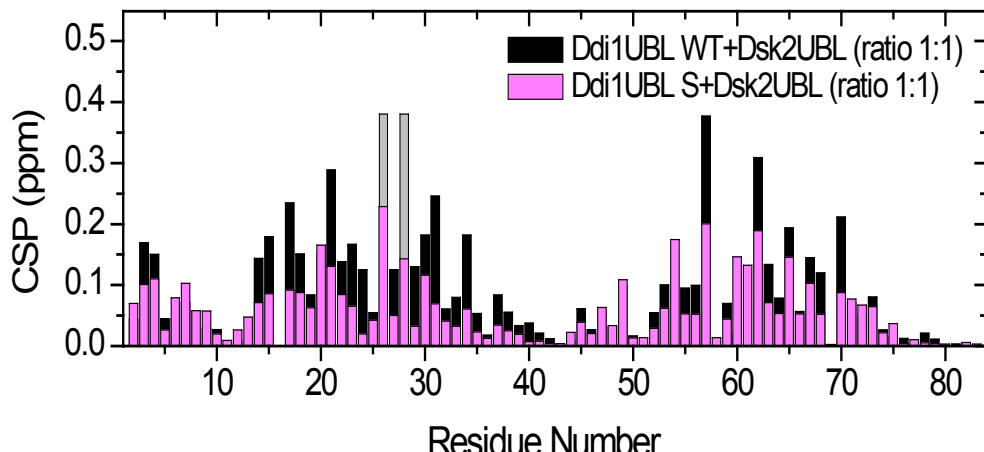
**Figure 4-24. Ddi1UBL mutants binding to Dsk2UBL.** (a)  $^1\text{H}$ - $^{15}\text{N}$  SOFAST-HMQC of  $250\mu\text{M}$   $^{15}\text{N}$ -Ddi1UBL\_S alone (red) and in the presence of Dsk2UBL at 1:1 ratio (blue). (b) Overlay of the spectrum of  $250\mu\text{M}$   $^{15}\text{N}$ -Ddi1UBL\_SK (red) and  $^{15}\text{N}$ -Ddi1UBL\_SK bound to Dsk2UBL also at 1:1 ratio (blue). (c)  $250\mu\text{M}$   $^{15}\text{N}$ -Ddi1UBL\_KSK (red) binding to UBL domain of Dsk2 (blue) also at 1:1 ratio. (d) HetNOE spectrum of Ddi1UBL\_KSK in the presence of Dsk2UBL at ratio 1:1; red peaks show positive signal intensities, green peaks represent negative signal intensities.

The goal of the designed mutations was to affect one of potential binding sites that involve the  $\alpha$ -helix. To determine if this was achieved the chemical shift perturbations of Ddi1UBL\_WT and Ddi1UBL mutants in the presence of Dsk2UBL were compared (Figure 4-25). The single mutation in Ddi1UBL did affect the recognition of Dsk2UBL; however, there are still perturbations present in the  $\alpha$ -helix of Ddi1UBL indicating that the second binding site was not fully diminished (Figure 4-25a).

In contrast, the Ddi1UBL\_SK mutant bound in a similar way as wild type, bound through the amino acids that were part of the  $\beta$ -sheet site, the first binding site (Figure 25b). Interestingly, the amino acids preceding the  $\alpha$ -helix and the  $\alpha$ -helix itself showed significantly lower chemical shift perturbations, proving that double mutation changing amino acids from hydrophobic to polar and charged changed the recognition of the ligand through a potential second binding site.

Finally, the most promising mutation Ddi1UBL\_SK was used to test binding properties to Ub<sub>2</sub>. Based on the spectra analysis there are still differences between K48-Ub<sub>2</sub> and K63-Ub<sub>2</sub> binding (Figure 4-26).

a)



b)

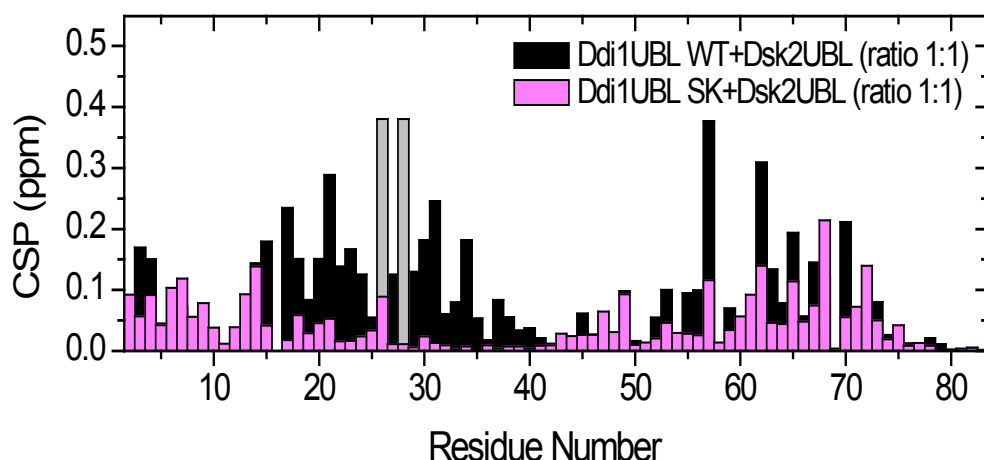


**Figure 4-25. Comparison of chemical shift perturbations of Ddi1UBL\_WT and Ddi1UBL mutants in the presence of Dsk2UBL. (a) CSP quantification of Ddi1UBL\_S binding to Dsk2UBL at 1:1 ration. (b) CSP plots for Ddi1UBL\_SK binding to Dsk2UBL also at 1:1 ratio.**

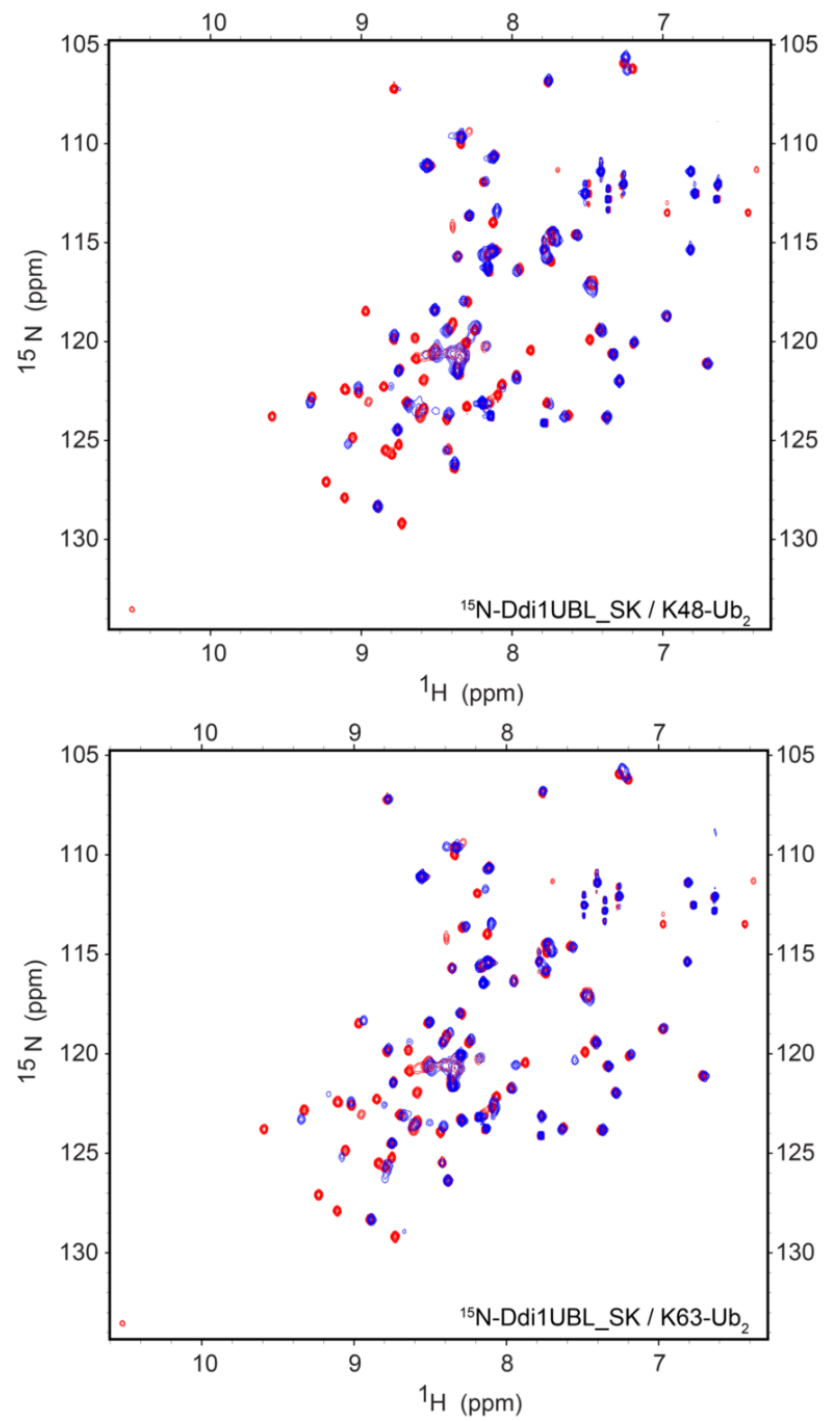


**Figure 4-26. Ddi1UBL\_SK binding to K48-Ub<sub>2</sub> and K63-Ub<sub>2</sub>. Spectra of 250 $\mu\text{M}$   $^{15}\text{N}$ -Ddi1UBL\_SK only are shown in red in both figures. Top, spectrum of  $^{15}\text{N}$ -Ddi1UBL\_SK in the presence of K48-Ub<sub>2</sub> at 1:1 ratio (blue). Bottom, spectrum of  $^{15}\text{N}$ -Ddi1UBL with K63-Ub<sub>2</sub> also at 1:1 ratio (blue).**

Despite the presence of introduced mutations in Ddi1UBL, K48-Ub<sub>2</sub> was still binding slightly different than mono Ub (Figure 4-27). The overall pattern of CSP differs for both ligands (Figure 4-28a). Moreover, more peaks attenuated in the spectrum of Ddi1UBL\_SK upon K48-Ub<sub>2</sub> than for Ub. Then again, K63-Ub<sub>2</sub> was bound in almost the same manner as mono Ub. The CSPs are almost the same for both Ub and K63-Ub<sub>2</sub> binding to Ddi1UBL\_SK. The small discrepancy that can be observed is that K63-Ub<sub>2</sub> has extra attenuation and few stronger CSPs (Figure 4-27 and 4-28b).

Different K48-Ub<sub>2</sub> and K63-Ub<sub>2</sub> binding to Ddi1UBL\_SK might indicate that the introduced mutations did not fully affect the second binding site, though the differences are smaller than for Ddi1UBL\_WT binding. The second possibility is that K48-Ub<sub>2</sub> in general causes slightly different changes in the chemical surrounding of the amide groups of Ddi1UBL than K63-Ub<sub>2</sub> does, and even diminishing the second binding site still results in spectrum of the bound state that will differ than spectrum upon Ub or K63-Ub<sub>2</sub> binding.

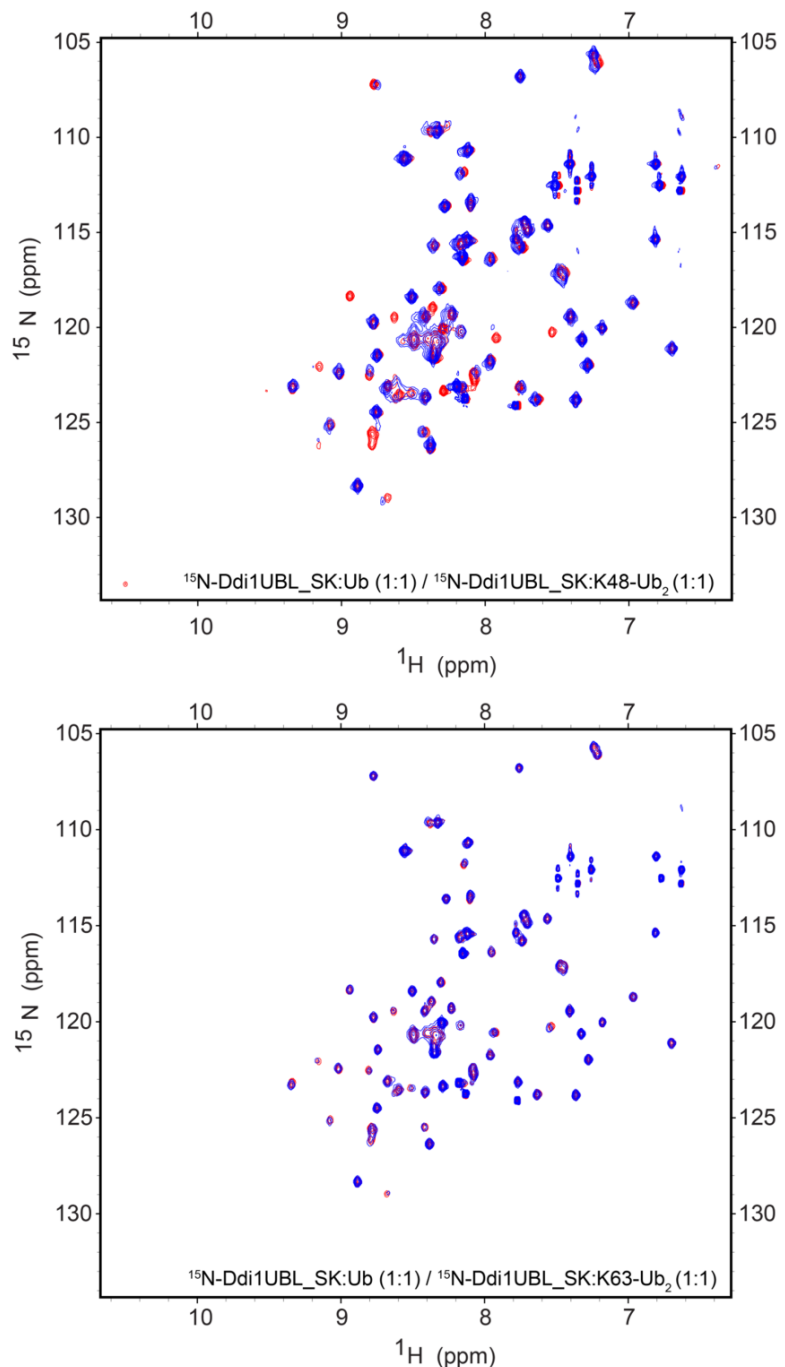


**Figure 4-27. Comparison of Ddi1UBL\_SK binding to Ub, K48-Ub<sub>2</sub> and K63-Ub<sub>2</sub>.**  
**On top, comparison of bound states of Ddi1UBL\_SK in the presence of monoUb (red) and in the presence of K48-Ub<sub>2</sub>(blue).** Both bound states are at the same ratio, 1:1. **On bottom, similar type of comparison, Ddi1UBL\_SK:monoUb spectrum at 1:1 ratio (red) is overlaid with spectrum of Ddi1UBL\_SK bound to K63-Ub<sub>2</sub> also at 1:1 ratio (blue).**

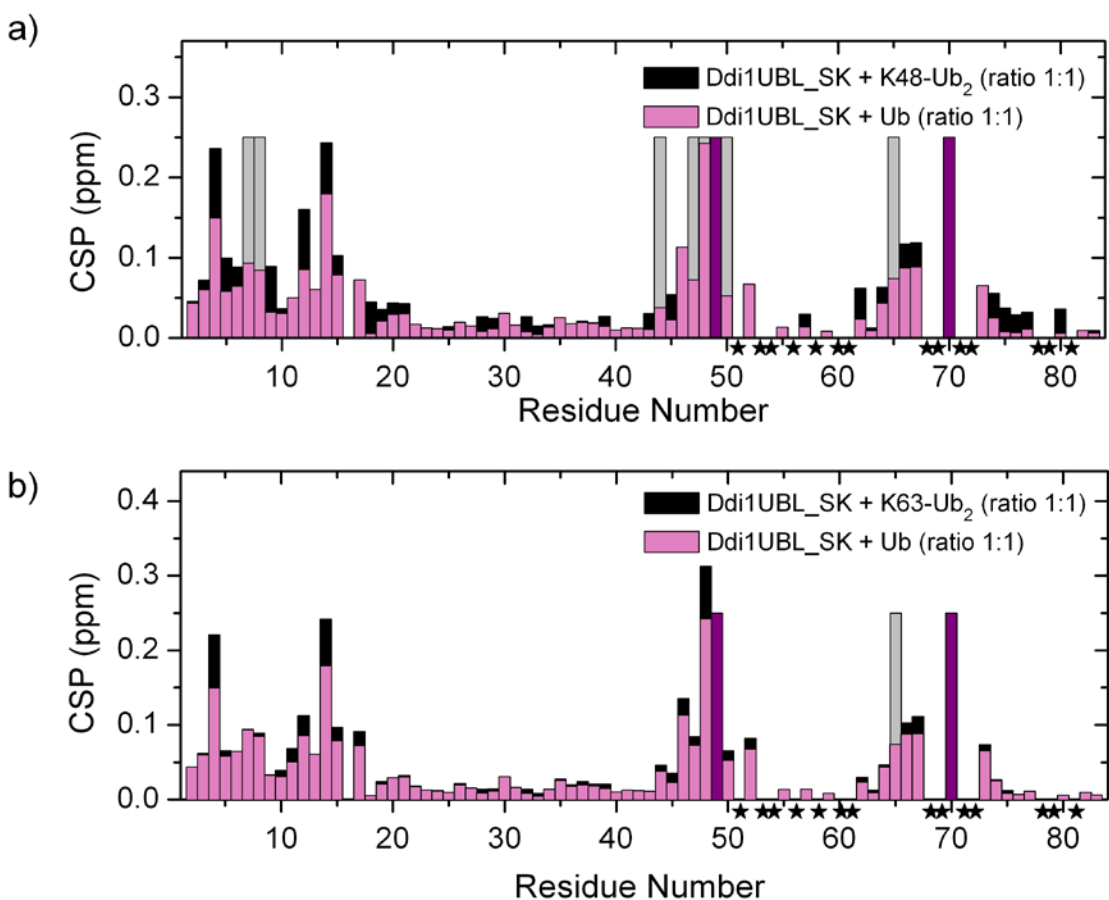


**Figure 4-28. CSP between free Ddi1UBL\_SK and Ddi1UBL\_SK bound to Ub, K48- and K63-Ub<sub>2</sub>.** (a) Comparison of CSP of Ddi1UBL\_SK upon Ub binding and CSP of Ddi1UBL\_SK upon K48-Ub<sub>2</sub> binding. (b) Similar comparison, as in a) but K63-Ub<sub>2</sub> was used as second ligand. All compared bound states are in 1:1 molar ratio of Ddi1UBL\_SK to its ligand. Gray bars show residues that attenuated upon Ub binding. Purple bars indicate residues that attenuated upon adequate Ub<sub>2</sub> binding. Stars show overlapping residues for which CSP values could not be estimated.

It must be emphasized that despite potential small discrepancies in recognition of both Ub<sub>2</sub> the bound states (Ddi1UBL\_SK:K48-Ub<sub>2</sub> and Ddi1UBL\_SK:K63-Ub<sub>2</sub>) when compared with each other show very similar peak positions for the number of residues (Figure 4-29). This would mean that at least these peaks are affected by recognition of Ub<sub>2</sub>s in a very similar way.

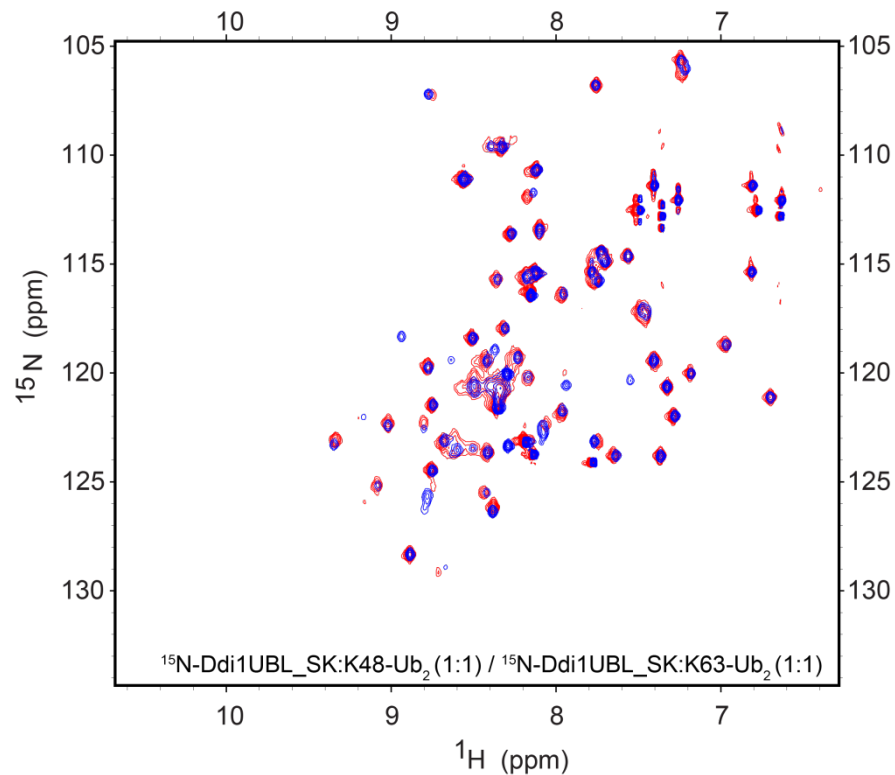


**Figure 4-29.** Comparison of Ddi1UBL\_SK spectra at bound states with K48-Ub<sub>2</sub> and K63-Ub<sub>2</sub>. In red <sup>15</sup>N-Ddi1UBL\_SK in the presence of K48-Ub<sub>2</sub> at 1:1 ratio, as blue peaks <sup>15</sup>N-Ddi1UBL\_SK in the presence of K63-Ub<sub>2</sub> at 1:1 ratio is shown.

# **Chapter 5. UBL domain of Ubp6, purification and NMR data collection**

Ubp6 is one of four deubiquitinase enzymes (DUB) in *S.cerevisiae* that associates with the base of the proteasome<sup>87,88</sup>. It is responsible for removing ubiquitin moieties from polyUb chains that are attached to the substrate protein targeted for degradation. It was proposed that Ubp6 is responsible for regulation of the nature and magnitude of proteasome activity<sup>89</sup>. Ubp6 is a cysteine protease whose activity increases 300-fold when bound to the proteasome<sup>87</sup>. It was shown that Ubp6 recognizes the proteasome's Rpn1 subunit through its UBL domain, what makes it a very interesting subject for biochemistry and biophysical studies.

## **5.1 Ubp6 construct design**

The construct of Ubp6UBL that was available for structural studies did not have a cleavable His-tag and an additional seven residues at the C-terminal end were present:

MRGSHHHHHGSSGETFEFNIRHSGKVYPITLSTDATSADLKSKAELTQVPSA  
RQKYMVKGLSGEESIKIYPLIKPGSTVMLLGTPDANLQPSLIS

For the convenience of further studies it was desired to clone this coding sequence in the pET15b plasmid, which contains N-terminal His-tag followed by a thrombin site. The pET15b plasmid was cut with NdeI and BamHI restriction enzymes. The same restriction sites were introduced into the primers used for the amplification of the sequence of interest.

After successful cloning the final Ubp6UBL construct had the following sequence:

MRSSHHHHHSSGLVPRGSMTFEFNIRHSGKVYPITLSTDATSADLKSKAEELT  
QVPSARQKYMVKGGLSGEESIKIYPLIKPGSTVMLLGTPDAN

## 5.2 Protein purification

Ubp6UBL coding sequence was cloned in pET15b vector and expressed in BL21(DE3) cells. The cells were grown in LB media till  $A_{600}=0.6\text{-}0.8$  and protein expression was induced with 1mM IPTG overnight at 20°C. Uniformly isotope labeled  $^{15}\text{N}$  and  $^{13}\text{C}/^{15}\text{N}$  Ubp6UBL protein was enriched with  $^{15}\text{NH}_4\text{Cl}$  and  $^{13}\text{C}_6\text{-D-glucose}$  (for double labeled sample) and grown in M9 minimal medium, and similar to the unlabeled sample cells, were induced overnight at 20°C. Proteins were purified using a 5mL HiTrap Chelating HP Column. The chromatogram and corresponding SDS-PAGE gel from HiTrap purification of unlabeled Ubp6UBL is shown in Figure 5-1 a) and b).

Protein eluted from the HiTrap column was dialyzed in PBS. The His-tag was cleaved by incubation with thrombin for 4 hours at room temperature. In the next step, the sample was passed through a 1mL benzamidine column. For the final purification the Ubp6UBL sample was applied to a Superdex 75 120mL column. The chromatogram and SDS-PAGE gel of the final sample is shown in Figure 5-1 c) and d).

Comments: The protein sample has a tendency to precipitate at high concentrations. Is recommend to mix the sample often during concentrations and buffer exchanges. The Ubp6UBL concentrated sample precipitates also in the presence of 10% glycerol.

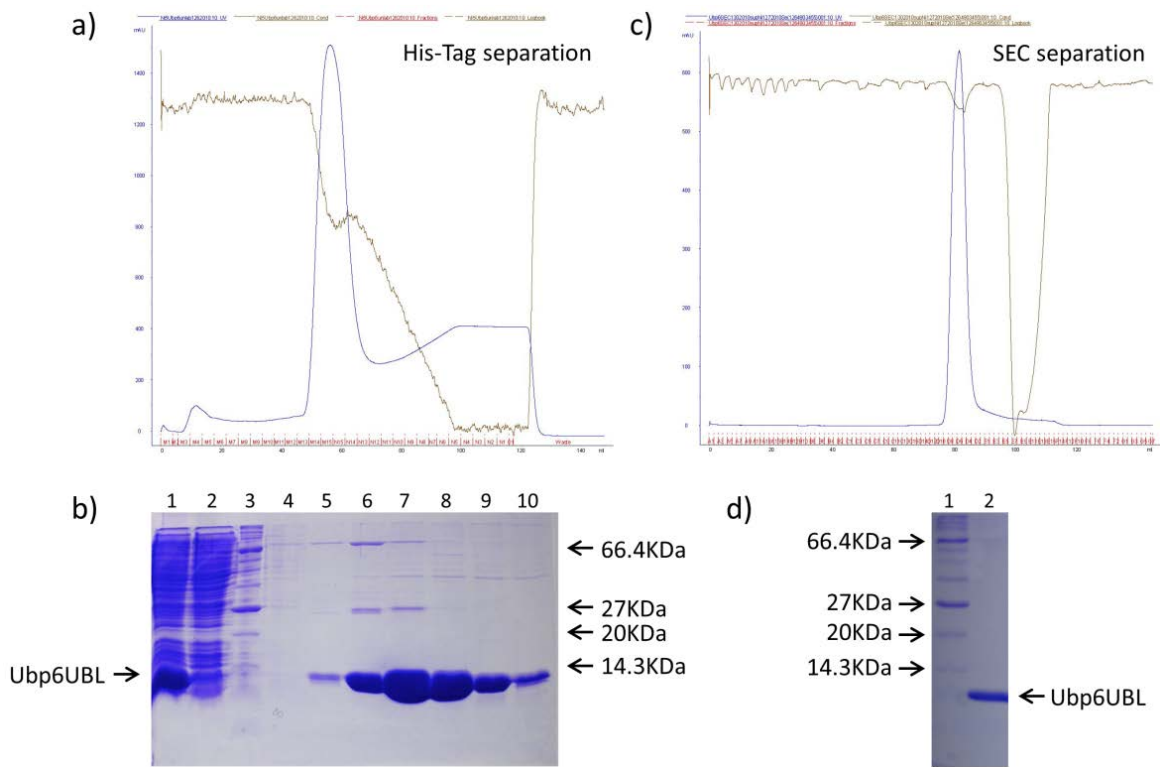


**Figure 5-1. Purification of unlabeled sample of Ubp6UBL.** (a) Chromatogram of sample purification on 5mL HiTrap Chelating HP Column. (b) 15% SDS-PAGE gel of HiTrap Chelating HP Column purification step of unlabeled Ubp6UBL, lane 1: lysate loaded into the column, lane 2: column loading flow through, lane 3: NEB Protein Marker, Broad Range (2-212 kDa), lane 4-10: HiTrap fractions M4, M13, M14, M15, N15, N14 and N13, respectively. (c) Chromatogram of final purification step of Ubp6UBL on Superdex 75 with 120mL column volume. (d) 15% SDS-PAGE gel of unlabeled Ubp6UBL after all purification steps. Lane 1: NEB Protein Marker, Broad Range (2-212 kDa), lane 2: purified Ubp6UBL sample.

### **5.3 Ubp6UBL NMR data collection for resonance assignment**

After purifying the new Ubp6UBL construct, the goal was to collect all spectra necessary for full resonance assignment of the UBL domain. In the future, as was done for Ddi1UBL, such assignment will be used to do sequential assignment which is very convenient for functional and structural studies. For that purpose, a series of NMR two and three dimensional experiments were collected with use of  $^{15}\text{N}$ -Ubp6UBL and  $^{13}\text{C}$ ,  $^{15}\text{N}$ -Ubp6UBL samples. The following experiments were collected: HNCO, HN(CA)CO, HN(CO)CA, HNCA, CBCA(CO)NH, HNCACB, HNCACO as well as 2D, 3D TOCSY and 2D, 3D NOESY.

### **5.4 Ubp6UBL has more than one conformation?**

After close examination of the  $^1\text{H}$ - $^{15}\text{N}$  HSQC spectrum of Ubp6UBL, it was interesting to note that there are more peaks in the spectrum than one would anticipate (Figure 5-2). For the 80 amino acid construct with 5 prolines in its sequence and excluding the first amino acid for which the amide is very often not observed, there should be 74 resonances, excluding side chains. Surprisingly, there are at least 94 peaks in the spectrum, counting only peaks of strong intensities but excluding peaks that probably come from  $\text{NH}_2$  in the side chains. The increased number of peaks in the spectrum can be explained either by the presence of more than one species in the spectrum, or that Ubp6UBL can have more than one conformation in solution. Ubp6UBL samples go through an extensive purification including specific affinity tag purification; therefore it is less probable that there will be an impurity with the same size and affinity properties as the Ubp6UBL construct.

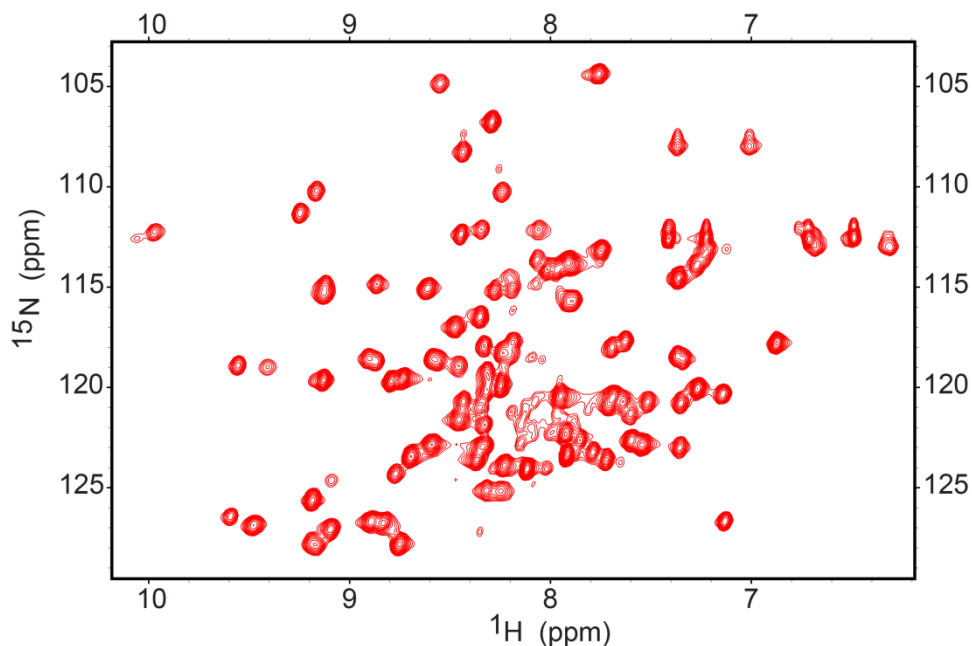


**Figure 5-2.**  $^1\text{H}$ - $^{15}\text{N}$ -HSQC spectrum of Ubp6UBL in 20mM phosphate buffer, pH=6.8, at 25°C.

Another possibility is that Ubp6UBL degrades with time into small peptides. It would be expected that such shorter fragments will be less structured and probably would gain some flexibility.

Interestingly, when the hetNOE spectrum was collected, the majority of peaks had positive signals indicating that they belonged to well-structured residues, and only a few signals showed negative signals that correspond to flexible amide groups (Figure 5-3).

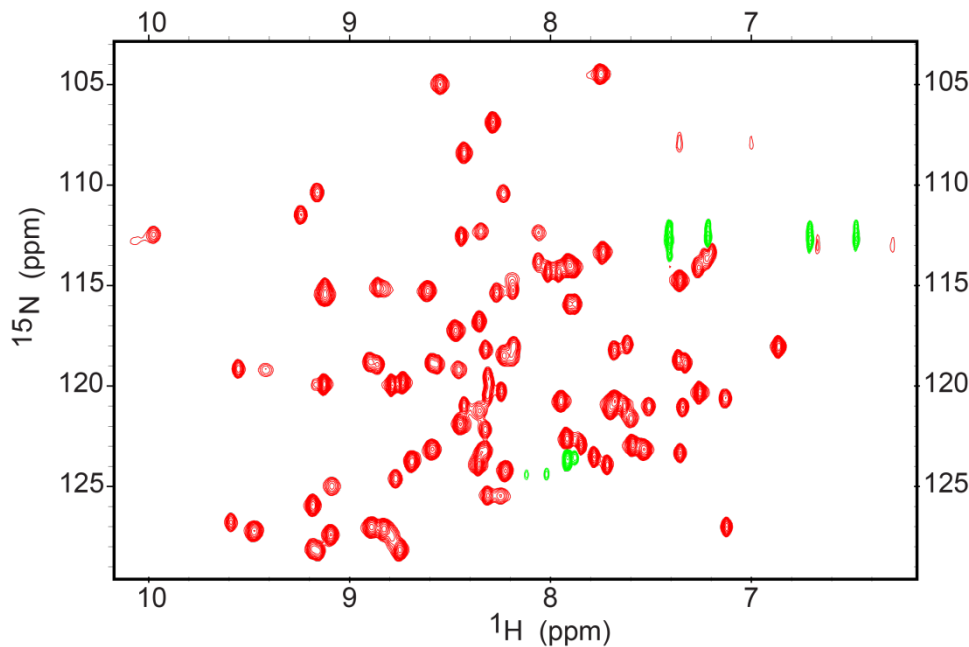


**Figure 5-3. HetNOE spectrum of Ubp6UBL. In red peak with positive signal intensities, in green peaks with negative intensities. Spectrum collected at 25°C temperature.**

Since the majority of signals in hetNOE are positive, this would not support the scenario that Ubp6UBL undergoes degradation resulting in a number of smaller, less structured peptides. If indeed the increased number of peaks is an indication of different conformations of amino acids in Ubp6UBL these peaks could undergo chemical exchange, which is temperature dependent. When the Ubp6UBL sample spectrum was measured at additional temperatures 17°C and 35°C, changes in the spectrum are observed (Figure 5-4). As highlighted on the spectrum, two types of changes can be easily noticed, one, when at low temperature there is only one signal but there are two peaks at higher temperature, and two, when the intensities between the two peaks, which likely corresponds to the same amide group, changes with the change of

temperature. Both phenomena are characteristic for chemical exchange when the nucleus exchanges intramolecularly between conformers, supporting the hypothesis that Ubp6UBL has more than one conformation in solution. It is worth mentioning that for some signals in triple resonance experiments two sets of carbon chemical shifts can be also observed.

In the future, resonance and sequential assignment must be performed. The possibility of Ubp6UBL having more than one conformation also has to be investigated further.

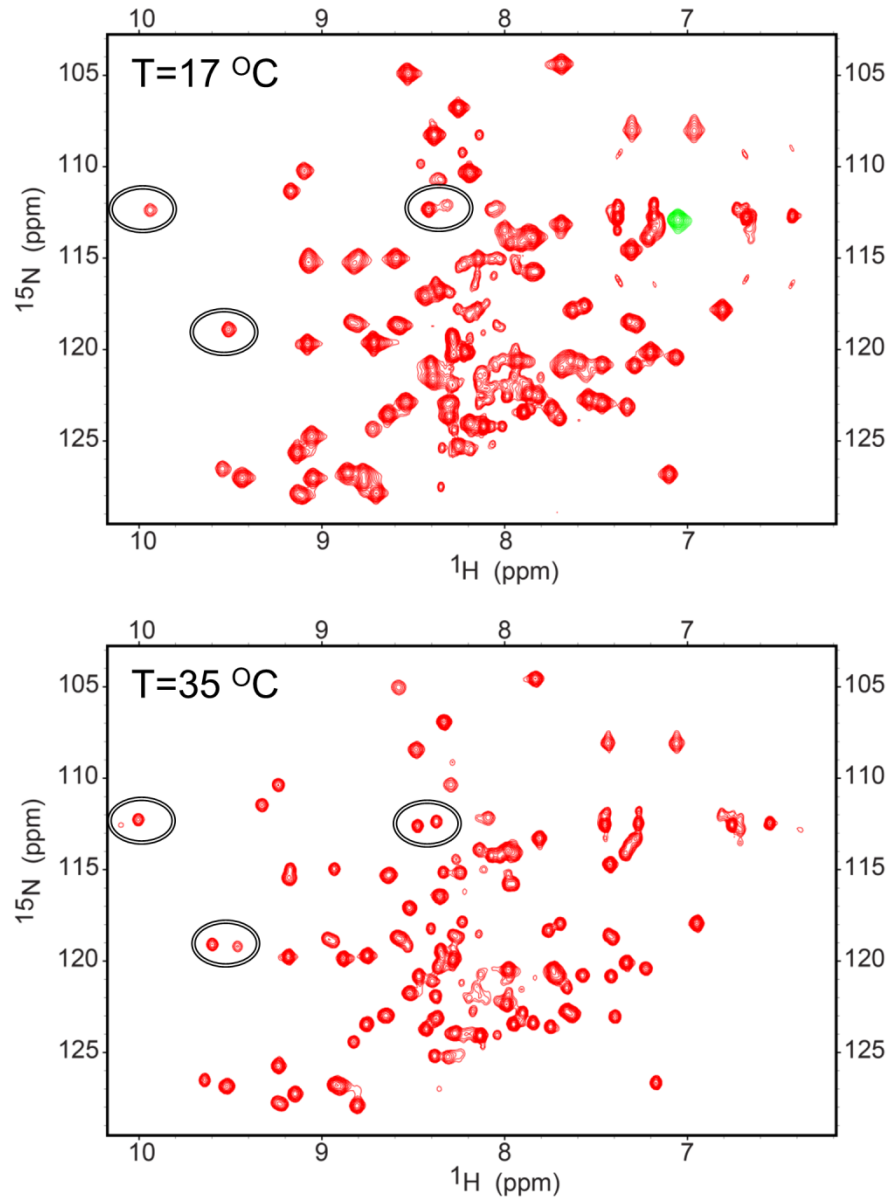


**Figure 5-4.**  $^1\text{H}$ - $^{15}\text{N}$  SOFAST-HMQC spectra of Ubp6UBL sample collected at low temperature,  $17^\circ\text{C}$  and higher temperature  $35^\circ\text{C}$ . The highlighted ellipsoids contain residues that probably undergo chemical exchange upon change of temperature.

# **Chapter 6. Discussion and future project direction**

## **6.1 Discussion**

This work presents a thorough characterization of Ddi1 from *S.cerevisiae* and provides important information about its potential function in the cell. The UBL domain is capable of recognizing Ub and Ub conjugates, shedding new light on this system, and is important in explaining how a protein without a UBA domain can perform its shuttling function.

Ddi1 is a multi-domain protein in which each domain performs a different function. All three main domains: UBL, RVP and UBA do not interact with each other and are connected through flexible linkers that allow them to tumble independently. This finding justifies the relevance of structural and functional studies of UBA and UBL domains individually. Despite low sequence identities the N-terminal fragment of Ddi1 has a ubiquitin-like fold. There are small discrepancies between this structure and the structure of Ub, such as secondary structure packing, the presence of a long flexible loop, and lack of a classical Ub hydrophobic patch. Surprisingly, the UBL domain of Ddi1 displayed completely unexpected binding properties. Based on our knowledge, the Ddi1UBL domain is the first UBL domain that has a ubiquitin-like fold but does not behave as ubiquitin with respect to its binding preferences. Here, it was shown that the UBL domain of Ddi1 is capable of interacting with Ub itself which is unusual and has not been observed for any other UBL domain before. Ddi1UBL utilizes the binding site that is located on the  $\beta$ -sheet, similar to the one on Ub. The interface between these two proteins is mainly based on hydrophobic residues stabilized by surrounding polar and

charged residues. Interestingly, this interaction is stronger than the UBA interaction with ubiquitin. The unique features of Ddi1 UBL discovered in this work allows for re-interpretation of some published data. The fluorescence studies published by Bertolaet et al., 2001 show that full-length Ddi1 interacts with Ub with an  $K_d$  of  $\sim 10 \mu\text{M}$ . Based on the results presented here, it can be concluded that the main source of strong binding was the Ub:Ddi1UBL interaction and not the Ub:Ddi1UBA interaction, as previously interpreted<sup>32</sup>.

In addition to the Ddi1UBL interaction with Ub, these studies show that it can also interact with the UBL domain of Dsk2. Unfortunately, the implications of this interaction for the function of Ddi1 are unclear. Nevertheless, this interaction involves two binding sites on the Ddi1UBL structure. One,  $\beta$ -sheet which is the same as for Ub binding, and another that includes the  $\alpha$ -helix with a UIM-like motif, which is again unique for the Ddi1 when compared to known UBL domains. Also, the second binding site discovered in this work helps the UBL domain of Ddi1 to distinguish between different Ub<sub>2</sub> linkages, which might be very important for selecting the proper linkage when performing the shuttling function.

It was shown in previous studies that turnover of the Ufo1 protein depends upon Ddi1<sup>56</sup>. Knowing that the presence of the UBL domain of Ddi1 and UIMs of Ufo1 is important for this phenomenon, we tested whether both domains interact with each other. Surprisingly, no direct interaction was observed between them. However, based on the unique properties of the Ddi1 UBL domain, such as selecting for polyUb chains and that UIMs of Ufo1 binds Ub, it can be proposed that the Ufo1:Ddi1 interaction is indirect and is mediated through ubiquitin chains. Interestingly, as Ddi1 is also

important for degradation of Ho endonuclease, and both proteins interact only while Ho endonuclease is already ubiquitinated, Ddi1 might interact with the Ub chain on Ho endonuclease not only through UBA but also through the UBL domain<sup>90</sup>. Since Ho endonuclease is recruited by Ufo1 to the SCF complex for ubiquitination, it is possible that (1) the UIM domains of Ufo1 stabilize ubiquitin chain build up on the substrate and once the chain has reached the appropriate length for signal degradation, the UBL domain of Ddi1 outcompetes the Ufo1UIM:Ub interaction with its stronger affinity and helps in releasing the ubiquitinated Ho endonuclease from the E3 ligase, (2) in a situation where Ufo1 is not near Ho endonuclease in space, the Ufo1:Ub:Ddi1 complex aids in bringing Ddi1 in close proximity to ubiquitinated Ho endonuclease, hence allowing the UBA domain of Ddi1 to reach the Ub chain on the substrate, and (3) despite Ufo1 and Ho endonuclease being functionally linked, their interactions with Ddi1 are independent processes.

Nevertheless, as a shuttle protein Ddi1 should bind ubiquitinated proteins and deliver them to the proteasome for degradation. For Ddi1 in *S.cerevisiae*, a number of possible modes of interaction with polyUb chains can be proposed (Figure 7-1). “Classical” UBL-UBA shuttle proteins (Rad23, Dsk2) utilize their UBA domain(s) to bind to the polyUb tag on a substrate, and use their UBL domain to bind to the Rpn1 subunit of the 19S regulatory particle (RP)<sup>82,91</sup>. The unusual dual functionality of the Ddi1 UBL, which is capable of binding both Ub and 19S RP, suggests that Ddi1 might not act as a classical shuttle protein. Both UBL and UBA of Ddi1 could be bound to polyUb (Figure 7-2), with subsequent dissociation of the UBL to bind to Rpn1 when in close proximity to 19S. Another scenario could be that Ddi1 forms heterodimer with

Rad23 through the UBA1 and acts as a tandem shuttle. It should be kept in mind that the same heterodimerization will increase the local concentration of the Ub-binding domains and protect the chain together with UBA2 domains of Rad23. Consequently, depending on the interaction Ddi1 is involved in, it will act either as a positive or negative regulator, delivering for degradation and consequently disassembling the polyUb chains or protecting the chains from degradation.

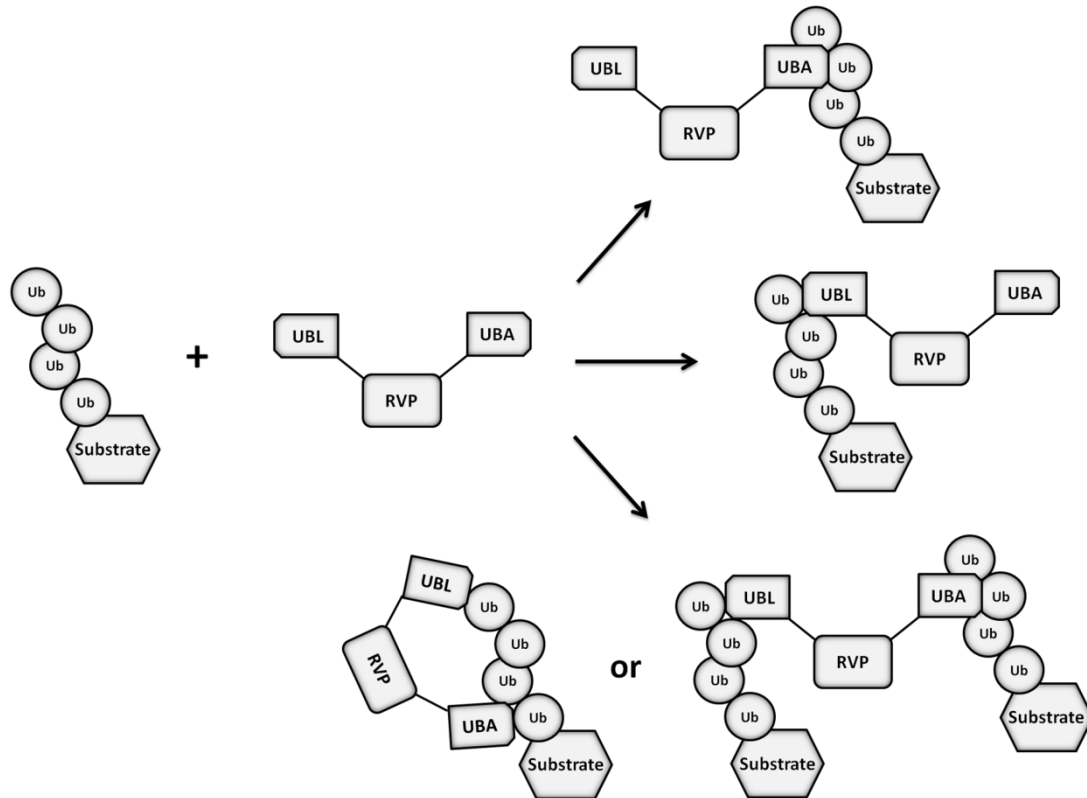
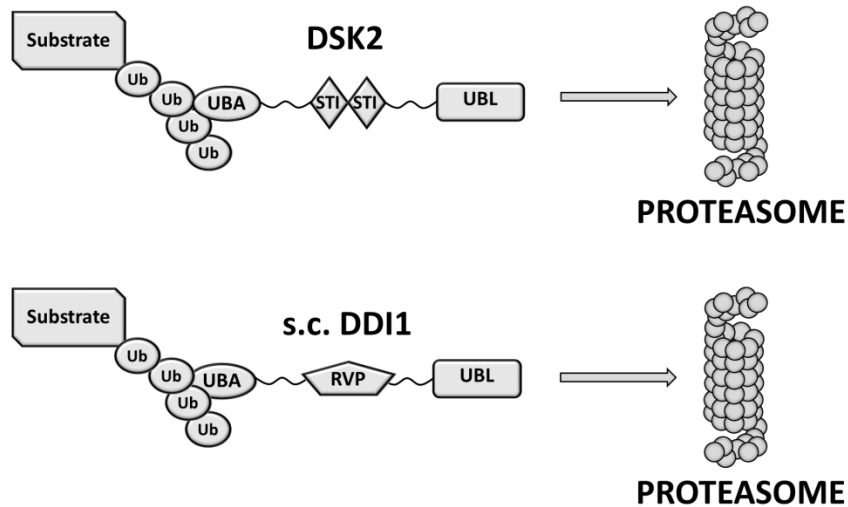


**Figure 6-1. Ddi1 recognition of ubiquitinated substrates in *S.cerevisiae*. Ddi1 has two domains UBA and UBL, that can recognize Ub, therefore it can use either or both of them to recognize Ub conjugates.**

## *Classical Shuttle*



## *Alternative Shuttle*

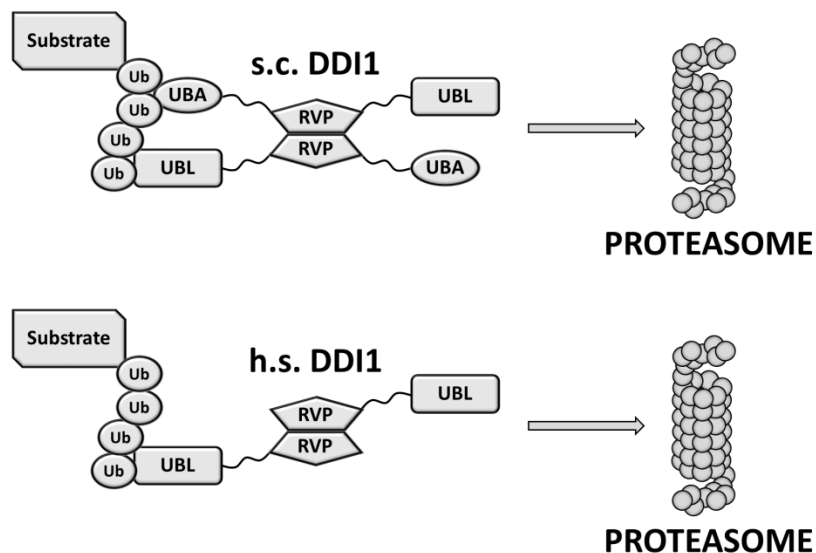


**Figure 6-2.** Schematic representation of a possible function of Ddi1 as a proteasomal shuttle in yeast and humans. Yeast denoted as s.c. and humans as h.s..

To summarize, the detailed role of Ddi1 and its unique UBL domain is not fully understood. UBL domain binding to Ub indicates that Ddi1 might not be a classical shuttle protein. Moreover, other UBL-UBA proteins have both UBA and UBL domains conserved among different eukaryotes while Ddi1 retains its UBL domain in higher eukaryotes but does not have a UBA domain any longer. This evolution may change might be added proof that Ddi1 performs its shuttle protein role differently than Rad23 and Dsk2. Finally, more studies need to be performed to fully understand the detailed function of the UBL domain of Ddi1 in the cell. Based on these findings, it will be required to redefine what it means for a domain to be ubiquitin-like.

## 6.2 Future project direction

The presented research introduced significant insights into the role of Ddi1; however it is not clear how in detail Ddi1 performs its function. First, it is not fully understood how Ddi1 is recognized by the proteasome. There were two studies that examined the Ddi1 interaction with proteasomal Rpn1 subunit; however they delivered contradictory results<sup>20,91</sup>. Therefore, further studies should focus on characterizing whether and how Ddi1 interacts with the proteasome. There are four main subunits that are potential docking sites for the Ddi1 as a shuttle: Rpn1, Rpn2, Rpn10 and Rpn13 and it is necessary to examine whether Ddi1 interacts with any of them. More interestingly, if any of these interactions are mediated through the UBL domain, it will be necessary to compare it with binding of already characterized partners and consequently try to explain how Ddi1 can perform its function utilizing mainly just the UBL domain.

Competition experiments would definitely deliver more information about such a possibility. Additionally, it will be fascinating to see if Ddi1 is capable of pulling any component of the proteasome from the cell extract. This would provide further evidence that Ddi1 is involved in the ubiquitin proteasomal system.

It must be emphasized that the above results were conducted with Ddi1 from *S.cerevisiae*. The same properties should be tested with constructs from other organisms, especially the UBL domain in Ddi1 from mammals. This is very important to keep in mind that the UBA domain is not present in mammals (Figure 1-16), therefore it would be essential for the Ddi1UBL domain from these organisms to also have Ub binding capability in order to perform Ddi1 shuttling function.

Finally, there are some discrepancies between the UBL domain in yeast and in human (Figure 7-3).

Ddi1UBL_Human	1 MLITVYCVRRDLS-----EVTFSLQVS PDFELRNFKVLCEAESRVPVE	43
	.  :        :....:   .  .. .: :.....	
Ddi1UBL_Yeast	1 -----MDLTISNELTGEIYGPIEVSEDMAL <u>TDLIALLQADCGFDKT</u>	41
Ddi1UBL_Human	44 EIQIIHMERLLIEDHC-SLGSYGLKDGDIVVLLQKDNVG	81
	:...:....: ... ...     ...   ... :.... :...	
Ddi1UBL_Yeast	42 KHDLYYNMDILDNSRTQSLKELGLKTDLALLIRGKISNS	80

**Figure 6-3. Sequence alignment of UBL domain of Ddi1 from *S.cerevisiae* and from *H.sapiens*. Lines indicate identity between sequences; colons indicate similarity. Underlined is the UIM like sequence in Ddi1UBL from *S.cerevisiae*. The EMBOSS program was used to align the sequences<sup>60</sup>.**

Based on Emboss alignment results, both UBL sequences share approximately 40% similarity. Interestingly, the LIALL sequence that is present in Ddi1UBL from *S.cerevisiae* is not present in the Ddi1 UBL domain in *H.sapiens*. This questions whether human Ddi1UBL will have the same binding properties, especially for Dsk2UBL and Ub<sub>2</sub>.

Ddi1 and particularly its UBL domain are very interesting subjects to study and clearly it is very important to understand its function and involvement in the ubiquitin proteasomal system. Future studies will help to answer the question of whether uncharacteristic properties of Ddi1UBL are in “response” to evolutionary loss of the UBA domain.

# **Chapter 7. Materials and methods**

## **7.1 Proteins constructs and purifications**

The Ddi1UBL construct used in these studies contains the UBL domain of yeast Ddi1 amino acids 2-80 (Uniprot P40087), 12 amino acids at the N-terminus with a His-tag (MRGSHHHHHGS) and 3 amino acids at the C-terminal (KLN). Since both extensions are not part of Ddi1 all amino acid numbering presented in the paper corresponds to the actual residue position in Ddi1. Ddi1UBL mutants, Ddi1FL, Dsk2FL, Rad23FL, Dsk2UBL, Rad23UBL and Ufo1UIM (Uniprot Q04511, 576-668 fragment containing three UIM motifs) constructs also contain His-tag extension for purification purpose. They were cloned in the pQE30 vector (Qiagen) and expressed in M15 cells, with the exception of Ufo1UIM which was cloned in pET28b (Novagen) and expressed in BL21(DE3)-Rosetta cells, and Ub which was in pET3a and expressed from BL21(DE3)-pJY2 cells. All above constructs were grown in LB media till  $A_{600}=0.6-0.8$  and induced with 1mM IPTG for 6h at 37°C, or overnight at 20°C. Isotopically labeled  $^{15}\text{N}$  or  $^{13}\text{C}/^{15}\text{N}$  Ddi1UBL was uniformly enriched with  $^{15}\text{NH}_4\text{Cl}$  or  $^{13}\text{C}_6\text{-D-glucose}$  in M9 minimal medium and induced overnight at 20°C. Proteins were purified using 5mL HiTrap Chelating HP Column followed by size exclusion separation on a Superdex 75 120mL column. Expression and purification of human Ub WT was performed as described elsewhere<sup>92</sup>.

## 7.2 Sequence analysis

All sequences used for analysis of the Ddi1 gene structure can be found in the Uniprot Database under the following ID numbers: Q8WTU0, Q95JI3, Q9DAF3, A0JPP7, F1MG01, A8B333, B9SX98, B9QR20, Q4UDI9, Q10256, Q5AY89, G3JEF4, Q2H085 and Q54JB0. Sequence comparison was performed using ClustalW/ClustalOmega software available at EMBL-EBI webpage and domain prediction software CDD and SMART<sup>93-98</sup>. Sequence alignment and quantification of sequence identity and similarity of Ddi1 UBA and UBL domains with human Ub (P0CG47), yeast Ub (P0CG63), Dsk2 (P48510), Rad23 (P32628) was performed using EMBOSS software<sup>60</sup>. Sequence comparison of  $\alpha$ -helix of Ddi1UBL with known UIM domains was also done with ClustalOmega<sup>94,95</sup>. Uniprot codes of sequences used for this comparison: P42567, Q12518, P55036, P38886, Q9UHP3, P40343, Q8GY23 and O14964.

## 7.3 NMR experiments

Final NMR samples were prepared in 20mM sodium phosphate buffer, pH 6.8, 5% D<sub>2</sub>O, 0.02% NaN<sub>3</sub>. In addition Ddi1FL, Ddi1UBL, Rad23UBL samples and Cys mutants of Ub contained 3mM TCEP. All measurements were collected on Avance III 600 MHz Brucker Biospin spectrometer equipped with CPTCI cryoprobe and on 800MHz Brucker Ascend equipped with CPQCI cryoprobe at 23°C. All spectra were processed using TopSpin 2.1 software and were analyzed using Sparky or CARA programs<sup>66,99,100</sup>. <sup>1</sup>H-<sup>15</sup>N HSQC and TROSY spectra were acquired for verification of the full-length construct with individual domains. Triple resonance NMR experiments:

HNCO, HN(CA)CO, HN(CO)CA, HNCA, CBCA(CO)NH, HNCACB were used for  $^1\text{H}_\text{N}$ ,  $^{15}\text{N}$ , C', C $\alpha$ , C $\beta$  resonance assignment. CC(CO)NH, H(CCO)HN along with 2D and 3D TOCSY were used to obtain complete proton and carbon Ddi1UBL assignment. 2D and 3D NOESY spectra were collected and analyzed to obtain inter-proton NOE distance constraints for Ddi1UBL.  $^{15}\text{N}$  relaxation measurements: T1, T2 and steady-state hNOE were performed as described previously<sup>101</sup>. The overall rotational correlation time ( $\tau_\text{c}$ ) was determined using ROTDIF<sup>79,101</sup>. The RDC measurements were performed in PEG/hexanol-based alignment medium<sup>102</sup> using IPAP-HSQC experiments<sup>73</sup> and analysed using ALTENS program to determine alignment tensors<sup>41</sup>.

## 7.4 NMR binding assays

All binding experiments were conducted by monitoring changes in the peak positions in  $^1\text{H}$ - $^{15}\text{N}$  SOFAST-HMQC spectra upon titrations, with the exception of Ddi1FL for which  $^1\text{H}$ - $^{15}\text{N}$  TROSY experiments were collected. The changes in peak positions were quantified as chemical shift perturbations (CSP) using the following equation  $\Delta\delta=[\Delta\delta_{\text{H}}^2+(\Delta\delta_{\text{N}}/5)^2]^{0.5}$ , where and are difference in the chemical shift for  $^1\text{H}$  and  $^{15}\text{N}$  respectively. Obtained CSP values were used to calculate the binding affinities by fitting different binding models using in-house software KDfit as detailed elsewhere<sup>41</sup>.

## 7.5 HD exchange experiments

1mM sample of  $^{15}\text{N}$  Ddi1UBL was lyophilized in 20mM sodium phosphate buffer pH 6.8. Subsequently, it was rapidly dissolved in D<sub>2</sub>O and used for NMR

experiments. A series of  $^1\text{H}$ - $^{15}\text{N}$  SOFAST-HMQC spectra were collected at 600MHz Bruker spectrometer at 23°C. All experiments were collected with the same experimental parameters with the exception of the number of scans. In total 45 spectra were collected over a time of ~4h, experiments 1 to 14 were collected with 4 scans and approximate experimental time of each was 2.5 minutes, 15 to 34 had 8 scans and every experiment took 5 min, in the last series 35-45 each experiment had 16 scans and took 10 min. The dead time between sample resuspension in D<sub>2</sub>O and first experiment was 8 min. It was assumed that buffering properties are very similar in H<sub>2</sub>O and D<sub>2</sub>O, and no major shifts will be observed in the spectrum. This hypothesis was confirmed after collecting spectra.

## 7.6 PRE experiments for complex structure calculations

The paramagnetic spin label, 1-oxyl-2,2,5,5-tetramethyl-3-pyrroline-3-methyl methanesulfonate (MTSL), was attached to a Cys side chain of each of the constructs: UbT12C, UbK63C and UbG75Cs, as described<sup>41,103</sup>. The paramagnetic relaxation enhancement (PRE) effects in Ddi1UBL were expressed for each amino acids as the ratio of the signal intensities in the  $^1\text{H}$ - $^{15}\text{N}$  HSQC spectra recorded with MTS defense in the oxidized and reduced states. All measurements were performed for  $^{15}\text{N}$ -Ddi1UBL mixed in 1:1 molar ratio with UbT12C-MTS defense, UbK63C-MTS defense or UbG75C-MTS defense. PRE data analysis such as reconstruction of the MTS defense position on Ub and distance between spin label and particular amino acid position was determined with a use of SLFIT program<sup>104</sup>.

## 7.7 Ddi1FL DUB activity assay

Reaction mixture contained 25  $\mu\text{M}$  of a given di-ubiquitin chain (K6-, K11-, K27-, K29-, K33-, K48-, K63-Ub2) and 5  $\mu\text{M}$  of FL Ddi1, in 50 mM Tris at pH 8.0. Total reaction volume was 50 $\mu\text{L}$  and each reaction was carried out at 30°C. Samples were taken at indicated time points, ran on SDS-PAGE gels, and stained with coomassie blue.

## 7.8 Sedimentation equilibrium

The molecular mass of Ddi1UBL was determined by sedimentation equilibrium measurement using Beckman Coulter Optima XL-1 instrument. The analytical ultracentrifuge was equipped with a four-hole An-60 rotor. The sample was placed in 12mm six-hole cells with charcoal-filled Epon centerpieces with sapphire windows. Ddi1UBL (250 $\mu\text{M}$ ) sample in 20mM sodium phosphate buffer, pH 6.8 with 3mM TCEP was centrifuged at three rotor speeds: 26000, 29000 and 32000 rpm at 20°C. Absorbance at 290nm was measured with 0.001 cm intervals and 5 replicates per step. All data were analyzed globally using the program WinNonLin<sup>105</sup>. The best fit was obtained for the single species model. The reduced molecular weight ( $\sigma$ ) obtained from this analysis allowed for the calculation of the molecular weight (M):

$$\sigma = ((M(1-\nu\rho)) / RT)\omega^2$$

$\nu$  is partial specific volume of the protein,  $\rho$  is buffer density,  $\omega$  is rotor angular velocity, R is gas constant and T is the absolute temperature.

## **7.9 Mass spectrometry**

The mass spectra of the diluted sample of Ddi1UBL were collected using electrospray positive mode with flow injection on JEOL AccuTOF-CS mass spectrometer and were deconvoluted using MagTran software.

## **7.10 Circular dichroism**

The spectra were measured in Jasco J-810 spectropolarimeter in continuous mode with 100nm/min scanning speed, 4sec response and 2nm bandwidth. The experiments were performed at 4.5 $\mu$ M Ufo1UIM concentration in 20mM NaP buffer at pH 6.8 in a cuvette with 10mm path length. Ellipticity was monitored in the range of 190-340 nm at temperature of 18°C.

## References

1. Ciechanover, A. The ubiquitin-proteasome proteolytic pathway. *Cell* **79**, 13-21 (1994).
2. Yamaguchi, R. & Dutta, A. Proteasome inhibitors alter the orderly progression of DNA synthesis during S-phase in HeLa cells and lead to rereplication of DNA. *Exp Cell Res* **261**, 271-83 (2000).
3. Conaway, R.C., Brower, C.S. & Conaway, J.W. Emerging roles of ubiquitin in transcription regulation. *Science* **296**, 1254-8 (2002).
4. Muratani, M. & Tansey, W.P. How the ubiquitin-proteasome system controls transcription. *Nat Rev Mol Cell Biol* **4**, 192-201 (2003).
5. Schubert, U. et al. Rapid degradation of a large fraction of newly synthesized proteins by proteasomes. *Nature* **404**, 770-4 (2000).
6. Rock, K.L. & Goldberg, A.L. Degradation of cell proteins and the generation of MHC class I-presented peptides. *Annu Rev Immunol* **17**, 739-79 (1999).
7. Hicke, L. A new ticket for entry into budding vesicles-ubiquitin. *Cell* **106**, 527-30 (2001).
8. Hicke, L. Protein regulation by monoubiquitin. *Nat Rev Mol Cell Biol* **2**, 195-201 (2001).
9. Hoege, C., Pfander, B., Moldovan, G.L., Pyrowolakis, G. & Jentsch, S. RAD6-dependent DNA repair is linked to modification of PCNA by ubiquitin and SUMO. *Nature* **419**, 135-41 (2002).
10. Spence, J., Sadis, S., Haas, A.L. & Finley, D. A ubiquitin mutant with specific defects in DNA repair and multiubiquitination. *Mol Cell Biol* **15**, 1265-73 (1995).
11. Ciechanover, A. The ubiquitin-mediated proteolytic pathway: mechanisms of action and cellular physiology. *Biol Chem Hoppe Seyler* **375**, 565-81 (1994).
12. Lee, D.H. & Goldberg, A.L. Proteasome inhibitors: valuable new tools for cell biologists. *Trends Cell Biol* **8**, 397-403 (1998).

13. Rock, K.L. et al. Inhibitors of the proteasome block the degradation of most cell proteins and the generation of peptides presented on MHC class I molecules. *Cell* **78**, 761-71 (1994).
14. Adams, J. et al. Proteasome inhibitors: a novel class of potent and effective antitumor agents. *Cancer Res* **59**, 2615-22 (1999).
15. McNaught, K.S. & Olanow, C.W. Proteasome inhibitor-induced model of Parkinson's disease. *Ann Neurol* **60**, 243-7 (2006).
16. McNaught, K.S., Jackson, T., JnoBaptiste, R., Kapustin, A. & Olanow, C.W. Proteasomal dysfunction in sporadic Parkinson's disease. *Neurology* **66**, S37-49 (2006).
17. Clarke, D.J. et al. Dosage suppressors of pds1 implicate ubiquitin-associated domains in checkpoint control. *Molecular and Cellular Biology* **21**, 1997-2007 (2001).
18. Elsasser, S., Chandler-Militello, D., Müller, B., Hanna, J. & Finley, D. Rad23 and Rpn10 serve as alternative ubiquitin receptors for the proteasome. *J Biol Chem* **279**, 26817-22 (2004).
19. Elsasser, S. & Finley, D. Delivery of ubiquitinated substrates to protein-unfolding machines. *Nat Cell Biol* **7**, 742-9 (2005).
20. Gomez, T.A., Kolawa, N., Gee, M., Sweredoski, M.J. & Deshaies, R.J. Identification of a functional docking site in the Rpn1 LRR domain for the UBA-UBL domain protein Ddi1. *BMC Biol* **9**, 33 (2011).
21. Hartmann-Petersen, R. & Gordon, C. Integral UBL domain proteins: a family of proteasome interacting proteins. *Semin Cell Dev Biol* **15**, 247-59 (2004).
22. Hicke, L., Schubert, H.L. & Hill, C.P. Ubiquitin-binding domains. *Nat Rev Mol Cell Biol* **6**, 610-21 (2005).
23. Kaplun, L. et al. The DNA damage-inducible UbL-UbA protein Ddi1 participates in Mec1-mediated degradation of Ho endonuclease. *Mol Cell Biol* **25**, 5355-62 (2005).
24. Kleijnen, M.F. et al. The hPLIC proteins may provide a link between the ubiquitination machinery and the proteasome. *Mol Cell* **6**, 409-19 (2000).
25. Lambertson, D., Chen, L. & Madura, K. Pleiotropic defects caused by loss of the proteasome-interacting factors Rad23 and Rpn10 of *Saccharomyces cerevisiae*. *Genetics* **153**, 69-79 (1999).

26. Saeki, Y., Saitoh, A., Toh-e, A. & Yokosawa, H. Ubiquitin-like proteins and Rpn10 play cooperative roles in ubiquitin-dependent proteolysis. *Biochem Biophys Res Commun* **293**, 986-92 (2002).
27. Husnjak, K. et al. Proteasome subunit Rpn13 is a novel ubiquitin receptor. *Nature* **453**, 481-8 (2008).
28. Díaz-Martínez, L.A., Kang, Y., Walters, K.J. & Clarke, D.J. Yeast UBL-UBA proteins have partially redundant functions in cell cycle control. *Cell Div* **1**, 28 (2006).
29. Rao, H. & Sastry, A. Recognition of specific ubiquitin conjugates is important for the proteolytic functions of the ubiquitin-associated domain proteins Dsk2 and Rad23. *J Biol Chem* **277**, 11691-5 (2002).
30. Kang, Y. et al. UBL/UBA ubiquitin receptor proteins bind a common tetraubiquitin chain. *J Mol Biol* **356**, 1027-35 (2006).
31. Verma, R., Oania, R., Graumann, J. & Deshaies, R.J. Multiubiquitin chain receptors define a layer of substrate selectivity in the ubiquitin-proteasome system. *Cell* **118**, 99-110 (2004).
32. Bertolaet, B.L. et al. UBA domains of DNA damage-inducible proteins interact with ubiquitin. *Nature Structural Biology* **8**, 417-422 (2001).
33. Chen, L., Shinde, U., Orton, T.G. & Madura, K. Ubiquitin-associated (UBA) domains in Rad23 bind ubiquitin and promote inhibition of multi-ubiquitin chain assembly. *EMBO Rep* **2**, 933-8 (2001).
34. Funakoshi, M., Sasaki, T., Nishimoto, T. & Kobayashi, H. Budding yeast Dsk2p is a polyubiquitin-binding protein that can interact with the proteasome. *Proc Natl Acad Sci U S A* **99**, 745-50 (2002).
35. Wilkinson, C.R. et al. Proteins containing the UBA domain are able to bind to multi-ubiquitin chains. *Nat Cell Biol* **3**, 939-43 (2001).
36. Beal, R., Devereaux, Q., Xia, G., Rechsteiner, M. & Pickart, C. Surface hydrophobic residues of multiubiquitin chains essential for proteolytic targeting. *Proc Natl Acad Sci U S A* **93**, 861-6 (1996).
37. Haririnia, A. et al. Mutations in the hydrophobic core of ubiquitin differentially affect its recognition by receptor proteins. *J Mol Biol* **375**, 979-96 (2008).
38. Sloper-Mould, K.E., Jemc, J.C., Pickart, C.M. & Hicke, L. Distinct functional surface regions on ubiquitin. *J Biol Chem* **276**, 30483-9 (2001).

39. Fushman, D. & Walker, O. Exploring the linkage dependence of polyubiquitin conformations using molecular modeling. *J Mol Biol* **395**, 803-14 (2010).
40. Varadan, R., Walker, O., Pickart, C. & Fushman, D. Structural properties of polyubiquitin chains in solution. *J Mol Biol* **324**, 637-47 (2002).
41. Varadan, R. et al. Solution conformation of Lys63-linked di-ubiquitin chain provides clues to functional diversity of polyubiquitin signaling. *J Biol Chem* **279**, 7055-63 (2004).
42. Varadan, R., Assfalg, M., Raasi, S., Pickart, C. & Fushman, D. Structural determinants for selective recognition of a Lys48-linked polyubiquitin chain by a UBA domain. *Mol Cell* **18**, 687-98 (2005).
43. Glickman, M.H. & Ciechanover, A. The ubiquitin-proteasome proteolytic pathway: destruction for the sake of construction. *Physiol Rev* **82**, 373-428 (2002).
44. Bachmair, A. & Varshavsky, A. The degradation signal in a short-lived protein. *Cell* **56**, 1019-32 (1989).
45. Al-Hakim, A. et al. The ubiquitous role of ubiquitin in the DNA damage response. *DNA Repair (Amst)* **9**, 1229-40 (2010).
46. Kirkpatrick, D.S. et al. Quantitative analysis of in vitro ubiquitinated cyclin B1 reveals complex chain topology. *Nat Cell Biol* **8**, 700-10 (2006).
47. Jin, L., Williamson, A., Banerjee, S., Philipp, I. & Rape, M. Mechanism of ubiquitin-chain formation by the human anaphase-promoting complex. *Cell* **133**, 653-65 (2008).
48. Deng, L. et al. Activation of the IkappaB kinase complex by TRAF6 requires a dimeric ubiquitin-conjugating enzyme complex and a unique polyubiquitin chain. *Cell* **103**, 351-61 (2000).
49. Pickart, C.M. & Fushman, D. Polyubiquitin chains: polymeric protein signals. *Curr Opin Chem Biol* **8**, 610-6 (2004).
50. Hochstrasser, M. Lingering mysteries of ubiquitin-chain assembly. *Cell* **124**, 27-34 (2006).
51. Thrower, J.S., Hoffman, L., Rechsteiner, M. & Pickart, C.M. Recognition of the polyubiquitin proteolytic signal. *EMBO J* **19**, 94-102 (2000).
52. Ciechanover, A. The ubiquitin-proteasome pathway: on protein death and cell life. *EMBO J* **17**, 7151-60 (1998).

53. Deffenbaugh, A.E. et al. Release of ubiquitin-charged Cdc34-S - Ub from the RING domain is essential for ubiquitination of the SCF(Cdc4)-bound substrate Sic1. *Cell* **114**, 611-22 (2003).
54. Hofmann, K. & Falquet, L. A ubiquitin-interacting motif conserved in components of the proteasomal and lysosomal protein degradation systems. *Trends Biochem Sci* **26**, 347-50 (2001).
55. Jelinsky, S.A., Estep, P., Church, G.M. & Samson, L.D. Regulatory networks revealed by transcriptional profiling of damaged *Saccharomyces cerevisiae* cells: Rpn4 links base excision repair with proteasomes. *Mol Cell Biol* **20**, 8157-67 (2000).
56. Ivantsiv, Y., Kaplun, L., Tzirkin-Goldin, R., Shabek, N. & Raveh, D. Unique role for the UbL-UbA protein Ddi1 in turnover of SCFUfo1 complexes. *Mol Cell Biol* **26**, 1579-88 (2006).
57. Liu, Y.L. & Xiao, W. Bidirectional regulation of two DNA-damage-inducible genes, MAG1 and DDI1, from *Saccharomyces cerevisiae*. *Molecular Microbiology* **23**, 777-789 (1997).
58. Gabriely, G., Kama, R., Gelin-Licht, R. & Gerst, J.E. Different domains of the UBL-UBA ubiquitin receptor, Ddi1/Vsm1, are involved in its multiple cellular roles. *Mol Biol Cell* **19**, 3625-37 (2008).
59. Sirkis, R., Gerst, J.E. & Fass, D. Ddi1, a eukaryotic protein with the retroviral protease fold. *Journal of Molecular Biology* **364**, 376-387 (2006).
60. Rice, P., Longden, I. & Bleasby, A. EMBOSS: the European Molecular Biology Open Software Suite. *Trends Genet* **16**, 276-7 (2000).
61. Bertolaet, B.L. et al. UBA domains mediate protein-protein interactions between two DNA damage-inducible proteins. *Journal of Molecular Biology* **313**, 955-963 (2001).
62. Sasaki, T., Funakoshi, M., Endicott, J.A. & Kobayashi, H. Budding yeast Dsk2 protein forms a homodimer via its C-terminal UBA domain. *Biochem Biophys Res Commun* **336**, 530-5 (2005).
63. Hiyama, H. et al. Interaction of hHR23 with S5a. The ubiquitin-like domain of hHR23 mediates interaction with S5a subunit of 26 S proteasome. *J Biol Chem* **274**, 28019-25 (1999).

64. Kaplun, L., Ivantsiv, Y., Kornitzer, D. & Raveh, D. Functions of the DNA damage response pathway target Ho endonuclease of yeast for degradation via the ubiquitin-26S proteasome system. *Proc Natl Acad Sci U S A* **97**, 10077-82 (2000).
65. Kaplun, L., Ivantsiv, Y., Bakhrat, A. & Raveh, D. DNA damage response-mediated degradation of Ho endonuclease via the ubiquitin system involves its nuclear export. *J Biol Chem* **278**, 48727-34 (2003).
66. Keller, R. *The Computer Aided Resonances Assignment Tutorial*, (CANTINA Verlag, 2004).
67. Sitkoff, D. & Case, D. Theories of chemical shift anisotropies in proteins and nucleic acids. *Progress in Nuclear Magnetic Resonance Spectroscopy* **32**, 165-190 (1998).
68. Schwarzinger, S., Kroon, G.J., Foss, T.R., Wright, P.E. & Dyson, H.J. Random coil chemical shifts in acidic 8 M urea: implementation of random coil shift data in NMRView. *J Biomol NMR* **18**, 43-8 (2000).
69. Wishart, D.S. & Case, D.A. Use of chemical shifts in macromolecular structure determination. *Methods Enzymol* **338**, 3-34 (2001).
70. Wishart, D.S., Sykes, B.D. & Richards, F.M. The chemical shift index: a fast and simple method for the assignment of protein secondary structure through NMR spectroscopy. *Biochemistry* **31**, 1647-51 (1992).
71. Wishart, D.S. & Sykes, B.D. The <sup>13</sup>C chemical-shift index: a simple method for the identification of protein secondary structure using <sup>13</sup>C chemical-shift data. *J Biomol NMR* **4**, 171-80 (1994).
72. Berjanskii, M.V. & Wishart, D.S. A simple method to predict protein flexibility using secondary chemical shifts. *J Am Chem Soc* **127**, 14970-1 (2005).
73. Ottiger, M., Delaglio, F. & Bax, A. Measurement of J and dipolar couplings from simplified two-dimensional NMR spectra. *J Magn Reson* **131**, 373-8 (1998).
74. Nilges, M., Macias, M.J., O'Donoghue, S.I. & Oschkinat, H. Automated NOESY interpretation with ambiguous distance restraints: the refined NMR solution structure of the pleckstrin homology domain from beta-spectrin. *J Mol Biol* **269**, 408-22 (1997).
75. Rieping, W. et al. ARIA2: automated NOE assignment and data integration in NMR structure calculation. *Bioinformatics* **23**, 381-2 (2007).

76. Brunger, A.T. et al. Crystallography & NMR system: A new software suite for macromolecular structure determination. *Acta Crystallogr D Biol Crystallogr* **54**, 905-21 (1998).
77. Clore, G. & Garrett, D. R-factor, free R, and complete cross-validation for dipolar coupling refinement of NMR structures. *Journal of the American Chemical Society* **121**, 9008-9012 (1999).
78. The Pymol Molecular Graphics System, Version 1.2r1. (Schrödinger, LLC.).
79. Walker, O., Varadan, R. & Fushman, D. Efficient and accurate determination of the overall rotational diffusion tensor of a molecule from <sup>(15)N</sup> relaxation data using computer program ROTDIF. *J Magn Reson* **168**, 336-45 (2004).
80. Tjandra, N., Feller, S.E., Pastor, R.W. & Bax, A. Rotational diffusion anisotropy of human ubiquitin from <sup>15</sup>N NMR relaxation. *Journal of the American Chemical Society* **117**, 12562-12566 (1995).
81. Haririnia, A., D'Onofrio, M. & Fushman, D. Mapping the interactions between Lys48 and Lys63-linked di-ubiquitins and a ubiquitin-interacting motif of S5a. *J Mol Biol* **368**, 753-66 (2007).
82. Zhang, D. et al. Together, Rpn10 and Dsk2 can serve as a polyubiquitin chain-length sensor. *Mol Cell* **36**, 1018-33 (2009).
83. Dominguez, C., Boelens, R. & Bonvin, A.M. HADDOCK: a protein-protein docking approach based on biochemical or biophysical information. *J Am Chem Soc* **125**, 1731-7 (2003).
84. de Vries, S.J. et al. HADDOCK versus HADDOCK: new features and performance of HADDOCK2.0 on the CAPRI targets. *Proteins* **69**, 726-33 (2007).
85. de Vries, S.J., van Dijk, M. & Bonvin, A.M. The HADDOCK web server for data-driven biomolecular docking. *Nat Protoc* **5**, 883-97 (2010).
86. Hubbard, S.J. & Thornton, J.M. NACCESS Computer Program. (Department of Biochemistry and Molecular Biology, University College London, 1993).
87. Leggett, D.S. et al. Multiple associated proteins regulate proteasome structure and function. *Mol Cell* **10**, 495-507 (2002).
88. Verma, R. et al. Proteasomal proteomics: identification of nucleotide-sensitive proteasome-interacting proteins by mass spectrometric analysis of affinity-purified proteasomes. *Mol Biol Cell* **11**, 3425-39 (2000).

89. Hanna, J. et al. Deubiquitinating enzyme Ubp6 functions noncatalytically to delay proteasomal degradation. *Cell* **127**, 99-111 (2006).
90. Tzirkin, R., Ivantsiv, Y., Klyman, E. & Raveh, D. The ubiquitin domain protein Ddi1 functions in DNA damage response mediated degradation of Ho endonuclease of yeast. *Yeast* **20**, S144-S144 (2003).
91. Rosenzweig, R., Bronner, V., Zhang, D., Fushman, D. & Glickman, M.H. Rpn1 and Rpn2 coordinate ubiquitin processing factors at proteasome. *J Biol Chem* **287**, 14659-71 (2012).
92. Zhang, D., Raasi, S. & Fushman, D. Affinity makes the difference: nonselective interaction of the UBA domain of Ubiquilin-1 with monomeric ubiquitin and polyubiquitin chains. *J Mol Biol* **377**, 162-80 (2008).
93. Goujon, M. et al. A new bioinformatics analysis tools framework at EMBL-EBI. *Nucleic Acids Res* **38**, W695-9 (2010).
94. Larkin, M.A. et al. Clustal W and Clustal X version 2.0. *Bioinformatics* **23**, 2947-8 (2007).
95. Sievers, F. et al. Fast, scalable generation of high-quality protein multiple sequence alignments using Clustal Omega. *Mol Syst Biol* **7**, 539 (2011).
96. Marchler-Bauer, A. et al. CDD: conserved domains and protein three-dimensional structure. *Nucleic Acids Res* **41**, D348-52 (2013).
97. Schultz, J., Milpetz, F., Bork, P. & Ponting, C.P. SMART, a simple modular architecture research tool: identification of signaling domains. *Proc Natl Acad Sci U S A* **95**, 5857-64 (1998).
98. Letunic, I., Doerks, T. & Bork, P. SMART 7: recent updates to the protein domain annotation resource. *Nucleic Acids Res* **40**, D302-5 (2012).
99. Keller, R. Optimizing the process of nuclear magnetic resonance spectrum analysis and computer aided resonance assignment. (Thèse de doctorat, ETH Zurich Thesis No. 15947 , Swit).
100. Goddard, T.D. & Kneller, D.G. SPARKY 3, University of California, San Francisco.
101. Hall, J.B. & Fushman, D. Characterization of the overall and local dynamics of a protein with intermediate rotational anisotropy: Differentiating between conformational exchange and anisotropic diffusion in the B3 domain of protein G. *J Biomol NMR* **27**, 261-75 (2003).

102. Ruckert, M. & Otting, G. Alignment of biological macromolecules in novel nonionic liquid crystalline media for NMR experiments. *J. Amer. Chem. Soc.* **122**, 7793-7797 (2000).
103. Varadan, R., Assfalg, M. & Fushman, D. Using NMR spectroscopy to monitor ubiquitin chain conformation and interactions with ubiquitin-binding domains. in *Ubiquitin and Protein Degradation, Methods in Enzymology*, Vol. 399 part B, Vol. 399 part B (ed. R.J.Deshaies) 177-192 (2005).
104. Ryabov, Y. & Fushman, D. Interdomain mobility in di-ubiquitin revealed by NMR. *Proteins* **63**, 787-96 (2006).
105. Johnson, M.L., Correia, J.J., Yphantis, D.A. & Halvorson, H.R. Analysis of data from the analytical ultracentrifuge by nonlinear least-squares techniques. *Biophys J* **36**, 575-88 (1981).